Palladian gold mineralisation (*ouro preto*) in Brazil: Gongo Soco, Itabira and Serra Pelada

Dissertation
for acquisition of a degree of Doctor
of Natural Sciences

presented by
Alexandre Raphael Cabral, M.Sc., B.Sc.
from Rio de Janeiro, Brazil

Approved by
the Faculty of Mathematics and Natural Sciences
of the Technical University of Clausthal

Day of examination: May 16, 2003

Über das Vorkommen von Palladiumhaltigem Gold (*ouro preto*) in Brasilien: Gongo Soco, Itabira und Serra Pelada

Dissertation
zur Erlangung des Grades eines
Doktors der Naturwissenschaften

vorgelegt von
Alexandre Raphael Cabral, M.Sc., B.Sc.
aus Rio de Janeiro, Brasilien

genehmigt von der
Mathematisch-Naturwissenschaftlichen Fakultät
der Technischen Universität Clausthal

Tag der mündlichen Prüfung: 16. Mai 2003

This dissertation was undertaken at the Department of Ore Geology Research of the Institute of Mineralogy and Mineral Resources of the Technical University of Clausthal.

Dean:	Prof. Dr. D. Mayer
Supervisor:	Prof. Dr. B. Lehmann
Co-supervisor:	Prof. Dr. H. H. Otto

Die vorliegende Arbeit wurde an der Abteilung Lagestättenforschung des Institutes für Mineralogie und Mineralische Rohstoffe der Technischen Universität Clausthal angefertigt.

Dekan:	Prof. Dr. D. Mayer
Referent:	Prof. Dr. B. Lehmann
Korreferent:	Prof. Dr. H. H. Otto

In memory of

Alexandre Vanucchi Leme (1950-1973)

on the occasion of the 30th anniversary of his assassination under torture by the military dictatorship. He was a 22-year-old student of Geology at *Universidade de São Paulo* (USP).

¡Color de sangre minera
tiene el oro del patrón!

Atahualpa Yupanqui

Acknowledgements

When I arrived in Germany, my research project was on some manganese oxide deposits in the Quadrilátero Ferrífero of Minas Gerais. Adventitious problems compelled me to change the advisory professor. On accepting me as a doctoral student, Professor Bernd Lehmann suggested that I should go for a noble metal. Consequently, I turned back to Gongo Soco, where I carried out field work in 1994 for my master degree. On that occasion I got to know Richard D. Jones, an exploration geologist who worked at Gongo Soco in the 1960's. He shared his knowledge on the deposit with me.

The research project was financed by a *Deutscher Akademischer Austauschdienst* (DAAD) scholarship and *Deutsche Forschungsgemeinschaft* (DFG). It has also benefited from a Hugh E. McKinstry Student Grant of the Society of Economic Geologists for the year 2000.

The former Socoimex Mineração Ltda (Minervino Bethonico and the Gongo Soco mine staff) is thanked for supporting field work and permission to visit the Gongo Soco mine since 1994. Orlando '*Landão*' Garcia, Muriel '*Murica*' Innocentini and Antônio Abdo are gratefully thanked for their valuable help during field work, for the wonderful samples and, especially, hospitality.

The same facilities have been supplied by the *Companhia Vale do Rio Doce* (CVRD) since it took over the Gongo Soco mine in 2000. José Tadeu L. Rodrigues (CVRD) has kindly provided access to the jacutinga deposits of Itabira. Henry F. Galbiatti, Marcelo da Costa Pereira and Antônio Augusto Seabra Gomes Jr. shared their knowledge on the jacutinga mineralisation of Itabira. Wilson '*Tonelada*' Brunetto also helped me to take good samples from Itabira.

Access to the Serra Pelada *garimpo* area and to drill cores, polished sections and private reports was possible due to the cooperation of CVRD, particularly of Paulo R. Amorim dos Santos Lima (*Paulão*), Carlos Henrique Cravo Costa and Rogério Kwitko Ribeiro. Rogério also was responsible for some SEM analyses.

I am particularly grateful to Dr. Volker Lüders (GeoForschungsZentrum Potsdam) for the fluid inclusion microthermometry data using infrared microscopy. Thanks are also due to Klaus Herrmann (TU Clausthal) for his meticulous assistance with the electron-microprobe analyses. Dr. Eike Gierth (TU Clausthal) assisted in taking photomicrographs and Wayan Warmada kindly helped with the fluid inclusion microthermometry at Clausthal. Ulf Hemmerling prepared good polished sections and Fred Türck provided some computational and laboratorial facilities. Some fellows, Frank Schultz and Jens Wittenbrink, gave a hand to customary problems that a foreigner has to face in Germany.

A doctoral dissertation is, as everything in life, a result of a particular historical process. Mine has partly been forged by my parents and grandparents (José Guilherme and Miriam, Guilherme and Yolanda), and now by my wife, Lisanea, who supported all sorts of vicissitudes at Clausthal.

Nothing, absolutely nothing would have been possible without those who do the every day work: the miners, Pimenta '*Veludo*', Antônio '*Negão*', Edivando, Toco, among others from Gongo Soco, Guillerme and Chico (Itabira), Fred and Paulo '*Pierre*' (Carajás), just to name a few *companheiros de verdade*.

Abstract

Gold mineralisation in which gold is alloyed with palladium is unusual. In Brazil, however, palladian gold is linked to large-scale gold rushes. In the Brazilian Gold Cycle (1695-1785), a Palaeoproterozoic banded iron formation (itabirite)-hosted, vein-style mineralisation presumedly accounted for much of the gold production from the Ouro Preto area, Minas Gerais. Remarkable examples of this mineralisation style are Gongo Soco and Itabira, Minas Gerais. In recent times, a spectacular gold rush was triggered by bonanza-style ore of palladian gold at Serra Pelada, Carajás mineral province, Pará.

Gongo Soco is an iron ore mine where gold is recovered, though intermittently, from cross-cutting, specularite-rich veins (*jacutinga*) and disseminations in itabirite and soft hematite ore. Palladian gold, of variable composition in terms of Pd, Ag and Hg, occurs as nuggets and aggregates with hematite. Gold grains typically have a dark coating composed distinctively of Pd–O species together with iron oxyhydroxide, i.e. the so-called *ouro preto* (black gold). A number of platinum-group minerals (PGM) are included in nuggets of palladian gold: isomertieite, mertieite-II, chrisstanleyite and selenides of empirical stoichiometry of $Pd_5(Hg,Sb,Ag)_2Se_6$ and $(Pd,Sb,Ag,Hg)_5Se_4$. Specular hematite included in gold is generally chromiferous. Native palladium is formed by a two-stage process of alteration: PGM → Pd–O → Pd. Cross-cutting relationships and the presence of mechanically twinned hematite suggest that at least some of the nugget gold is post-Brasiliano Orogeny in age (<0.6 Ga). Fluid inclusion microthermometry in cogenetic specular hematite points to minimum temperatures of about 160°C and moderately saline fluids. Bulk-rock chemical analyses of auriferous (*jacutinga*) veins indicate enrichment in Au, Pd, Fe, Mn, Ba, Hg and Cr compared to fresh, non-altered itabirite.

Itabira is a world-class iron ore district. Like Gongo Soco, auriferous veins cross-cut the foliated host rock (itabirite) and, consequently, a late- to post-Brasiliano age is inferred. Palladian gold and PGM occur as fracture infill and, occasionally, as inclusions in specularite. The PGM include palladseite, sudovikovite, isomertieite, atheneite and hongshiite (PtCu). Grains of hongshiite are haloed by a porous rim of native platinum, resembling the weathering-derived, core-and-mantle pattern of residual gold particles in placers and lateritic profiles. The veins are enriched in Au, Pd, Pt, Cr, Mn and Hg compared to host itabirite.

The Serra Pelada Au–Pd–Pt deposit is hosted by weakly metamorphosed sedimentary rocks of Late Archaean age. Remains of its near-surface bonanza ore, now completely mined out, were studied in a drill core, recovered in 1982, with abundant coarse-grained dendrites of palladian gold in a completely disaggregated, ferruginous, clayey material. PGM, occurring as inclusions in, or attached to, palladian gold are “guanglinite”, Sb-bearing “guanglinite”, atheneite, isomertieite, Se-bearing phases (sudovikovite and palladseite, as well as Pd–Pt–Se, Pd–Se, Pd–Hg–Se and Pd–Bi–Se phases), and native palladium. A mineral assemblage of fine-grained palladian gold (about 2 wt % Pd), isomertieite and a Ba-bearing Mn oxide (possibly romanèchite) post-dates the dendrites of palladian gold (about 7 wt % Pd). Fluid inclusions in quartz consist of Ca-rich brines that homogenise from about 100 to 175°C. The drill core shows enrichments of up to three orders of magnitude for Ag, As, Ba, Cr, and Sb, and of four orders and more for Au, Pd, Pt and Hg compared to the country rock.

Regardless of different geological settings and intrinsic particularities, all three deposits have mineralogical and geochemical features in common that point to highly oxidising (hematite stability field) and relatively shallow-level conditions, typical of hydrothermal selenide vein-type deposits formed at relatively low temperatures (<300°C).

Contents

1
Introduction

> "Whether the gold which (…) is associated with the same metals in different parts of the Province; as well as that which, in other matrices and strata, contains different alloys, in the same neighbourhood (…) – however inviting as a subject for speculation – can scarcely be discussed, with advantage, in a descriptive memoir".
>
> *On the Gold-Mines of Minas Geraes*, *in Brazil*, by W. J. Henwood, 1871.

This is a descriptive memoir on the mineralogy and geochemistry of auriferous ore from three exceptional deposits, i.e. the Gongo Soco and Itabira iron ore deposits in the Quadrilátero Ferrífero of central Minas Gerais, and the Serra Pelada deposit in the Carajás mineral province of southern Pará, in which gold is alloyed with palladium in sediment-hosted, sulphide-poor, epigenetic mineralisation. It complements published data by the author (CABRAL et al. 2001, CABRAL et al. 2002a, b, c, d; KWITKO et al. 2002; CABRAL & LEHMANN 2003; CABRAL et al. 2003), in partial fulfilment of the requirements of his doctoral degree. The research had to diverge from its original course, which first was targeted on Gongo Soco only, to also include Itabira and Serra Pelada, as access to the ore deposits and internal files, permission to sample and logistical support were granted by Companhia Vale do Rio Doce (CVRD).

Palladian gold mineralisation is unusual and occurrences of economic importance seem to be known from Brazil only. The first evidence of a natural gold–palladium alloy came from a gold grain from Brazil (GEHLEN 1811). Historically, in the Brazilian Gold Cycle (1695-1785), much of the gold production from the area around the city of Ouro Preto, Minas Gerais, is presumed to have come from gold mineralisation hosted by banded iron formation, i.e. itabirite (e.g. ESCHWEGE 1833; FERRAND 1894; SCOTT 1902, HUSSAK 1904). The auriferous portions of itabirite have traditionally been called *jacutinga* (HARTT 1870; HUSSAK 1904), a vein-style mineralisation, of which Gongo Soco and Itabira are the outstanding examples. Many researchers were intrigued by the virtually sulphide-free, bonanza gold ore of *jacutinga* deposits (e.g. HUSSAK 1904, 1906; BENSUSAN 1929; OLIVEIRA 1932; FREYBERG 1932; DORR & BARBOSA 1963; DORR 1965; GUIMARÃES 1970; LADEIRA 1991; OLIVO et al. 1995, 2001; VARAJÃO et al. 1999), but substantial work on ore mineralogy and ore geochemistry is still needed. This is precisely the case of Gongo Soco: the published chemical analyses of its ore and gold nuggets can only be found in early accounts (e.g. FARADAY 1828; JOHNSON & LAMPADIUS 1837; HENWOOD 1871a; HUSSAK 1904), where remarkable findings were then reported. One of these, by JOHNSON & LAMPADIUS (1837), that the typical dark colour of the Gongo Soco gold, i.e. *ouro preto* (vide JEDWAB & CASSEDANNE 1998) was due to coatings of Pd–O species and iron oxyhydroxide could only be confirmed recently (CABRAL et al. 2001). This memoir records ore microscopy, coupled with scanning electron microscopy (SEM) and electron-microprobe analysis (EMPA), and reconnaissance bulk-rock chemical and fluid inclusion data, suggesting that the Gongo Soco *jacutinga* mineralisation occurs as relatively low-temperature open-space infill under highly oxidising hydrothermal conditions.

Among the *jacutinga*-style gold deposits worked in the eighteenth and nineteenth centuries in the Quadrilátero Ferrífero (Fig. 1), the most famous was Gongo Soco. It was the first major underground mine in Brazil, with a production of 12.9 tonnes of gold between 1826 and 1856 (HENWOOD 1871a). Of the entire produce, about 68% were obtained "in clusters, nuggets, and other coarse gold treated by hand at the washing-house" (HENWOOD 1871a). Its spectacular auriferous "bunches" (pockets), from which Hart in May 1827 "brought out of the mine, in a miner's hat, eleven pounds of gold" (HART 1827), motivated copious reports by early workers, as compiled by HENWOOD (1871a) and FERRAND (1894). The first chemical investigations date back to 1826 when palladium was identified (GARDNER 1826). After the closure of the mine at the end of 1856, the old underground workings collapsed and were flooded, and thus became inaccessible; the formerly imposing mine installations were brought to ruin (Fig. 2a) Only recently, open-pit mining operations have reached the level of the old underground workings (Fig. 2b). At present, gold is an intermittent by-product of iron ore mining at Gongo Soco (several tens of kilograms per year).

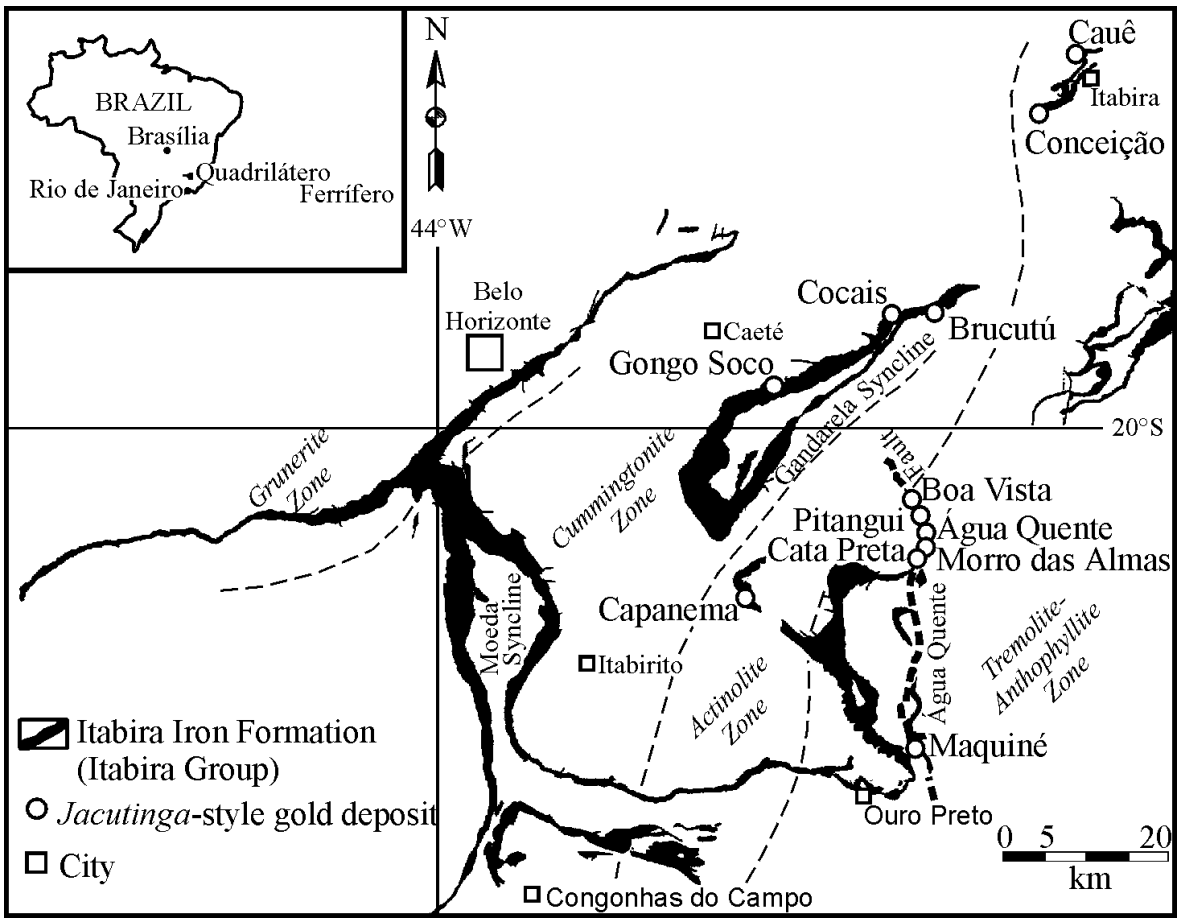

Fig. 1: Location of *jacutinga*-style gold deposits (open circles) in relation to the Itabira Iron Formation (Itabira Group), shown in black (after DORR 1969), with the metamorphic zones of PIRES (1995), dashed lines. Gold is currently mined as a by-product of iron ore at Cauê, Conceição and Gongo Soco. Note that the old *jacutinga* deposits in the eastern part of the Quadrilátero Ferrífero (i.e. Maquiné to Boa Vista) are located along the N–S-trending Água Quente Fault (FERREIRA FILHO & FONSECA 2001), a major Brasiliano (0.8-0.6 Ga) structure of the Fazendão Thrust Front (CHEMALE et al. 1994), with present-day hot-spring activity.

Like Gongo Soco, the currently world-class iron ore district of Itabira commenced as a gold-mining centre after the first discoveries were made in 1720 (SAINT-HILAIRE 1830). Only scattered records of the historical production of gold from the auriferous *jacutinga* seams are available (HENWOOD 1846, 1871a; Scott 1902). Nowadays, gold is mined as a by-product (about 600 kg per year) in the iron ore mines of Itabira. The Au–Pd mineralisation (*jacutinga*) of Itabira has been considered to be structurally controlled by mylonitic foliation and/or stretching lineation (POLÔNIA & SOUZA 1988; OLIVO et al. 1995, 2001). However, new data based on the mapping of working faces by mine geologists (GALBIATTI et al. 1997; GALBIATTI 1999; PEREIRA et al. 1999) and on ore microscopy (CABRAL et al. 2002d) indicate that the mineralisation occurs as late open-space infill. These findings are addressed in this dissertation, as well as new mineralogical and geochemical data.

Fig. 2: (a) Ruins of the blast furnace at Gongo Soco. Photograph taken in 1969 by R. D. Jones. (b) View (looking south) of a collapsed old shaft, exposed by the development of iron ore (open-pit) mining at Gongo Soco. Photograph taken in 1999 by R. D. Jones.

In recent times, the most impressive gold rush took place at Serra Pelada and focused again on palladian gold mineralisation (MEIRELES & SILVA 1988). Discovered in 1980 in the near-surface lateritic portion, the Serra Pelada deposit rapidly attracted an indigent multitude of *garimpeiros* (Fig. 3), who manually mined the bonanza gold ore until the *garimpo* (open pit) collapsed and flooded at a depth of about 130 m. From 1980 to 1984, 32.6 tonnes of gold were extracted (MEIRELES & SILVA 1988), but unofficial figures place the amount closer to 70 tonnes of gold. Although much information had been accumulated in unpublished internal reports of CVRD, the first detailed investigations on the Serra Pelada deposit have just been released recently (TALLARICO et al. 2000a; MORONI et al. 2001; GRAINGER et al. 2002; GÜNER et al. 2002). Since the bonanza gold ore is completely mined out, no material from the near-surface mineralisation could be examined. Fortunately, a 20-year-old drill core, recovered in 1982 from the central part of the Serra Pelada *garimpo*, has provided samples with coarse-grained aggregates of gold. The drill core is considered to be representative of the near-surface bonanza ore. Bulk-rock chemical analysis of selected depth intervals of this drill core and electron-microprobe analysis of gold aggregates have shown astonishingly high grades of gold, palladium and platinum related to palladian gold in association with rare minerals of palladium and platinum (CABRAL et al. 2002a, b). This dissertation presents complementary data to those two articles.

As an epilogue, some particular mineralogical and geochemical aspects are discussed. Emphasis is placed on the similarities in terms of ore mineralogy and ore geochemistry between the geologically distinct deposits of the Quadrilátero Ferrífero (Gongo Soco and Itabira) and Serra Pelada, which point to analogous ore-forming conditions.

Fig. 3: The Serra Pelada *garimpo* (open pit). The photograph, entitled "Babilônia", was taken by Breno A. Santos in August 1982.

2
Gongo Soco: a typical case of palladian gold mineralisation (*ouro preto*)

> ‘The lines and veins are followed with pick and without blasting; their contents supply a soft and crumbling iron ore, which requires little stamping, and the ‘line gold’ thus procured is of superior quality. Often by following the filaments which radiate to all directions from a common centre, the miner finds a nucleus or nugget of large size, but inferior in standard to the line gold, and losing more in the smelting-pot. The carat at Gongo Soco was 19–20. Some describe the gold as dark yellow with palladium (…)”.
>
> *The highlands of the Brazil*, Vol. I, by R. F. Burton, 1869.

Gongo Soco was one of the most famous gold mines of colonial Brazil. Rather more than two thirds of the gold produced from 1826 and 1856 at Gongo Soco by the Imperial Brazilian Mining Association were hand picked and occurred “in masses, plates and threads” (HENWOOD 1871a). The gold, though erratically distributed, was so incredibly concentrated in “bunches” (pockets) that only a few days accounted for the month produce (Fig. 4). Since the early days of gold mining by the English company, it was realised that palladium was associated with gold (GARDNER 1826) and all palladium for the Wollaston medal, coined in 1845 by the Geological Society of London, was obtained from Gongo Soco (HENWOOD 1871a). It was also noted that the proportions of other metals in unrefined gold varied with depth (Fig. 5). Remarkably, Gongo Soco provided the first evidence for the existence of natural Pd–O compounds (GARDNER 1826; JOHNSON & LAMPADIUS 1837).

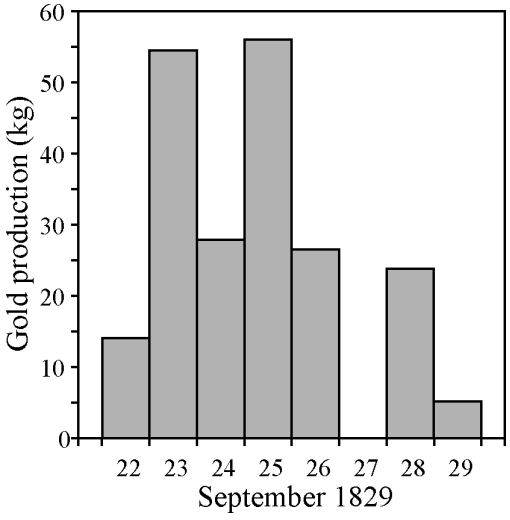

Fig. 4: Quantity of gold extracted from bonanza-style ore shoots at Gongo Soco (HENWOOD 1871a).

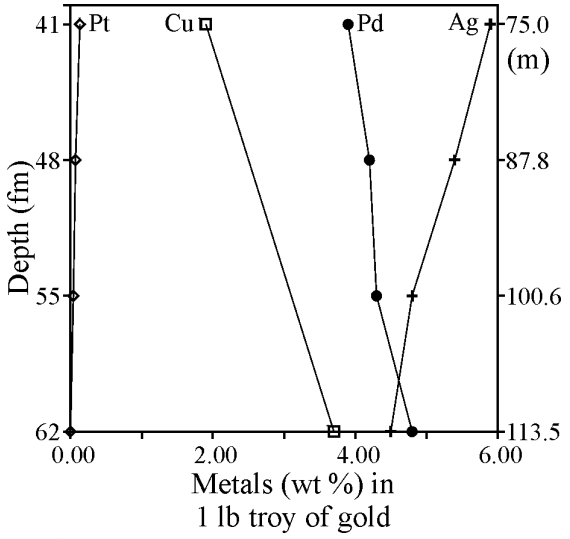

Fig. 5: Variation of metals at different depths in unrefined gold (HENWOOD 1871a).

This chapter records mineralogical, microchemical and microstructural features of *ouro preto* nuggets from Gongo Soco, i.e. nuggets partially coated by iron oxyhydroxide and Pd–O species, preceded by a brief account on regional geology and *jacutinga* mineralisation of the Quadrilátero Ferrífero. Reconnaissance fluid inclusion and bulk-rock chemical data of auriferous veins are as well presented.

Geological setting and the Gongo Soco iron ore mine

Gongo Soco is one of numerous iron ore deposits in the Quadrilátero Ferrífero of Minas Gerais. It is hosted by the Itabira Iron Formation of HARDER & CHAMBERLIN (1915), later designated as the Itabira Group (DORR et al. 1957; DORR 1969). With a minimum Pb/Pb age of 2.4 Ga (BABINSKI et al. 1995), the Itabira Group is the middle unit of the Minas Supergroup and consists of a continuous sequence of chemical sedimentary rocks subdivided into two formations: (1) the Cauê Formation, a thick iron formation (itabirite), which grades upwards into the (2) dolomitic rocks of the Gandarela Formation. It is underlain by the Caraça Group, which comprises quartzite, conglomerate, sericite schist (basal Moeda Formation) and phyllite (Batatal Formation), and is overlain by the Piracicaba Group, of quartzite and phyllite with minor iron formation. The Minas Supergroup, with ages between 2580 Ma (base of the Caraça Group, i.e. the Moeda Formation) and 2050 Ma (RENGER et al. 1994), rests unconformably on the Archaean Rio das Velhas Supergroup, a greenstone-belt sequence (LOBATO et al. 2001a, and references therein).

The map pattern of the Quadrilátero Ferrífero is dominated by a dome-and-keel architecture, in which granitic domes are surrounded by interconnecting sedimentary belts containing the Rio da Velhas Supergroup and the Minas Supergroup (Fig. 6). There are other pronounced structures that do not conform to the dome-and-keel pattern. One of these is the Gandarela Syncline (Fig. 1), a regional-scale overturned structure (MOORE 1969; CHEMALE et al. 1994), where Gongo Soco is situated.

The structural complexity suggested by the map pattern has resulted in controversial models of tectonic evolution. For example, some authors support the superposition of two main tectonic events: (1) the ~2.0 Ga Transamazonian Orogeny, an extensional event with development of regional synclines and uplift of granite-gneiss domes; and (2) the ~0.6 Ga Pan-African-Brasiliano Orogeny, a compressive event characterised by a west-verging fold-and-thrust belt (e.g. DOSSIN et al. 1992; CHEMALE et al. 1994; ALKMIM & MARSHAK 1998). Alternatively, HIPPERTT & DAVIS (2000) advance the idea that the main evolution of the regional synclines and domes occurred during the Pan-African-Brasiliano Orogeny. The merits of this dispute are not discussed here, but it must be mentioned that there is apparently a consensus among structural geologists that the pervasive tectonic fabrics observed in the supracrustal rocks of the central and eastern parts of the Quadrilátero Ferrífero are related to the Brasiliano fold-and-thrust tectonics (CHAUVET & MENEZES 1992; MARSHAK et al. 1992; CHAUVET et al. 1994; CHEMALE et al. 1994; ALKMIM & MARSHAK 1998; HIPPERTT & DAVIS 2000). The fabrics include mylonitic foliation (S_1) and ESE-plunging stretching lineation, as well as mesoscopic folds with E–W-trending axes and N–S-trending crenulation lineation.

The Brasiliano deformation had an important influence on the economic geology of the Quadrilátero Ferrífero, particularly the development of foliated hematite fabrics in itabirite and associated high-grade hematite orebodies (ROSIÈRE et al. 2001). Late Brasiliano collapse tectonics produced extensional domains that locate auriferous quartz veins in the Ouro Preto

area (CHAUVET et al. 1994, 2001). Locally, hydrothermal manganese mineralisation can be recognised (CABRAL & SATTLER 2001; CABRAL et al. 2002e).

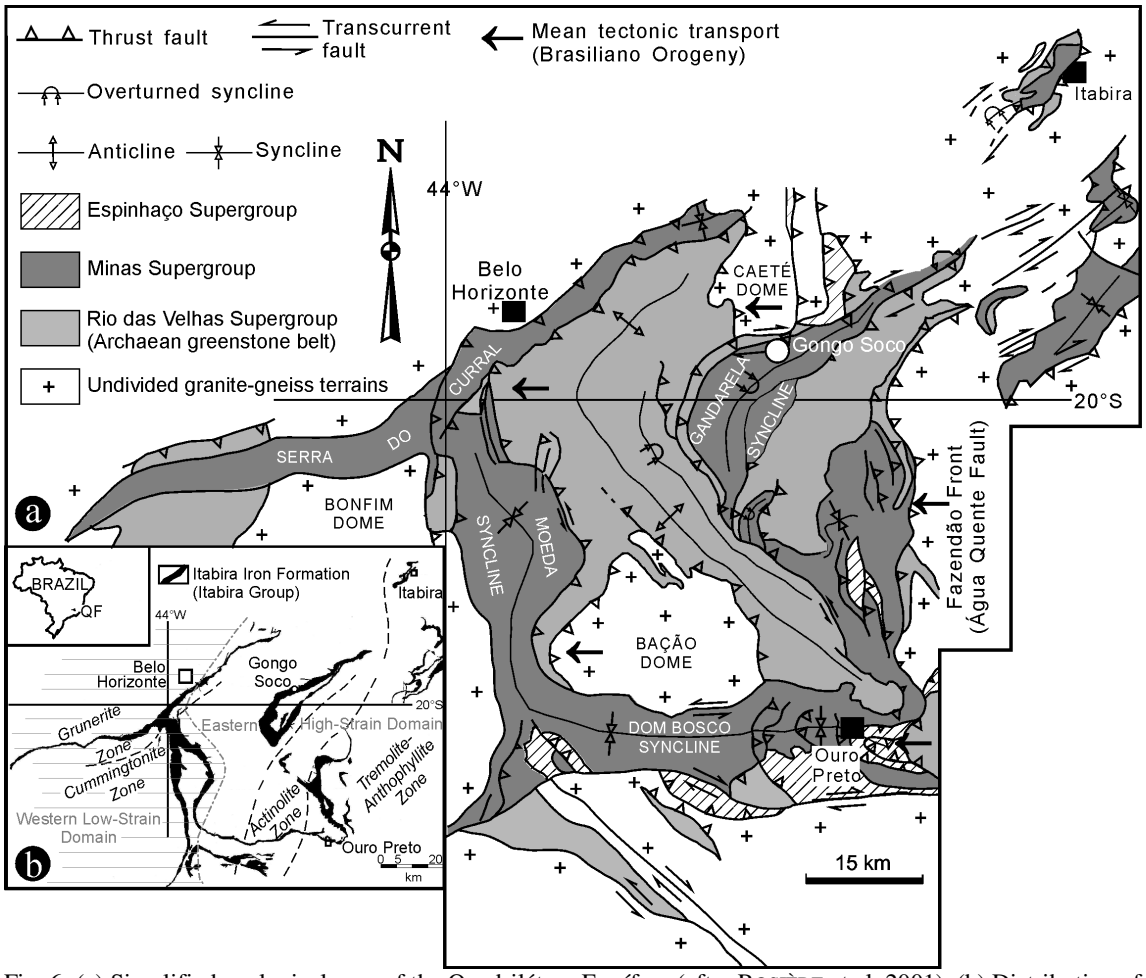

Fig. 6: (a) Simplified geological map of the Quadrilátero Ferrífero (after ROSIÈRE et al. 2001). (b) Distribution of the Itabira Iron Formation (Itabira Group), with metamorphic zones (dashed lines, after PIRES 1995) and strain domains (after ROSIÈRE et al. 2001).

The metasedimentary rocks show a regional zonation in metamorphic grade. The metamorphic grade increases from greenschist facies in the western and central parts of the Quadrilátero Ferrífero to almandine-amphibolite facies in its eastern part (PIRES 1995, and references therein). The metamorphic zones (chlorite, biotite and staurolite) delineated by HERZ (1978) were redefined by PIRES (1995) for the Itabira Group, with grunerite and cummingtonite zones occupying, respectively, the western and central parts of the Quadrilátero Ferrífero, and actinolite and tremolite-anthophyllite zones occurring in the eastern part (Figs. 1, 6b). Gongo Soco is localised within the cummingtonite zone.

The Cauê Formation at Gongo Soco is between 300 and 400 m thick. It strikes generally at azimuths 078-083° and dips about 45° south. Both the enclosing itabirite and the high-grade hematite orebody have a prominent, isoclinally folded, metamorphic foliation, defined by the planar orientation of hematite (specular hematite). The deposit is slightly discordant to the strike of the enclosing itabirite, spindle-shaped in plan, about 200 m wide at its mid-point and 1300 m long (Fig. 7), and has a strike about 110° with a gentle eastward plunge. The orebody is composed largely of soft hematite amounting to 66 Mt at about 66.6% Fe and 0.6% Mn (Table 1).

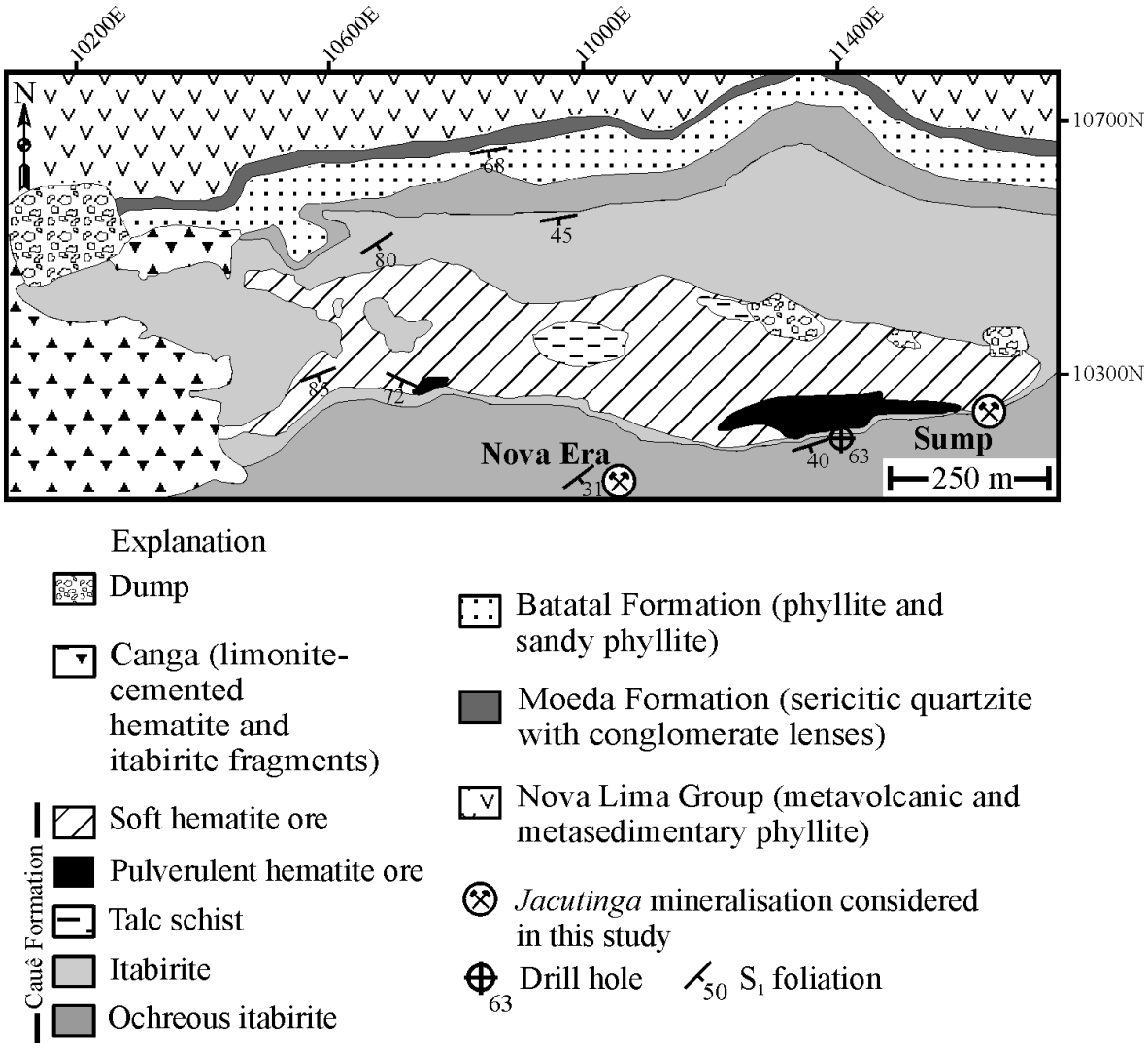

Fig. 7: Simplified geological map of the Gongo Soco iron ore mine, modified after R.D. Jones, R.L. Earhart and J.M. Lucas (unpublished data, 1962) by O.G. Rocha Filho and M.D. Innocentini in March 2001.

Table 1: Iron ore reserves (January 2001) of the Gongo Soco mine

Ore type	Reserve (Mt)	Fe (%)	SiO_2 (%)	Al_2O_3 (%)	P (%)	Mn (%)
Soft hematite	66.0	66.6	2.0	0.7	0.03	0.6
Pulverulent hematite*	6.9	62.7	2.9	1.0	0.06	2.7
Friable itabirite	25.5	45.8	31.0	0.9	0.05	0.3

* At Gongo Soco, distinction between soft and pulverulent hematite ore is based on the manganese content: fine-grained hematite ore with more than 1.5 % Mn is called pulverulent ore.

Jacutinga: palladian gold mineralisation in Minas Gerais

This section summarizes the general characteristics of the *jacutinga*-style gold deposits in Minas Gerais as described by previous workers. Recently, Olivo and co-workers have investigated the *jacutinga* orebodies of Itabira (OLIVO & GAUTHIER 1995; OLIVO et al. 1994, 1995, 1996, 2001). These are addressed in the next chapter.

Jacutinga is "75–84 per cent. of micaceous iron (…) with free gold in lines and potholes" (BURTON 1869, p. 132). It is an itabirite-hosted, virtually sulphide-free, characteristically palladium-bearing, auriferous mineralisation, made up essentially of soft, specular hematite with variable amounts of quartz and subordinate kaolinite, talc, limonite and manganese oxide (HENWOOD 1871a; HUSSAK 1904). The name *jacutinga* was originally given by the slaves who worked the deposits because of a fancied resemblance to the plumage of a bird, the *Penelope* (HARTT 1870, HENWOOD 1871a), combining the indigenous Tupi words *jacu* – bird, and *tinga* – white. It is possible that the white colour referred to kaolinite, since the occurrence of kaolinite as small aggregates in *jacutinga* was considered to be diagnostic of gold ore (GORCEIX 1881). The term has since acquired almost as many definitions as there are authors who have written about it (cf. Table 7 of FREYBERG 1932). For instance, it has been used to designate either the friable, soft portions of itabirite (CORREA DA COSTA 1878; GORCEIX 1881; FREYBERG 1932), or the bonanza-style gold ore hosted by itabirite (HUSSAK 1904). Hussak's definition was later adopted and recommended by HARDER & CHAMBERLIN (1915) in order to avoid the use of the term *jacutinga* in the iron ore terminology.

The auriferous mineralisation (*jacutinga*) occurs as narrow veins (from a few millimetres to generally no more than half a metre in width) running parallel to, and/or cross-cutting, the foliation of host itabirite (Fig. 8), and as pockets (HENWOOD 1871a; TOUZEAU 1892; HUSSAK 1904). One of the peculiarities of the *jacutinga*-style mineralisation is the occurrence of "lines of gold". They refer to threadlike fissures and small pockets in which gold may be found as "laminae and reticulated threads" (HENWOOD 1871a; cf. DE BOVET 1883; TOUZEAU 1892). From one of these lines at Maquiné (see Fig. 1 for location) about 5 cwt. (long hundredweight?, 254 kg) were taken out and yielded over 100 ounces (3.1 kg) of gold by washing (TOUZEAU 1892).

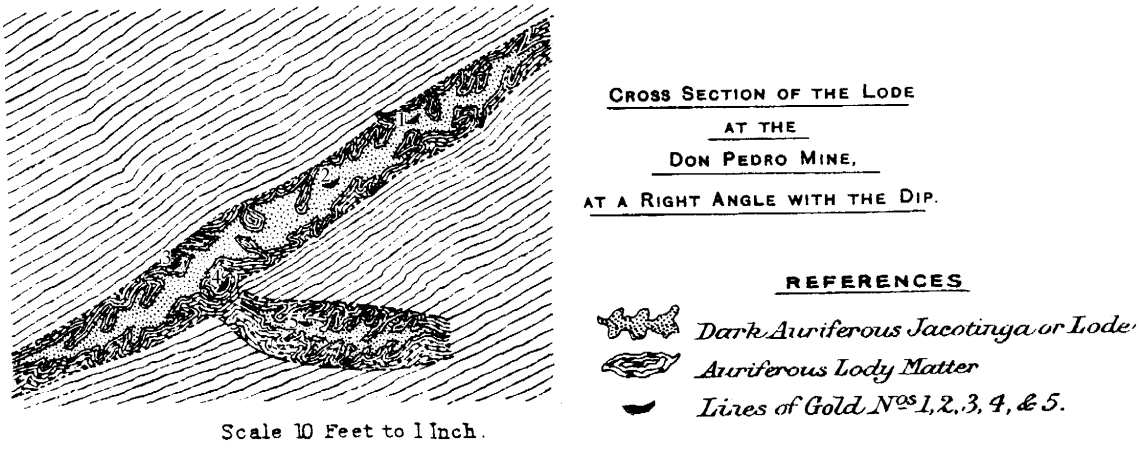

Fig. 8: TOUZEAU's (1892) cross-section of a bonanza-style ore shoot at the old Maquiné gold mine (also known as Dom Pedro). Note that the *jacutinga* vein runs parallel to, and cross-cuts, the host itabirite. Scale: 1.2 m to 1 cm.

Tourmaline is a common accessory component in *jacutinga* deposits (HUSSAK 1904). Cassiterite and rutile were also recorded at Gongo Soco, Maquiné and Itabira (HUSSAK 1904), as well as zircon (Gongo Soco and Maquiné). Gold occurs as free and visible granules, flakes and threads in soft *jacutinga*, but not in hard hematite ore (HENWOOD 1871a). Much of the gold is of darkish colour, i.e. *ouro preto* (HUSSAK 1904, 1906; BENSUSAN 1929). Such dark colour, though not explicitly stated, was due in part to Pd–O-bearing compounds (GARDNER 1826; JOHNSON & LAMPADIUS 1837).

Of the *jacutinga* gold deposits shown in Figure 1, Água Quente is the only one where gold mineralisation is associated with present-day hot spring activity. The temperature of water bubbling up out of *jacutinga* is as high as 35.5°C (HELMREICHEN 1847; HENWOOD 1871b). The mineralisation occurs as concordant and cross-cutting veins from which about 300 kg of gold were obtained from 1847 to 1853 (HENWOOD 1871a). The gold is reported to be free of palladium and copper, but alloyed with silver (HENWOOD 1871a).

Local enrichment of manganese seems to have been a guide to itabirite-hosted gold ore (HOCHEDER 1833; HENWOOD 1871a; THOMAS 1905). It was then proposed that pulverulent manganese was the best pathfinder element for *jacutinga*-style gold deposits (OLIVEIRA 1932).

The jacutinga-style mineralisation of Gongo Soco

The *jacutinga* mineralisation of Gongo Soco occurs as ore shoots, a few centimetre to about 1-3 metre in width, which cross-cut itabirite (Fig. 9). Millimetre-sized aggregates of talc and kaolinite are dispersed in a groundmass of fine-grained specularite, imparting a distinctive spotted appearance to the *jacutinga* ore shoots. Within the ore shoots, three types of specularite aggregates can be distinguished: (1) pockets of coarse-grained specularite intergrown with massive quartz; (2) tension gashes and pockets, a few centimetres wide, of fibrous, friable quartz and specularite; and (3) veinlets (<1 cm wide) of specularite. Cross-cutting relations among the quartz-specularite aggregates are not clear, but the veinlet-type appears to be the latest. Although *jacutinga* veins can readily be recognised in Figure 9, the boundaries of the mineralisation are difficult to be delimited because gold is also dispersed in itabirite and soft hematite ore as veinlets.

Two *jacutinga* orebodies are considered here. One occurs as decimetre-wide seams cutting ochreous itabirite (Fig. 9a), known as Nova Era; the other is a vein-like body in itabirite at the "Sump area", here designated as Sump orebody (Fig. 9b). Both are localised in fractures and faults that cross-cut the metamorphic foliation. As the Sump orebody has sporadically been mined and, consequently, well-exposed, a brief account of its structural setting is given below.

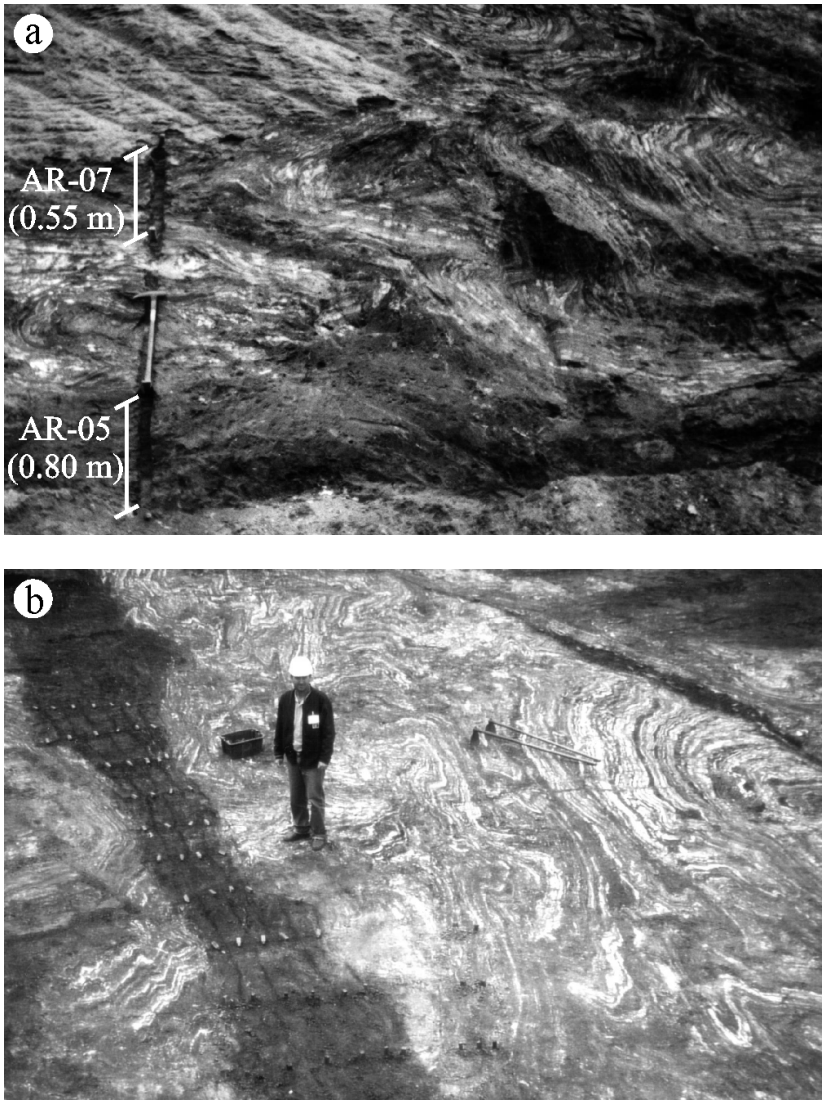

Fig. 9: (a) *Jacutinga* (dark, with sample pegs) truncates ochreous itabirite (below and above the 50 cm-long hammer) in the Nova Era area; photo toward SSE. Sample AR-06 is located between those shown in the photo. (b) E–W-trending *jacutinga* vein (dark, with sample pegs) cross-cuts complexly folded itabirite in the Sump area; photo toward ESE.

The Sump orebody

The Sump orebody (Fig. 9b) is a 45 m-long, E–W-trending, cross-cutting, sub-vertical ore shoot in soft itabirite (Fig. 10). It is about 3 m wide at its eastern end and irregularly tapers off towards the west. The foliation of the host itabirite (S_1) dips toward the south-east at 30-45° (Fig. 10a), being obliterated by a steeper S-dipping transposition foliation, i.e. S_2 (Fig. 10b). The ore shoot consists of soft hematite (fine-grained specularite) and accessory talc and kaolinite, and contains centimetre-long, steeply west-dipping, tension gashes filled by quartz, specularite and gold (Fig. 10c). Specularite-rich veinlets (<1 cm in width) also occur in the ore shoot.

Both S_1 and S_2 are cut by the sub-vertical ore shoot. A mineral lineation parallels the mesoscopic fold axes; both plunge toward the ESE at 25-35°. This set of structures

corresponds to those related to the Brasiliano tectonism in the Quadrilátero Ferrífero (e.g. CHEMALE et al. 1994; ALKMIM & MARSHAK 1998).

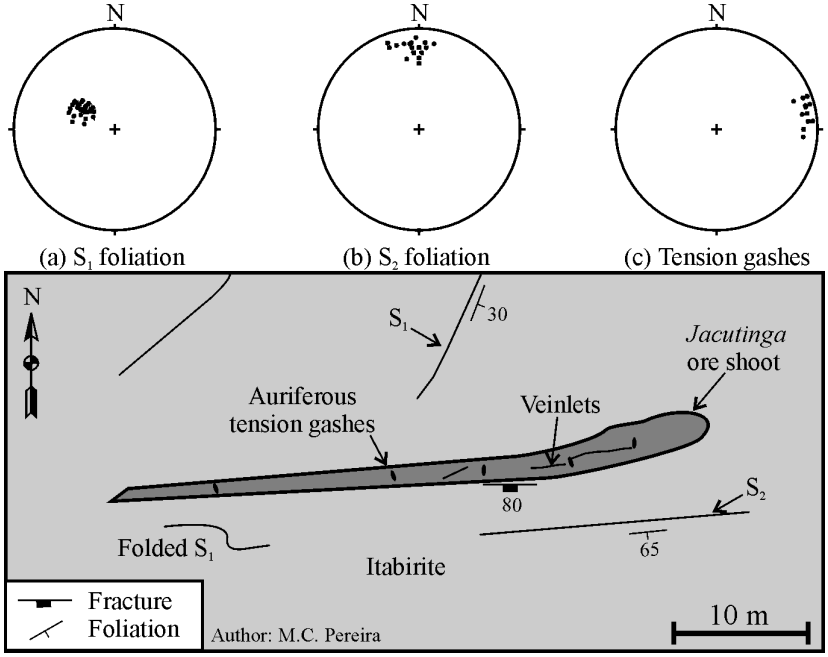

Fig. 10: Geological sketch of the Sump *jacutinga* orebody (modified by A.R. Cabral after unpublished report by M.C. Pereira, CVRD, 2001). Stereograms (pole to plane, lower hemisphere): (a) main foliation, S_1; (b) transposition surface, S_2; (c) tension gashes in the *jacutinga* vein.

Sample material and analytical techniques

Gold nuggets and gold-bearing iron ore fragments were recovered from a Knelson concentrator at the iron ore plant. Polished sections and mineral grains were studied by electron-microprobe analysis (Cameca SX100, Technical University of Clausthal) and with a scanning electron microscope, equipped with an EDS detector (Philips XL30 SEM, Companhia Vale do Rio Doce, Brazil). The analytical conditions are those reported in CABRAL et al. (2001), with the exception of platinum and selenium, for which the *L*α lines and pure metals as standards were used. Occasional modifications in the X-ray emission lines and analytical conditions used are noted in the tables.

Bulk samples for chemical analysis were collected from 0.25-1.15 m-long and 0.1-0.2 m-wide channels in *jacutinga* and host itabirite. The sample material is friable. Splits of about 0.3 kg were taken from bulk samples of 2–4 kg. The splits were ground in an agate mill. Aliquots of 30–60 g were submitted for chemical analyses at Activation Laboratories, Ancaster, Ontario, using analytical packages with INAA (instrumental neutron activation analysis), ICP, ICP-MS (inductively coupled plasma mass spectroscopy) and XRF (X-ray fluorescence spectroscopy) techniques. Gold, palladium and platinum were determined by fire assay ICP-OEM (optical emission spectroscopy), and mercury by cold vapour FIMS (flow injection mercury system). Five samples from the Sump area were analysed for the other platinum-group elements by NiS fire assay combined with INAA.

Crystals of specular hematite intergrown with quartz were examined by V. Lüders using infrared microscopy for fluid inclusion microthermometry at the GeoForschungsZentrum Potsdam. Sample preparation and analytical techniques are described elsewhere (LÜDERS et al. 1999).

Nuggets and aggregates of gold

Diverse nuggets of gold and gold-bearing aggregates occur at Gongo Soco. Some nuggets of gold are characteristically dark, i.e. *ouro preto* (Fig. 11a), others have whitish to brownish hues and are locally spotted with dark areas (Figs. 11b, c). Gold also is attached to quartz (Fig. 11d) and cross-cuts hematite ore (Figs. 11e, f). In all cases, crystals of specular hematite are attached to the surface of gold.

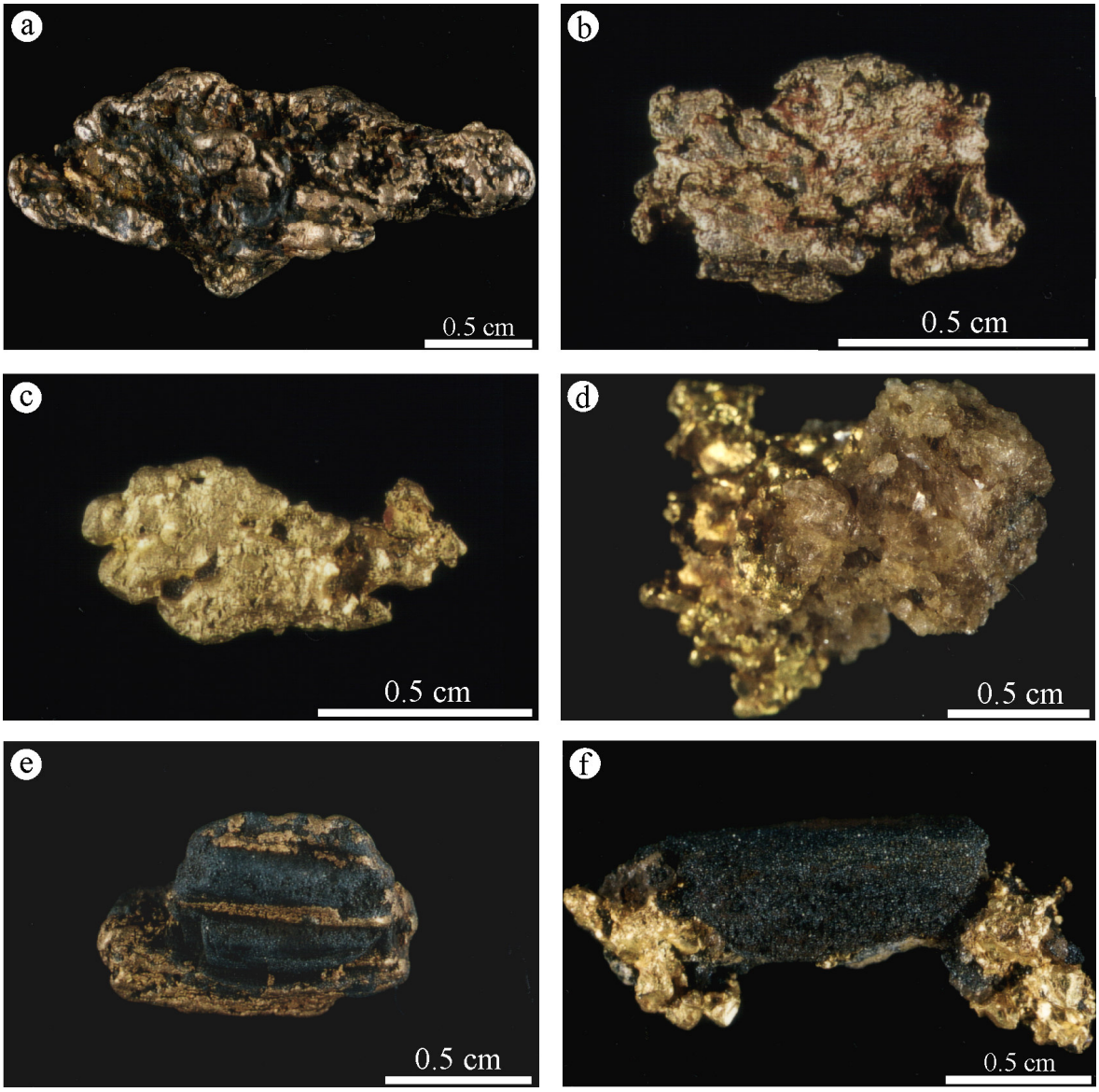

Fig. 11: Photographs of nuggets and aggregates of gold, recovered from a Knelson concentrator at the Gongo Soco iron ore plant. (a) Typical nugget of *ouro preto*. (b) Nugget of gold with a brownish tint and darker spots. (c) Nugget of gold of a whitish hue. (d) Gold attached to quartz. (e) Gold, with a brownish tint, cross-cuts the S_1 foliation defined by fine-grained hematite. (f) Gold grown over hematite ore.

Ore microscopy and mineral chemistry

The ore microscopy and electron-microprobe study presented here is based chiefly on nuggets of gold and aggregates of coarse-grained gold (>0.1 cm) and hematite. Microscopic investigation indicates that gold occurs as: (1) open-space infill in fragments of hematite ore (Fig. 12a); (2) intergrowth of fine-grained gold (<100 µm) with Cr-bearing specular hematite (Fig. 12b); (3) massive nugget with inclusions of Pd–Sb–As minerals (Fig. 12c); (4) brecciated nugget cemented by iron and manganese oxide minerals (Fig. 12d); (5) infill in, and dissemination over, Pd–O material (Fig. 12e); (6) fine-grained crystals of yellow colour associated with Pd–O material (Fig. 12f). The last two are observed on the surface of gold nuggets. Laths of specular hematite invariably accompany gold.

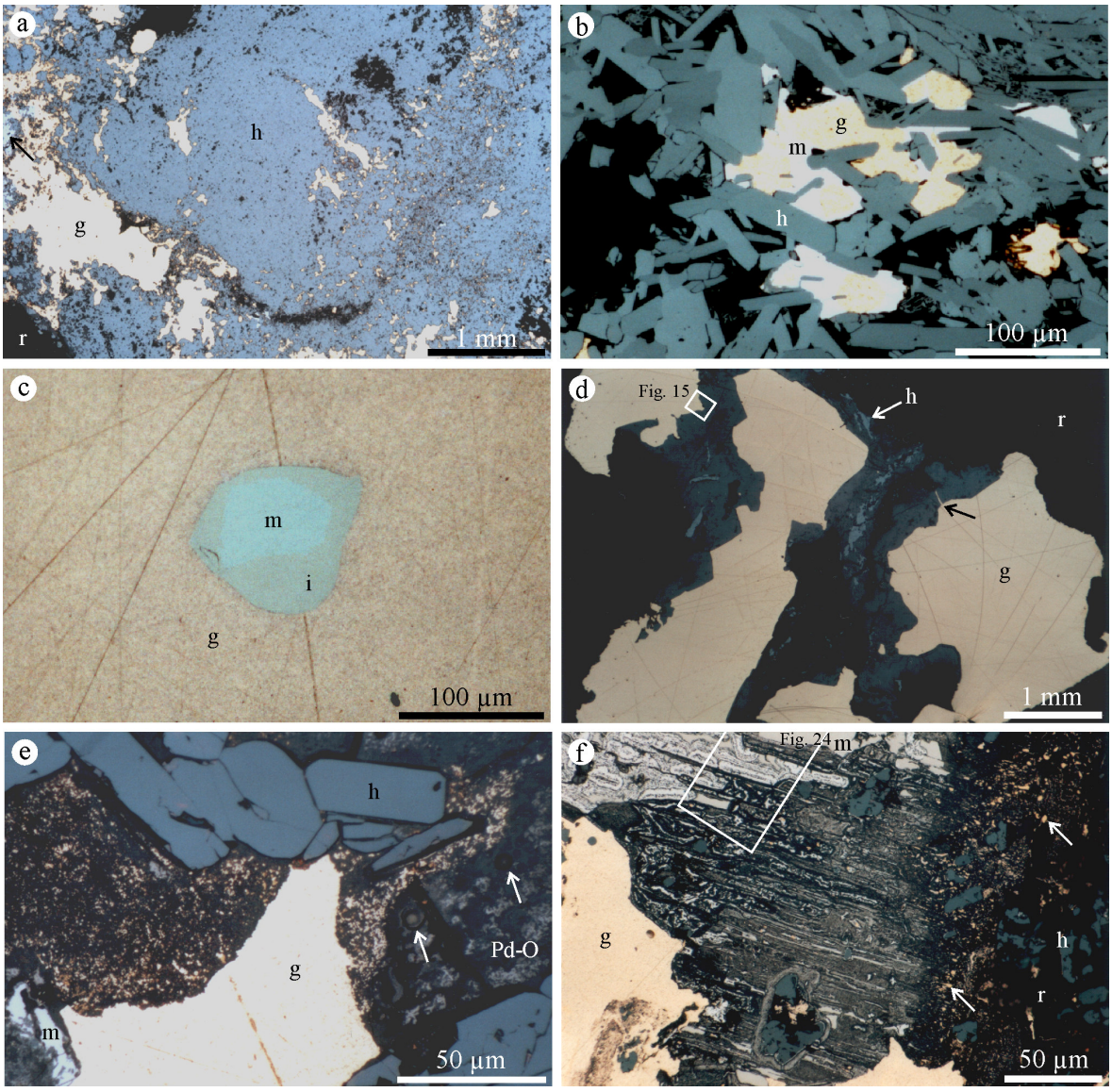

Fig. 12: For captions vide next page.

Fig 12: Photomicrographs of nuggets of gold and gold-bearing aggregates. Abbreviations: g, gold; h, hematite; i, isomertieite; m, mertieite-II; r, resin. (a) Cross-section of the aggregate of Figure 11e, where gold cross-cuts, and infills interstices in, fragmented hematite ore. Black arrow denotes mertieite-II. Reflected light, air, sample Au-4. (b) Intergrowth of gold, mertieite-II and Cr-bearing specular hematite as open-space infill in fragment of hematite ore. Reflected light, oil immersion, sample Au-18. (c) Zoned crystal with a mertieite-II core and an isomertieite mantle included in gold nugget. Reflected light, oil immersion, sample Au-12. (d) Fragmented nugget of gold cemented by a Mn–Ba oxide mineral in which coarse-grained crystals (up to about 500 µm in length, white arrow) of specular hematite occur. The cement (dark grey), into which gold protrudes (black arrow), is cut by a Mn–Fe–Ba–O matrix with fine-grained (about 10 µm in length), subhedral crystals of hematite (centre, dark areas). Reflected light, air, sample Au-15. (e) Gold penetrates into Pd–O material with relic of mertieite-II. The Pd–O material is located on the surface of a gold nugget. White arrows indicate curvilinear cracks formed after electron-microprobe analyses. Note that an alteration front emanates from the gold, impregnating the Pd–O material with fine-grained, Ag-bearing gold. Reflected light, oil immersion, sample Au-22. (f) Surface of a gold nugget where mertieite-II decays to Pd–O material (light grey), from which colloform native palladium (bright white) emerges. The linear fabric and the colloform banding resemble the birds eye texture of pyrrhotite alteration to pyrite–marcasite (RAMDOHR 1969). Yellow, fine-grained gold (white arrows) preferentially occurs at the most external part. Reflected light, oil immersion, sample Au-8.

Gold composition

As suggested by its different hues (HUSSAK 1904; Fig. 11 herein), gold composition is variable. Just a glimpse of the electron-microprobe data presented in Tables 2 and 3 confirms that individual nuggets of gold have diverse composition in terms of palladium and silver. Such compositional inhomogeneity is illustrated in Figure 13.

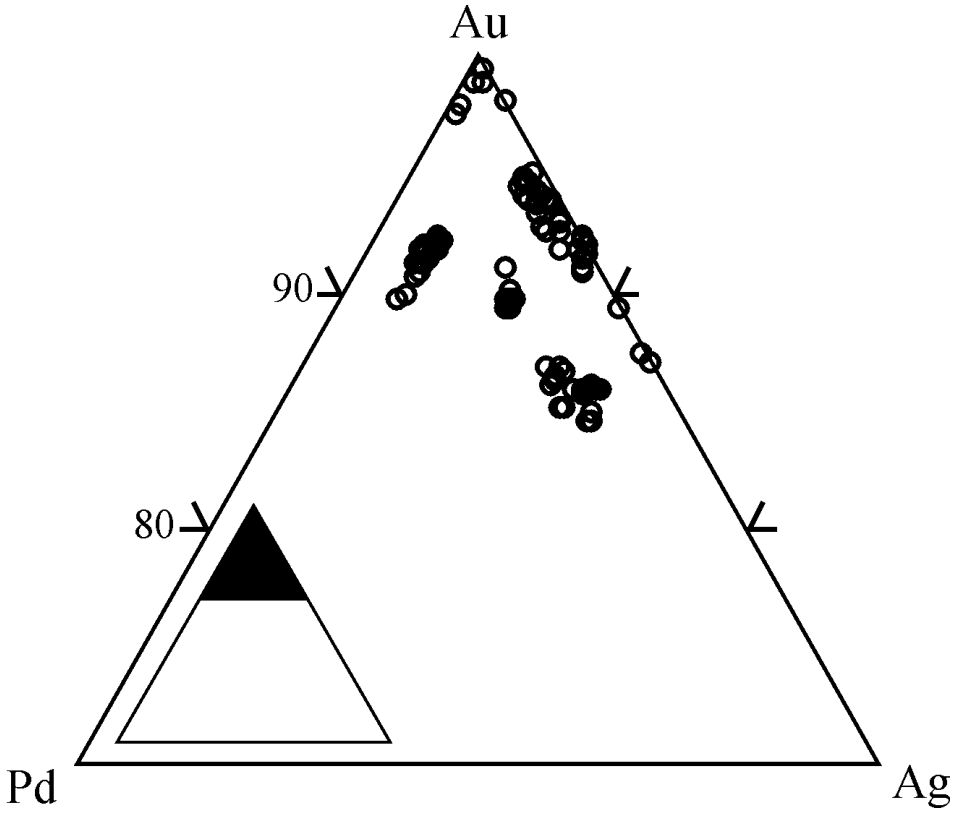

Fig. 13: Composition of nuggets and aggregates of gold from Tables 2 and 3 (in wt %).

Table 2: Electron-microprobe analyses of gold

Sample *Fig.*	(wt%)	Au	Pd	Ag	Hg	Cu	Fe	Total
Au-4	00A 1	92.72	0.85	5.22	0.33	1.19	<0.06	100.31
aggregate	00A 2	93.31	0.84	5.18	0.30	1.19	<0.06	100.82
11e, 12a	0A 3*	98.31	0.65	0.43	<0.3	<0.08	<0.06	99.39
	1A 1	92.64	0.84	5.11	0.39	1.16	0.58	100.72
	1A 2	92.73	0.67	4.89	<0.3	1.21	0.42	99.92
	2A 1	92.18	0.63	5.15	0.33	1.13	0.19	99.61
	4A 1	93.20	0.65	4.92	<0.3	1.12	0.38	100.27
Au-5	1	85.09	3.53	9.32	0.83	0.98	<0.06	99.75
nugget	2	84.95	4.19	9.49	0.97	1.02	<0.06	100.62
	3	85.90	3.54	9.71	0.65	0.99	<0.06	100.79
	4	85.42	3.89	8.93	0.95	0.95	<0.06	100.14
	5	85.08	3.92	9.48	1.02	1.02	<0.06	100.52
	6	85.19	3.90	9.54	0.97	1.04	<0.06	100.64
	7	84.71	4.16	9.38	0.98	0.97	<0.06	100.20
	8	85.70	3.84	9.53	0.78	1.00	<0.06	100.85
Au-7	7A-10	87.81	5.31	2.24	1.50	2.82	0.00	99.68
nugget	5A-1	89.59	5.09	2.46	1.00	2.67	0.07	100.88
	5A-2	89.63	5.23	2.35	0.88	2.51	0.00	100.60
	5A-3	89.06	5.11	2.25	0.99	2.72	0.12	100.25
	5A-10	89.12	5.15	2.26	1.08	2.66	0.25	100.52
	5A-13	88.81	5.37	2.24	0.81	2.64	0.00	99.87
	5A-14	89.08	5.09	2.45	0.65	2.57	0.51	100.35
	5A-15	89.88	5.14	2.47	0.73	2.54	0.00	100.76
	5A-16	87.67	5.47	2.29	1.89	2.75	0.00	100.07
	5A-17	88.03	5.35	2.36	1.68	2.81	0.00	100.23
	5A-18	89.56	5.18	2.24	0.99	2.58	0.00	100.55
	5A-19	88.78	5.18	2.43	1.02	2.51	0.34	100.26
Au-7	8A 1	87.91	6.20	2.10	1.86	2.33	0.35	100.75
veinlet	8A 2	89.52	5.13	2.41	0.63	2.47	0.56	100.72
17a	8A 4	88.16	6.41	1.94	1.32	2.34	0.57	100.74
	8A 5	82.75	7.49	1.96	5.53	1.96	0.54	100.23
	8A 6	87.26	6.34	2.29	0.93	2.18	0.19	99.19
	8A 7	86.60	6.67	2.10	2.23	2.38	0.51	100.49
	8A 8	89.11	5.47	2.32	0.97	2.45	0.19	100.51
	8A 9	87.85	6.17	2.17	1.33	2.32	0.35	100.19
	8A 10	87.34	5.80	2.28	2.58	2.18	0.38	100.56
	8A 11	88.14	6.22	2.25	1.42	2.30	0.19	100.52
	8A 12	82.82	7.10	2.13	6.03	1.81	0.36	100.25
Au-11	27A 1	94.92	0.46	4.32	<0.3	<0.08	<0.06	99.70
nugget	27A 2	95.21	1.03	4.20	0.48	0.22	<0.06	101.14
11c, 22	27A 3	94.93	0.83	4.23	0.35	<0.08	<0.06	100.34
	27A 4	94.94	0.98	4.27	0.32	0.22	<0.06	100.73
	27A 5	95.21	0.94	4.24	0.47	0.23	<0.06	101.09
	27A 6	94.72	0.84	4.34	0.33	0.13	<0.06	100.36
	27A 7	94.69	0.98	4.18	0.49	0.19	<0.06	100.53
	28A 1	94.99	0.90	4.16	0.37	0.20	<0.06	100.62

Table 2 (cont.): Electron-microprobe analyses of gold

Sample *Fig.*	(wt%)	Au	Pd	Ag	Hg	Cu	Fe	Total
Au-12	7A 3	88.69	6.03	2.10	1.00	2.74	<0.06	100.56
nugget	7A 4	88.86	6.03	1.90	1.09	2.72	<0.06	100.60
12c	8A 2	89.22	6.02	2.10	0.98	2.55	<0.06	100.87
	10A 1	89.41	5.69	1.93	0.85	2.32	<0.06	100.20
	10A 3	88.91	5.85	2.01	1.14	2.67	<0.06	100.58
Au-15	1[c]	92.12	1.15	5.36	0.58	0.83	<0.06	100.04
nugget	2[m]	90.16	0.36	8.00	0.49	0.50	<0.06	99.51
12d, 15	3[m]	88.60	0.18	10.33	0.50	0.37	<0.06	99.98
	4[m]	89.67	0.67	8.19	0.95	0.52	<0.06	100.00
	5[m]	89.50	0.62	8.12	0.75	0.54	<0.06	99.53
	6[c]	92.34	1.15	5.43	0.53	0.92	<0.06	100.37
	7[c]	92.89	1.21	4.53	0.45	0.98	<0.06	100.06
	8[p]	90.26	1.06	6.83	0.78	0.61	<0.06	99.54
	9[c]	92.93	1.24	4.14	<0.3	1.18	<0.06	99.49
	10[c]	91.63	1.23	5.94	0.62	0.88	<0.06	100.30
	11[c]	91.64	1.28	5.90	0.70	0.82	<0.06	100.34
	12[m]	92.06	0.63	6.67	0.49	0.71	<0.06	100.56
	14[m]	87.33	0.34	12.15	0.53	0.38	<0.06	100.73
	15[c]	91.66	1.21	6.02	0.67	0.75	<0.06	100.31
	16[m]	86.13	0.12	12.65	0.40	0.28	<0.06	99.58
	17[m]	91.87	0.51	6.31	0.33	0.75	<0.06	99.77
	18[c]	92.54	1.20	4.83	0.36	1.15	<0.06	100.08
Au-18	18A 2[†]	92.70	0.45	6.35	<0.3	0.08	1.68	101.26
aggregate	15A 1	93.90	0.47	5.57	<0.3	<0.08	<0.06	99.94
12b	15A 2[†]	93.16	0.35	5.63	<0.3	<0.08	0.99	100.13
	20A 3	94.41	0.36	5.76	<0.3	0.11	0.46	101.10
	20A 5	94.29	0.51	5.69	<0.3	0.10	0.10	100.69
Au-22	14A 1	92.61	<0.04	7.91	<0.3	<0.08	<0.06	100.52
Nugget	14A 2*	100.03	<0.04	0.43	<0.3	<0.08	<0.06	100.46
12e, 21	30A 3	91.92	0.05	7.76	<0.3	<0.08	<0.06	99.73
	30A 4[‡]	99.89	0.31	0.78	<0.3	<0.08	<0.06	100.98
	13A 4	92.53	0.06	7.58	<0.3	0.09	<0.06	100.26
	13A 12	93.00	0.17	7.69	<0.3	<0.08	<0.06	100.86
	13A 13[‡]	99.10	<0.04	1.88	<0.3	<0.08	<0.06	100.98
	15A 1	92.50	0.21	8.15	<0.3	0.08	<0.06	100.94
	22c 12	93.27	0.34	7.87	<0.3	<0.08	<0.06	101.48
Au-25	1	87.30	3.98	6.27	0.96	1.96	<0.06	100.47
Nugget	2	87.12	3.93	6.09	1.01	1.97	<0.06	100.12
11a, 20b	3	86.64	3.83	6.16	1.05	1.92	0.12	99.72
	4	88.62	3.31	5.26	0.68	1.74	0.09	99.70
	5	87.60	3.78	6.26	0.97	1.97	<0.06	100.58
	6	87.30	3.61	5.99	0.97	1.92	<0.06	99.79
	7	87.57	3.67	6.25	0.71	1.97	<0.06	100.17
	8	86.96	4.09	6.18	1.18	1.98	<0.06	100.39
	9	86.77	3.86	6.18	0.93	1.96	<0.06	99.70
	10	86.44	4.02	6.23	1.03	1.93	0.08	99.73
	11	87.00	3.97	5.88	1.19	1.95	<0.06	99.99

[c] core; [m] mantle; [p] slender protrusion; * veinlet of yellow gold, a few µm wide; [†] euhedral crystal of gold (~10 µm) included in mertieite-II; [‡] obtuse-angled triangular patch of yellow gold (~150 µm).

Table 3: Electron-microprobe analyses of gold of empirical formula $(Au,Hg)_3(Ag,Pd,Cu)$*

Sample		Weight per cent							Atomic proportions							
Fig.		Au	Pd	Ag	Hg	Cu	Fe	Total	Au	Hg	ΣAu	Ag	Pd	Cu	Fe	ΣAg
Au-8	1	84.55	2.67	10.84	1.05	1.24	0.14	100.49	2.950	0.036	2.986	0.691	0.172	0.134	0.017	1.014
nugget	2	83.75	2.78	10.86	1.07	1.31	<0.06	99.77	2.943	0.037	2.980	0.697	0.181	0.143	—	1.020
12f	3	84.39	2.55	11.19	0.82	1.19	<0.06	100.14	2.960	0.028	2.988	0.717	0.166	0.129	—	1.012
	4	83.68	2.83	10.84	1.01	1.28	<0.06	99.64	2.945	0.035	2.980	0.697	0.184	0.140	—	1.020
	5	83.85	2.84	10.77	0.75	1.27	<0.06	99.48	2.956	0.026	2.982	0.693	0.185	0.139	—	1.018
	6	84.22	2.93	10.88	1.10	1.22	<0.06	100.35	2.945	0.038	2.983	0.695	0.190	0.132	—	1.017
	7	84.35	2.69	11.03	0.91	1.24	0.13	100.35	2.942	0.031	2.974	0.703	0.174	0.134	0.016	1.026
Au-9	19	84.07	3.15	10.49	0.75	1.35	<0.06	99.81	2.950	0.026	2.976	0.672	0.205	0.147	—	1.024
nugget	22	84.70	3.00	10.85	0.60	1.34	<0.06	100.49	2.951	0.021	2.972	0.690	0.193	0.145	—	1.028
11b	23	83.27	4.42	10.13	1.07	1.38	<0.06	100.27	2.889	0.036	2.926	0.642	0.284	0.148	—	1.074
	24	83.49	4.17	10.27	1.21	1.37	<0.06	100.51	2.894	0.041	2.935	0.650	0.268	0.147	—	1.065
	25	83.78	4.39	10.19	1.20	1.36	<0.06	100.92	2.891	0.041	2.932	0.642	0.280	0.145	—	1.068
	26	83.96	3.55	10.25	0.87	1.45	<0.06	100.08	2.931	0.030	2.960	0.653	0.229	0.157	—	1.040
	28	84.08	3.51	10.31	0.87	1.36	<0.06	100.13	2.938	0.030	2.968	0.658	0.227	0.147	—	1.032
	29	83.67	3.14	10.68	0.67	1.36	<0.06	99.52	2.939	0.023	2.963	0.685	0.204	0.148	—	1.037
Au-16	1	98.11	2.03	0.44	<0.3	<0.08	<0.06	100.58	0.956	—		0.008	0.037	—	—	
nugget	2	83.94	3.59	11.72	0.36	0.67	<0.06	100.28	2.935	0.012	2.947	0.748	0.232	0.073	—	1.053
14, 20a	3	98.21	1.69	0.29	<0.3	<0.08	<0.06	100.19	0.964	—		0.005	0.031	—	—	
	4	83.74	3.61	11.53	0.54	0.67	<0.06	100.09	2.936	0.019	2.955	0.738	0.234	0.073	—	1.045
	5	84.20	3.46	11.52	0.50	0.65	<0.06	100.33	2.951	0.017	2.968	0.737	0.224	0.071	—	1.032

* Atomic proportions on the basis of 4 atoms, excepting microanalyses 1 and 3 of sample Au-16 (1 atom per formula unit).

Generally, massive nuggets of gold are individually homogeneous in composition, i.e. not compositionally zoned. They have, however, variable compositions. At least three of the nuggets investigated show similar compositions that suggest a specific alloy of empirical formula $(Au,Hg)_3(Ag,Pd,Cu)$ (Table 3). Locally, nugget gold is cut by veinlets (up to about 5 µm wide) of yellow gold at its margins. The yellow gold manifests itself as irregular veinlets, obtuse-angled triangular patches and, as portrayed in Figure 14, vermiform segments. Compared to the enclosing gold, the vermiform segments are enriched in gold, but impoverished in silver and palladium (Table 3).

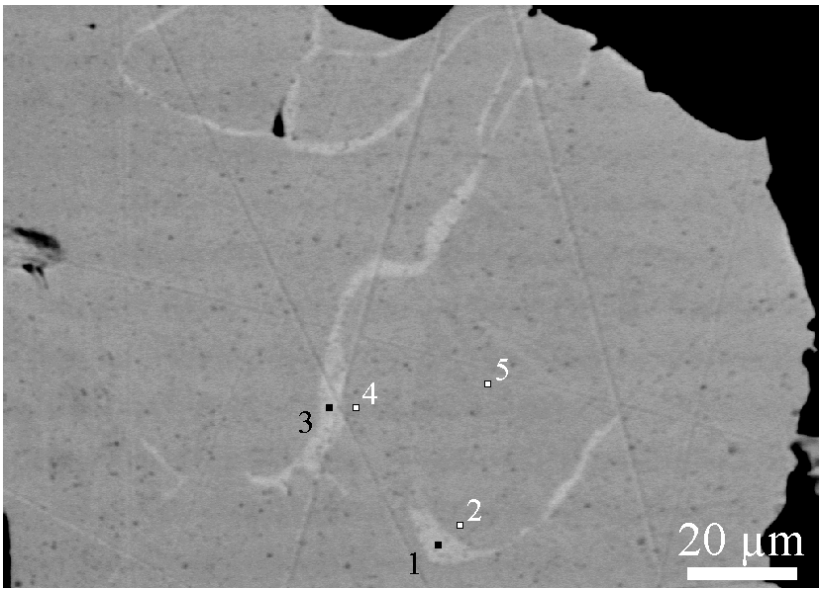

Fig: 14: Backscattered electron image (BSE) of massive nugget of gold. The vermiform segments (white) are enriched in gold, but depleted in silver and palladium, compared to the enclosing (nugget) gold. Black: resin. Numbers refer to microanalyses in Table 3, sample Au-16.

Only one case of compositional zoning in nuggets of gold has been recorded. It is in the fragmented nugget of gold of Figure 12d, in which a core-and-mantle pattern occurs locally at the contact with a coating of barium-bearing manganese oxide (Fig. 15a,b). Interspersed on the surface of gold are masses of a Pd–O phase, sometimes associated with what appears to be a relic of an As-bearing Pd–Sb phase (Fig. 15a). The contact between core and mantle is occasionally marked by darker segments (Fig. 15c), which consist of a Pd–Cu–O phase (Fig. 15d, e, f, g).The mantle is depleted in gold, but enriched in silver relative to the core (Figs. 15b, 16).

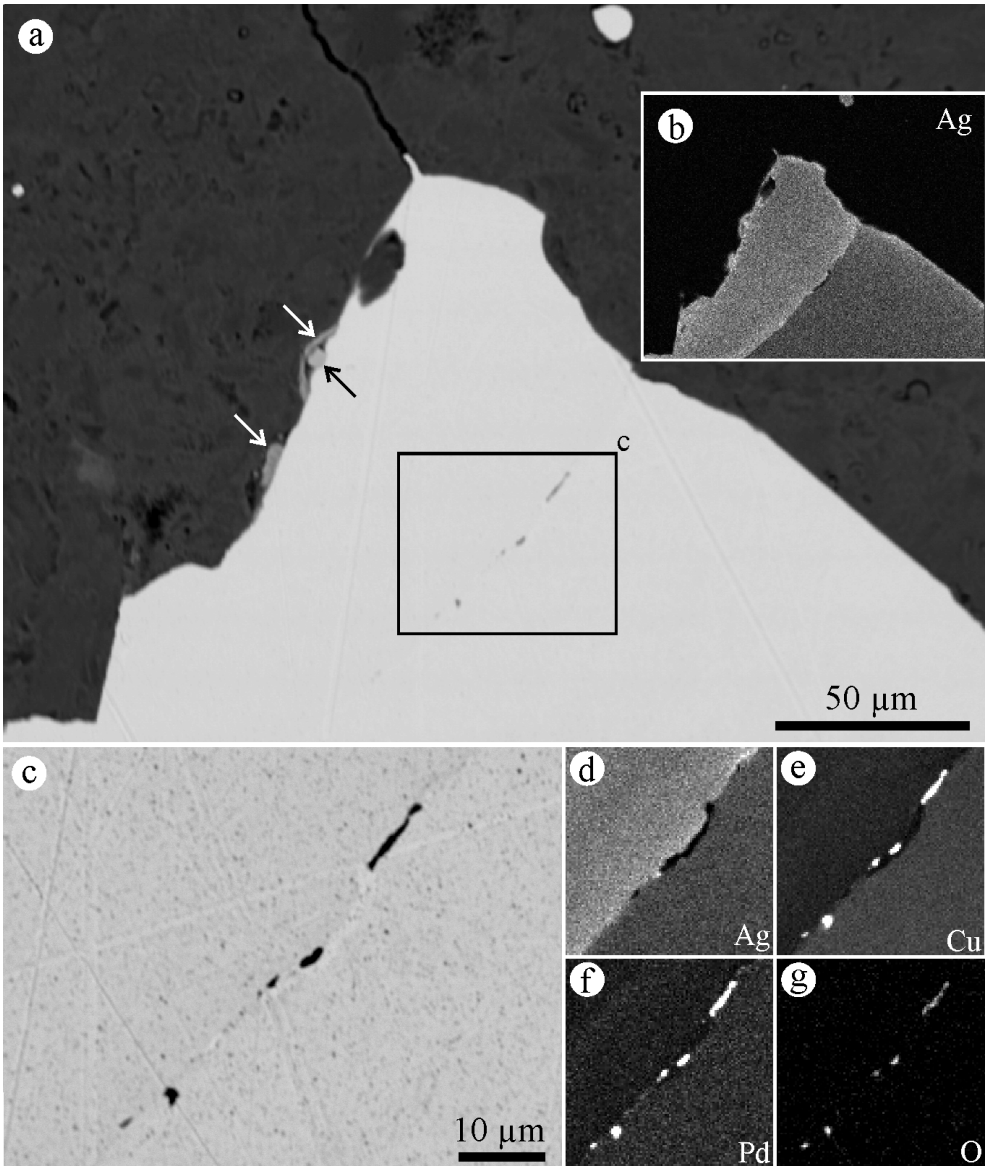

Fig. 15: (a) BSE image of the area squared in Figure 12d at the contact between gold (white) and an envelope of barium-bearing manganese oxide (dark grey). Note that gold protrudes into the Mn–Ba–O phase. Masses of Pd–O phase (white arrows) occur on the surface of gold, as isolated patch and as coating on an As-bearing Pd–Sb phase (black arrow). (b) X-ray element distribution of Ag$L\alpha$. (c) BSE image of the area squared in (a), with X-ray element distributions of (d) Ag$L\alpha$, (e) Cu$K\alpha$, (f) Pd$L\alpha$ and (g) O$K\alpha$.

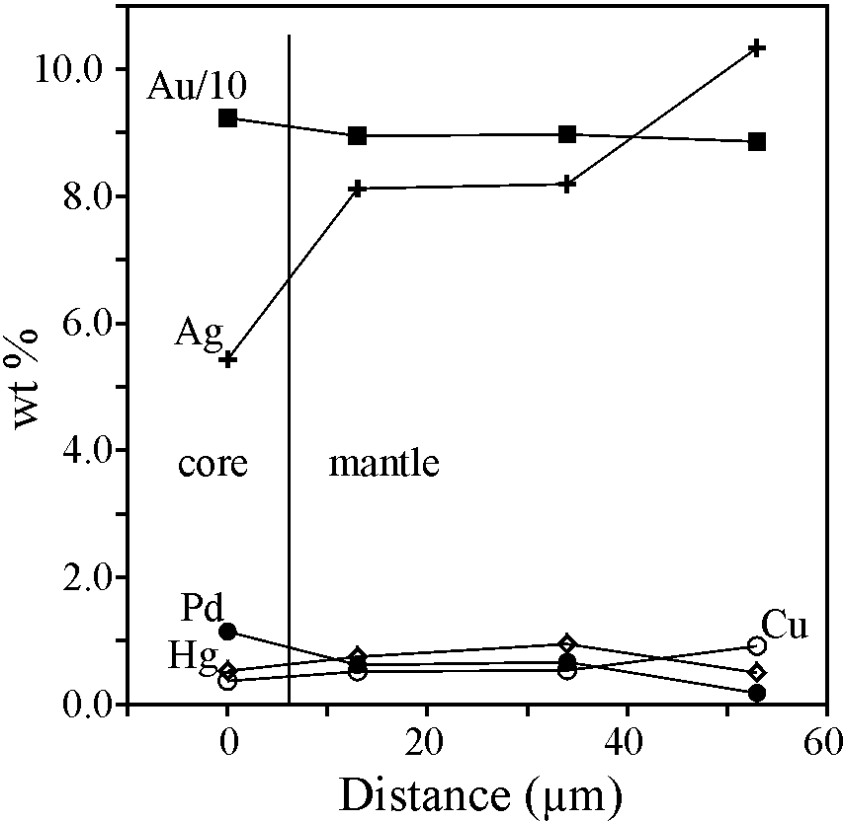

Fig. 16: Composition of gold across the contact between the core and mantle shown in Figure 15 (microanalyses 3, 4, 5 and 6 of Table 2).

Sample Au-7 (Table 2) is a fragmented nugget of gold. Its fragmented structure results from microfractures healed by laths of specular hematite, kaolinite and fine-grained crystals of gold (<100 µm) (Fig. 17a). The gold crystals, which are referred to as veinlet gold, have a more variable composition in terms of palladium and mercury than the coarser, host fragments of gold, i.e. nugget gold (Fig. 17b). Palladium is positively correlated with mercury (Fig. 17b). The finding that mercury is alloyed with gold at Gongo Soco confirms previous observations (GARDNER 1827).

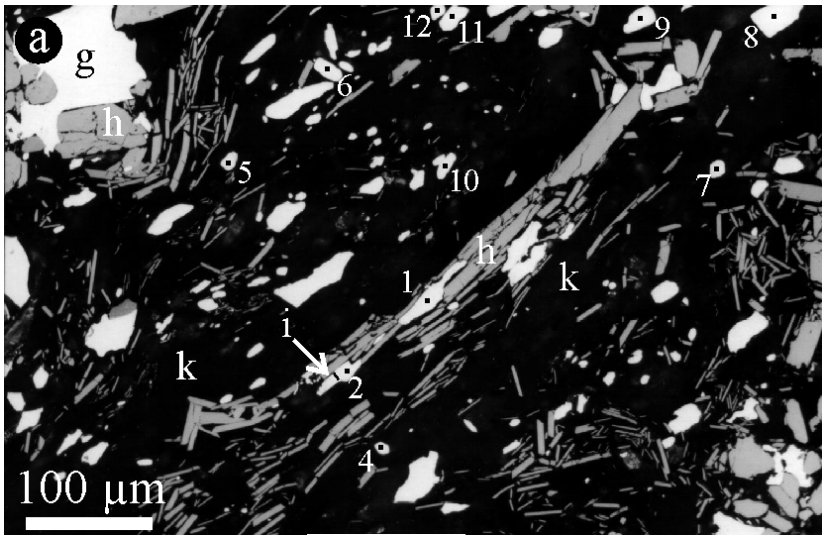

Fig: 17: For captions vide next page.

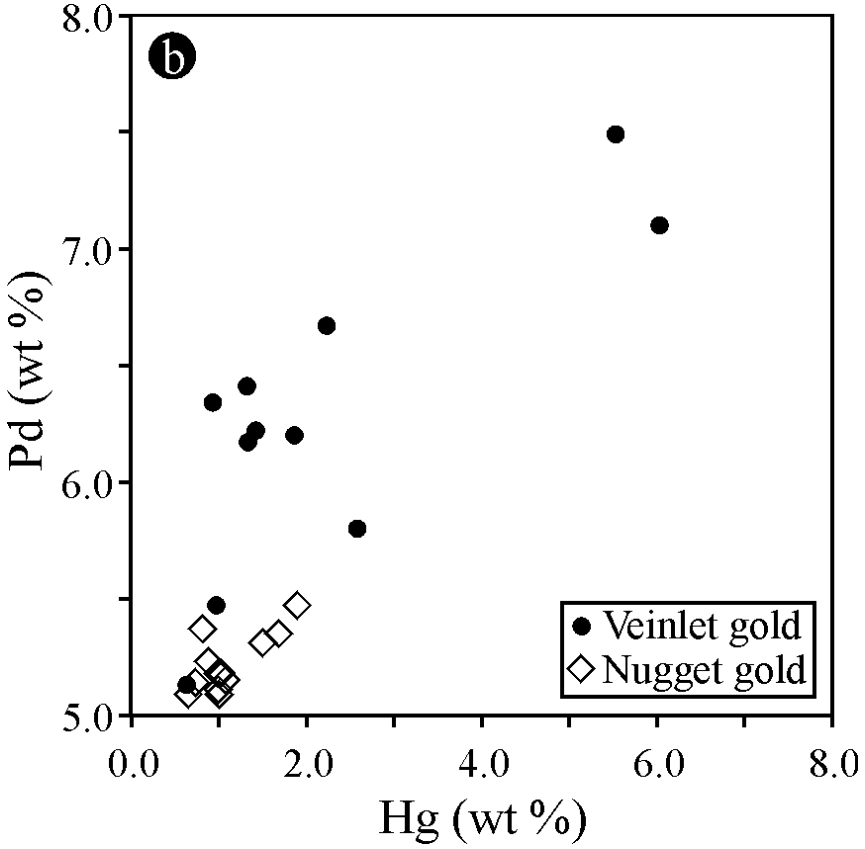

Fig: 17: (a) Reflected-light photomicrograph (oil immersion) of a microfracture in a nugget of gold (sample Au-7) healed by kaolinite, k, specular hematite, h, fine-grained crystals of gold, g (white) and isomertieite, i (white arrow). Numbers refer to microanalyses in Table 2. (b) Variation diagram for palladium and mercury in crystals of veinlet gold, as numbered in a, and the host gold (nugget gold, Table 2).

Minerals included in nuggets of gold

A number of minerals occur as inclusions in nuggets of gold. The minerals are specular hematite and arsenide-antimonides, as well as selenides, of palladium.

Specular hematite is commonly included in nuggets of gold as laths, ranging from about 10 µm to as long as 1 mm. It is also found intergrown with gold as open-space infill (Fig. 12b). The specular hematite included in nuggets is chromiferous, with contents varying from 0.1 to as high as 6 wt % Cr_2O_3 (Table 4). There is a conspicuous compositional difference between the specular hematite associated with (palladian) gold and that forming the S_1 foliation of soft hematite ore. The latter lacks chromium, but is higher in titanium (Fig. 18a, Table 4). Some crystals of hematite appear to have been segmented within the nuggets (Fig. 18b). Other crystals of hematite are mechanically twinned and occur as inclusion in, and in limonite-like coating on, nuggets of gold (Fig. 18c).

Table 4: Electron-microprobe analyses of hematite

	1	2	3	4	5	6	7	8	9	10
(wt %)										
SiO_2	<0.02	<0.02	<0.02	<0.02	<0.02	<0.02	<0.02	<0.02	0.14	<0.02
TiO_2	0.06	0.09	<0.02	<0.02	0.07	0.47	1.02	1.57	0.23	0.88
Cr_2O_3	0.12	1.45	4.35	6.41	2.09	<0.01	<0.01	<0.01	<0.01	0.12
Fe_2O_3	98.69	97.56	94.97	92.00	96.36	99.71	99.17	98.81	99.12	99.14
Au_2O_3	1.12	0.83	<0.3	<0.3	1.11	<0.3	<0.3	<0.3	<0.3	<0.3
MnO	<0.01	<0.01	<0.01	<0.01	<0.01	<0.01	<0.01	0.06	0.06	<0.01
Total	99.99	99.93	99.32	98.41	99.63	100.18	100.19	100.44	99.55	100.14

The mineral was analysed for titanium and chromium under 20 kV and 40 nA, using the *K*α emission line, and TiO_2 and pure metal (Cr) as standards.
Columns 1-5: specular hematite included in (palladian) gold
Columns 6-10: foliation-forming, specular hematite

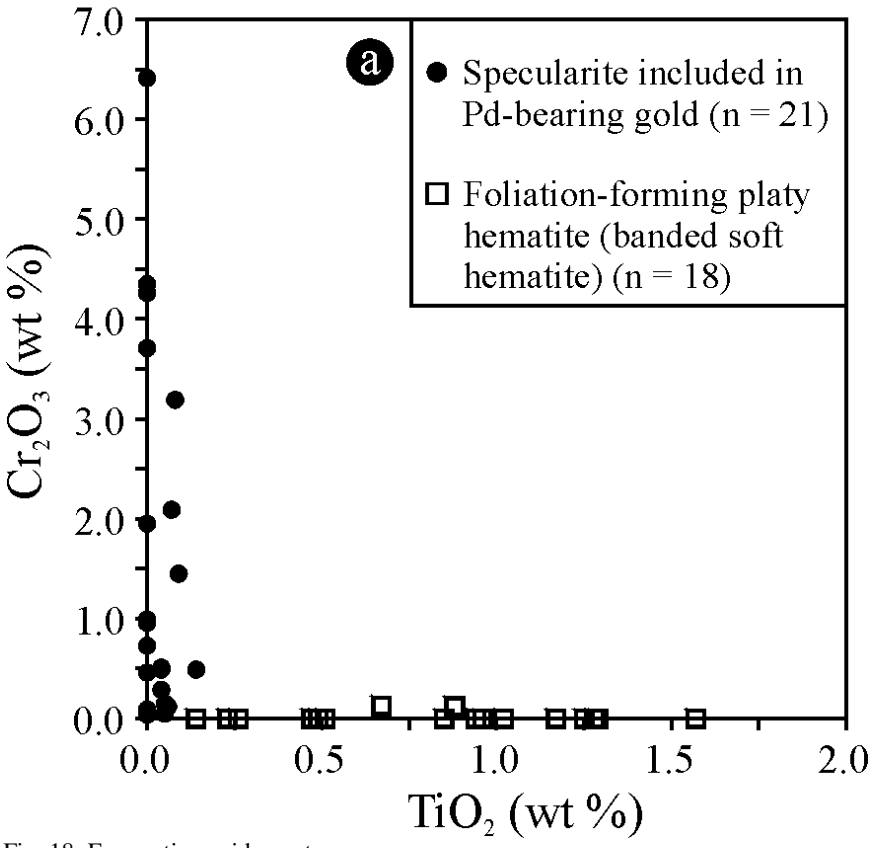

Fig. 18: For captions vide next page.

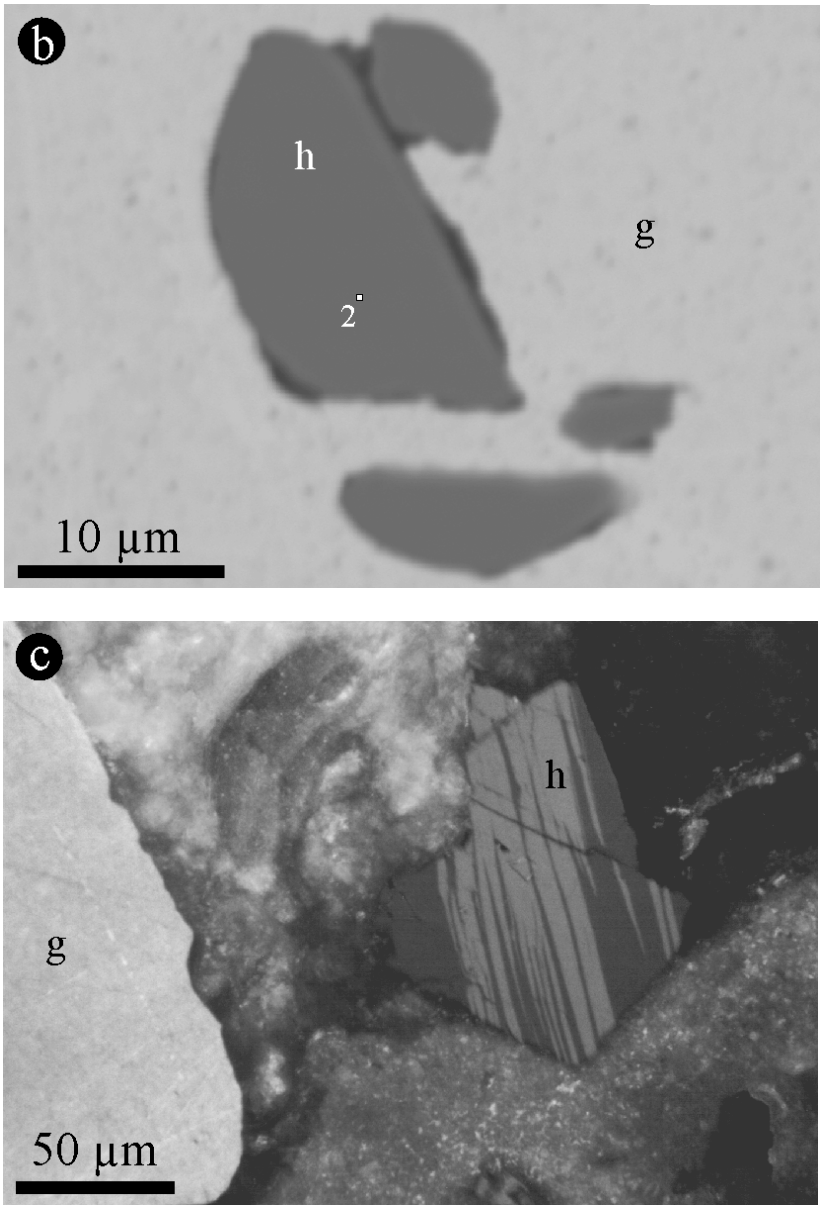

Fig. 18: (a) Compositional difference in terms of Cr_2O_3 and TiO_2 between specular hematite included in gold and S_1 foliation-forming, specular hematite of soft hematite ore. See Table 4 for representative microanalyses. (b) BSE image of a segmented crystal of Cr-bearing hematite included in gold nugget (sample Au-16). Number corresponds to microanalysis in Table 4. (c) Reflected-light photomicrograph (oil immersion, inclined nicols) of mechanically twinned, Cr-bearing hematite, h, in limonite-like coating on nugget of gold, g (sample Au-5).

Arsenide-antimonides of palladium occur as inclusions in, and on the surface of, nuggets of gold, and also as open-space infill (Fig. 12b). The minerals have compositions close to those of mertieite-II, $Pd_8(Sb,As)_3$, and isomertieite, $Pd_{11}(Sb,As)_4$ (Table 5), and have been described elsewhere (CABRAL et al. 2002c). The Pd–Sb–As minerals abound in nuggets of gold alloyed with more than 2 wt % Pd. There are inclusions of zoned crystals, with As-poor core and As-rich mantle (Fig. 12c). Where properly included in nuggets of gold (>2 wt % Pd), the Pd–Sb–As minerals tend to contain some platinum (CABRAL et al. 2002c, Table 5). Both mertieite-II and isomertieite are also situated on the surface of gold nuggets (Fig. 19a), where they are frequently fractured and mantled to varying degree by a Pd-oxygenated

coating (Figs. 19b, c). Microfracturing and brecciation of Pd–Sb–As inclusions in nuggets of gold are unexpected, but ubiquitously observed at Gongo Soco (Fig. 20a). Some breccia fragments are mantled by zones of colloform native palladium and Pd–O phase (Fig. 20b).

Table 5: Electron-microprobe analyses of arsenide-antimonides of palladium

	1	2	3	4	5	6	7	8	9	10
Dimensions	150x	50x	50x	Fig.	100x	Fig.	Fig.	80x	Fig.	10x
(µm)	200	130	400	12f	200	20b	20b	150	12b	30
Sample	Au-5	Au-5	Au-5	Au-8	Au-8	Au-25	Au-25	Au-16	Au-18	Au-4
Analysis no.	9	10	35	8	18	18	24	7	20A 6	4A 2
(wt %)										
Pd	72.41	72.99	72.29	71.70	71.94	73.46	73.83	74.40	72.07	71.26
Pt	<0.3	<0.3	<0.3	<0.3	<0.3	0.48	0.39	0.42	<0.3	<0.3
Au	<0.2	0.33	<0.2	<0.2	<0.2	0.48	0.46	<0.3	<0.3	0.35
Cu	<0.08	2.13	0.10	0.14	0.16	1.50	1.52	0.89	<0.08	0.42
Sb	23.97	15.22	23.51	23.77	23.68	14.88	14.95	15.19	24.69	24.96
As*	3.96	9.84	4.15	3.79	4.09	9.43	9.54	8.52	2.88	2.67
Sn	0.06	0.05	0.09	0.08	0.08	0.06	0.04	0.05	0.09	0.09
Total	100.40	100.56	100.14	99.48	99.95	100.29	100.73	99.47	99.73	99.75
apfu	11	15	11	11	11	15	15	15	11	11
Pd	8.042	10.521	8.034	8.034	8.011	10.704	10.701	10.990	8.104	8.012
Pt	—	—	—	—	—	0.038	0.031	0.034	—	—
Au	—	0.026	—	—	—	0.038	0.036	0.000	—	0.021
Cu	—	0.514	0.019	0.026	0.030	0.366	0.369	0.220	—	0.079
ΣPd	8.042	11.061	8.052	8.061	8.040	11.146	11.137	11.244	8.104	8.112
Sb	2.327	1.918	2.284	2.328	2.305	1.895	1.894	1.961	2.427	2.453
As	0.625	2.015	0.655	0.603	0.647	1.952	1.964	1.788	0.460	0.426
Sn	0.006	0.006	0.009	0.008	0.008	0.008	0.005	0.007	0.009	0.009
ΣSb	2.958	3.939	2.948	2.939	2.960	3.854	3.863	3.756	2.896	2.888

apfu: atoms per formula unit (11 atom for mertieite-II, 15 atoms for isomertieite).

* Crystals 1-7 were analysed for arsenic using the $L\alpha$ emission line and InAs as standard. Crystals 1, 2, 5 are situated on the surface of nuggets of gold (crystal 1 is partially mantled by 2); crystal 3 is on the wall of a goethite-filled vug within the nugget; crystal 8 is included in gold; crystal 10 is interstitial to specular hematite.

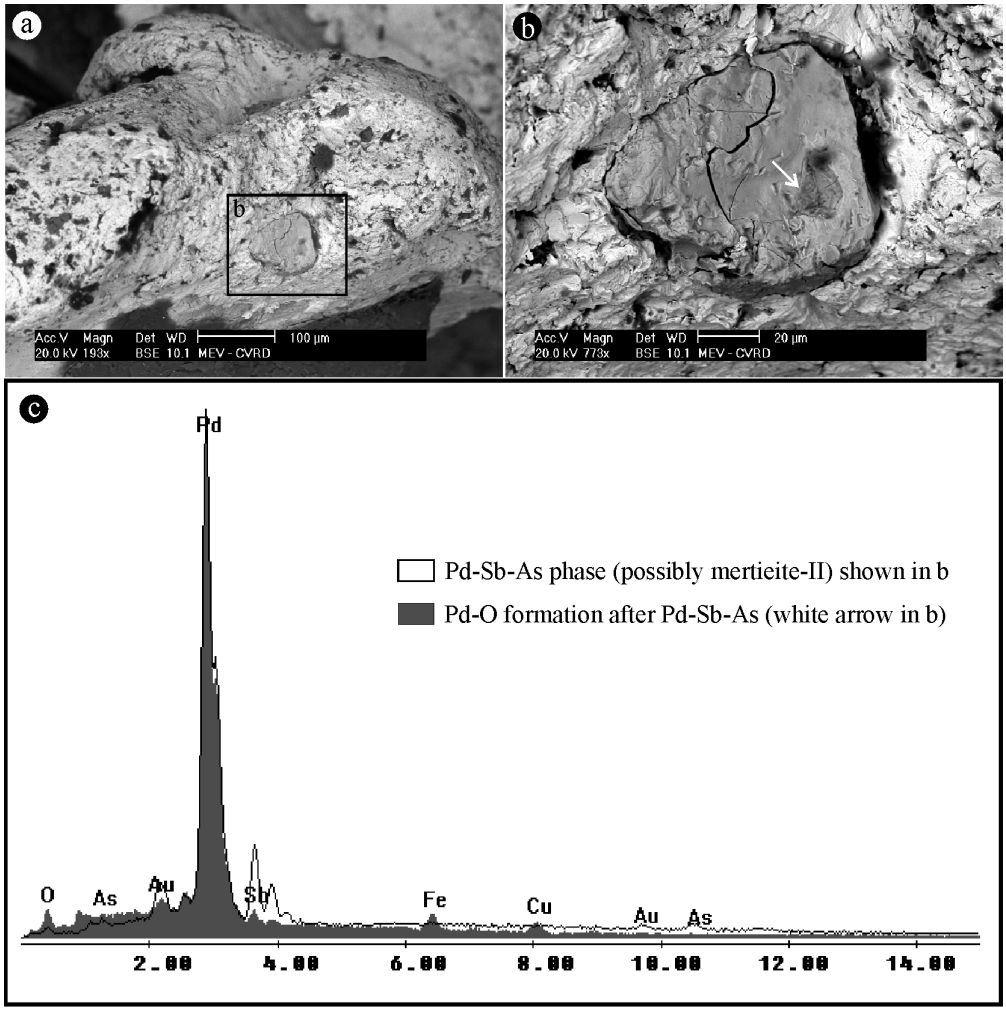

Fig. 19: (a) BSE image of a gold nugget, sample Au-6. (b) BSE image of the area squared in (a) to highlight that the Pd–Sb–As mineral is microfractured and has a Pd–O coating (white arrow). (c) Energy dispersive (ED) spectra of the Pd–Sb–As mineral and its Pd–O coating.

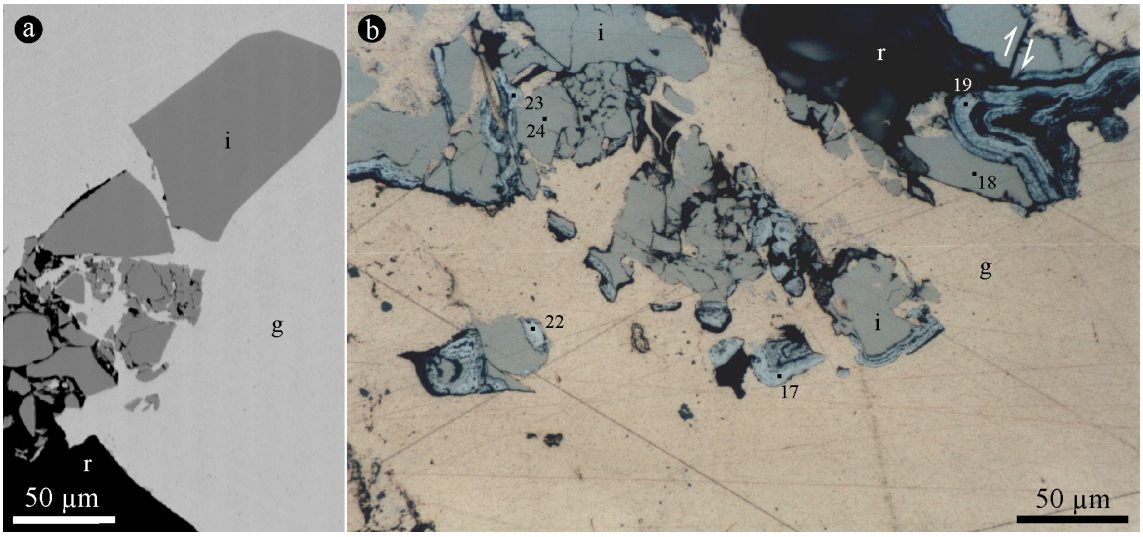

Fig. 20: (a) BSE image of a brecciated crystal of isomertieite, i, at the edge of a nugget of gold, g (sample Au-16). (b) Reflected-light photomicrograph, oil immersion, of brecciated isomertieite, i, included in nugget of gold, g (cross-section of sample Au-25 shown in Figure 11a). Arrows indicate relative displacement. Some fragments are corroded by zones of collofom native palladium (bright white) associated with Pd–O phase (dark grey).

Selenides of palladium have been observed as sub- to euhedral crystals (<100 µm in length) included in one nugget of gold. The nugget consists of palladium-poor, silver-bearing gold (Table 2, sample Au-22). Electron-microprobe analyses indicate mineral compositions analogous to chrisstanleyite, $Ag_2Pd_3Se_4$, and apparently unnamed Sb–Ag–Hg-bearing palladium selenides (Table 6). Chrisstanleyite is intimately associated with specular hematite (Fig. 21a) and occasionally forms composite crystals with naumannite and tiemannite (Fig. 21b). Crystals of Sb–Ag–Hg-bearing palladium selenide are segmented in a domino-like pattern (Fig. 21c).

Clausthalite, PbSe, is also an occasional inclusion in nuggets of gold, found as composite crystals with Cr-bearing specular hematite and, noticeably, as brecciated aggregates of Ca–Mg carbonate and chromiferous hematite (Figs. 22a, b).

Table 6: Electron-microprobe analyses of selenide minerals*

	1	2	3	4	5	6	7	8	9	10
	13A 7	14A 3	15A 2	15A 3	15A 4	13A 20	13A 20a	13A 20b	13A 20c	13A 20d
(wt %)										
Pd	54.45	38.81	<0.03	39.04	0.23	39.39	42.75	42.90	43.09	43.22
Hg	3.63	<0.3	<0.3	<0.3	68.55	15.41	5.37	1.91	3.34	2.77
Au	0.53	0.51	16.63	2.46	3.51	1.39	1.30	2.68	3.01	2.39
Ag	4.02	24.70	59.21	25.39	<0.2	2.93	6.38	7.20	6.89	7.01
Cu	1.43	<0.08	<0.08	<0.08	<0.08	<0.08	0.31	0.33	0.35	0.41
Sb	<0.03	<0.03	<0.03	<0.03	<0.03	5.83	8.58	9.23	8.98	9.06
Se	37.33	36.68	21.97	36.51	29.20	36.05	36.03	36.86	36.48	36.29
S	0.04	0.04	<0.03	0.05	<0.03	<0.03	0.03	0.04	0.03	0.05
Total	101.43	100.74	97.81	103.45	101.49	101.00	100.75	101.15	102.17	101.20
apfu	9	9	3	9	2	13	9	9	9	9
Pd	4.319	3.086	—	3.061	0.006	4.882	3.521	3.482	3.494	3.518
Hg	0.153	—	—	—	0.934	1.013	0.235	0.082	0.144	0.120
Au	0.023	0.022	0.278	0.104	0.049	0.093	0.058	0.117	0.132	0.105
Ag	0.315	1.938	1.806	1.964	—	0.358	0.518	0.576	0.551	0.563
Cu	0.190	—	—	—	—	—	0.043	0.045	0.048	0.056
Sb	—	—	—	—	—	0.632	0.618	0.655	0.636	0.644
Se	3.991	3.931	0.916	3.858	1.011	6.022	3.999	4.032	3.987	3.981
S	0.011	0.011	—	0.013	—	—	0.008	0.011	0.008	0.013

* Sample Au-22. Interference from the surrounding gold may account for some totals exceeding 100 wt %. Column: 1, empirical $(Pd,Ag,Cu,Hg)_5Se_4$; 2 and 4, chrisstanleyite, $Ag_2Pd_3Se_4$; 3, Au-bearing naumannite, Ag_2Se; 5, tiemannite, HgSe; 6, empirical $Pd_5(Hg,Sb,Ag)_2Se_6$; 7-10, empirical $(Pd,Sb,Ag,Hg)_5Se_4$.

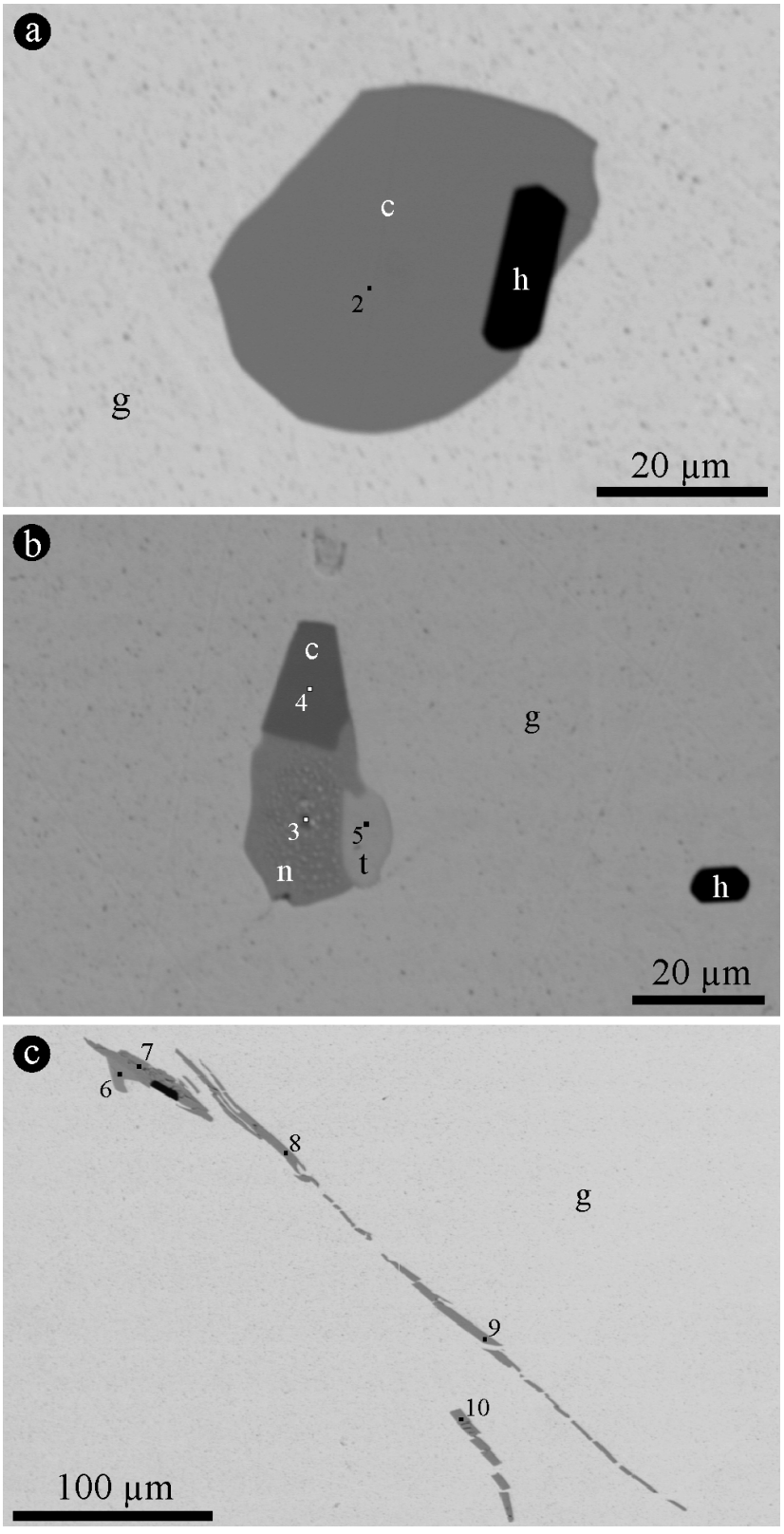

Fig. 21: BSE images of selenide minerals from sample Au-22. Numbers refer to microanalyses in Table 6 (columns 2–10). (a) Crystal of chrisstanleyite, c, with an inclusion of hematite, h, within gold, g. (b) Composite crystals of chrisstanleyite, naumannite, n, and tiemannite, t. (c) Segmented and relatively displaced crystals of Sb–Ag–Hg-bearing Pd selenide.

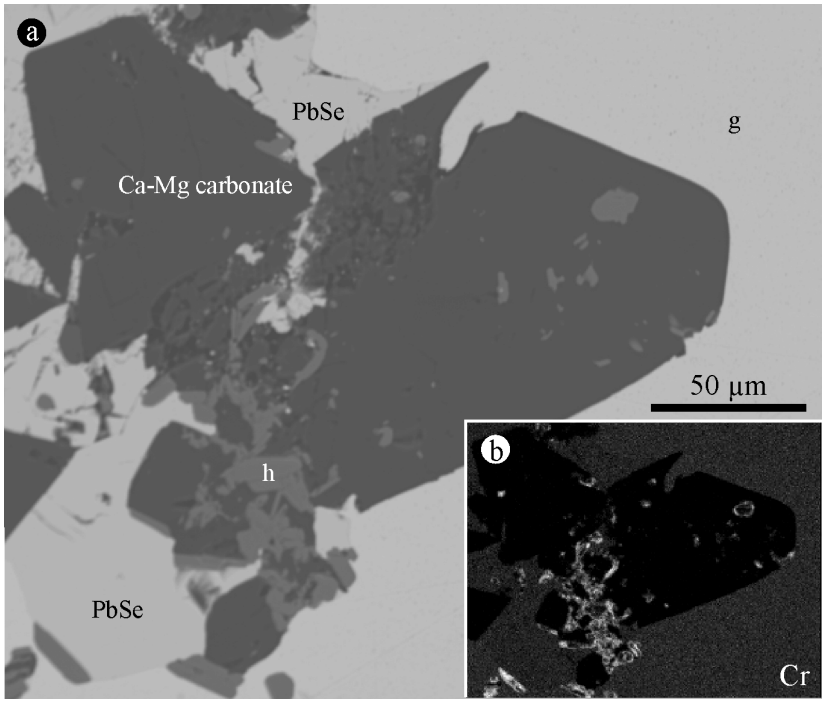

Fig. 22: (a) BSE image of a brecciated aggregate of clausthalite, PbSe, Ca–Mg carbonate and chromiferous hematite, h. (b) X-ray mapping for Cr*K*α (sample Au-11).

Pd–O compounds and native palladium

Pd–O compounds are located on the surface of gold grains (Figs. 23a, b), and thus contribute to the characteristic dark colour of gold grains from Gongo Soco. They occur as masses with relics of, and as halos on, arsenide-antimonide of palladium (Fig. 12e, 23c). Data on Pd–O compounds have recently been published (CABRAL et al. 2001, 2003; CABRAL & LEHMANN 2003), and only a few microprobe analyses are presented here to complement Figure 12e (Table 7). Low analytical totals and low oxygen contents characterise the Pd–O material of Figure 12e. Such a deficiency in oxygen is possibly due to undetected amounts of water, as evidenced by curvilinear fissures formed after microprobe analysis. It should be pointed out that the analytical conditions for oxygen were higher compared to those used by AUGÉ & LEGENDRE (1994) and CABRAL et al. (2001).

Table 7: Electron-microprobe analyses of Pd–O material of Figure 12e

	1	2	3	4
Pd (wt %)	76.05	73.22	76.82	74.75
Cu	11.79	11.49	12.03	12.63
Hg	<0.2	<0.2	0.29	<0.2
Fe	0.15	0.26	1.66	0.72
Mn	0.89	2.13	0.80	1.51
Au	2.92	2.33	1.96	1.84
As	0.09	0.23	<0.07	0.08
O	1.61	3.00	2.19	2.59
Total	93.50	92.66	95.75	94.12

The material was analysed for oxygen under 20 kV and 40 nA, using the *K*α emission line and Al_2O_3 as standard. The white arrows in Figure 12e indicate the locus of the first two microanalyses.

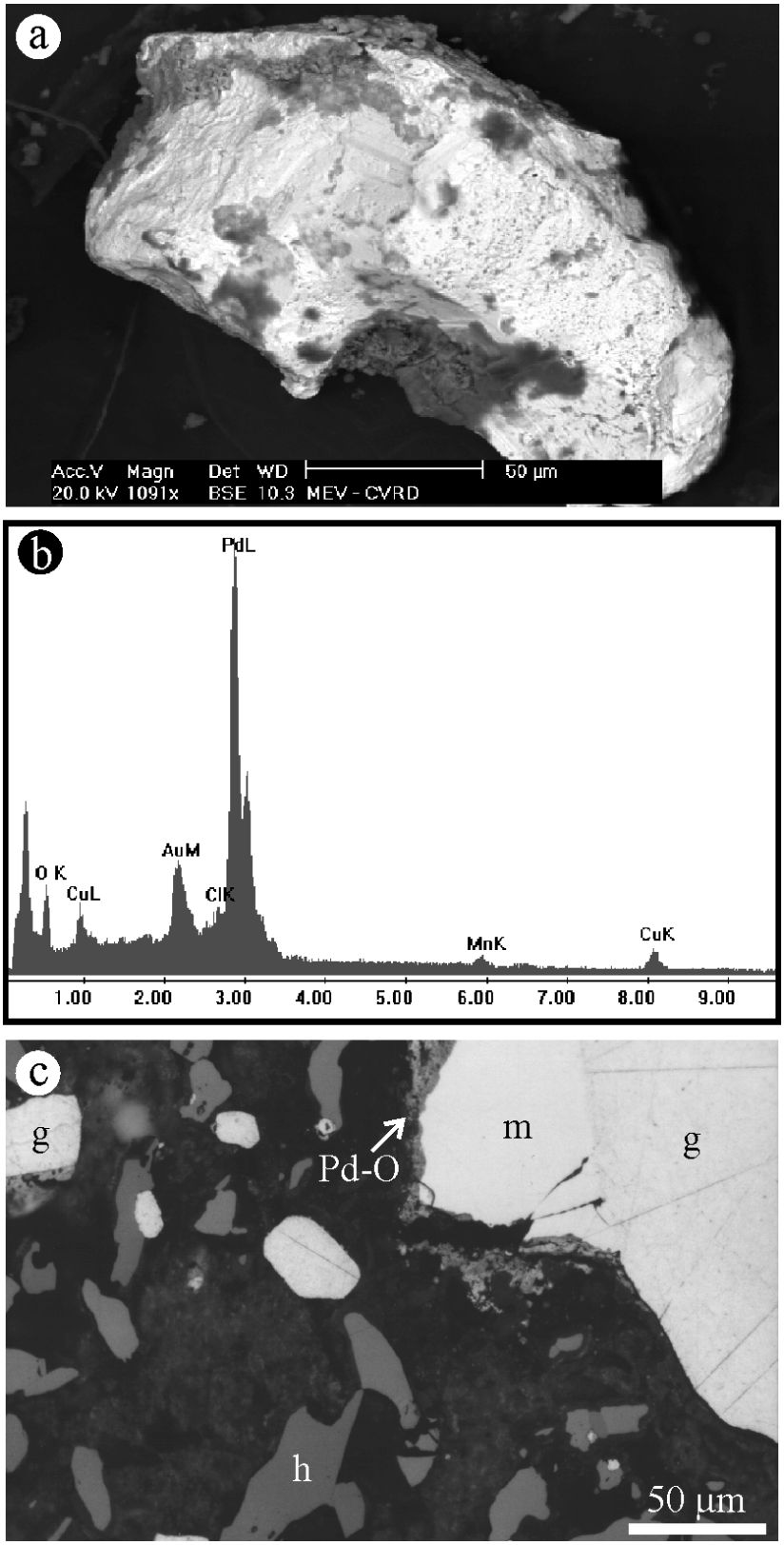

Fig. 23: (a) BSE image of a grain of *ouro preto* (black gold), characterised by coating of Pd–O material (grey, top) and iron oxyhydroxide (dark grey, bottom). (b) ED spectrum of the Pd–O coating shown in (a). (c) Gold, g, and specularite, h, within goethite-like groundmass (shades of grey), reflected light, oil immersion. Mertieite-II, m, is rimmed by a greyish halo of Pd–O. The Pd–O halos on crystals of Pd–Sb–As, together with iron oxides, give the dark colour to the *ouro preto* of Gongo Soco.

Native palladium is invariably associated with Pd–O material. Microstructural evidence has suggested that native palladium is derived from Pd–O by a desiccation-like process, i.e. deoxygenation and dehydration (CABRAL & LEHMANN 2003). Further investigation of nuggets of gold has revealed that native palladium occurs as colloform bands on arsenide-antimonides of palladium (Fig. 12f, 20b). Figure 12f can be divided into three domains that represent an oxygen gradient: (1) an inner, anoxic domain of mertieite-II (Table 5, column 4), (2) an intermediate, oxygen-deficient domain of linear colloform bands of native palladium, and (3) an external, oxygen-rich domain of Pd–O. The Pd–O domain has a linear fabric that conforms with the intermediate domain, a fact that suggests parallel arrays of microcracks, from which a whitish phase more enriched in palladium forms and inherits the linear pattern. In the intermediate domain, bands of native palladium alternate with films of Pd–O (Fig. 24a). X-ray mapping for Pd (Fig. 24b), Sb (Fig. 24c), Fe (Fig. 24d) and O (Fig. 24e) shows relics of a Sb-rich Pd mineral (mertieite-II) roughly parallel to the linear fabric of native palladium bands, among which films of Fe-bearing Pd–O are conformably interspersed. It is interesting to note that these microstructures are analogous to those produced by the alteration of pyrrhotite to pyrite–marcasite (i.e. birds eye texture, RAMDOHR 1969). Figure 12f records therefore an oxygen gradient that seems to corroborate the idea of a margin-directed removal of oxygen from the Pd–O mass (after a precursor palladium mineral) to form native palladium inside (CABRAL & LEHMANN 2003).

Compositionally, native palladium tends to be pure (CABRAL & LEHMANN 2003). Electron-microprobe data on native palladium should be considered with caution because of poorly polished surface and porosity, and interference from adjoining Fe–Cu-bearing Pd–O and Pd–Sb–As phases, and gold (Table 8).

Table 8: Electron-microprobe analyses of native palladium of Figure 20b

Analysis no.	17	19	22	23
(wt %)				
Pd	91.91	93.47	89.54	94.04
Pt	0.52	0.41	0.41	0.36
Au	2.17	0.50	1.43	0.89
Fe	0.74	1.35	0.76	1.75
Cu	0.39	0.34	0.69	0.38
Sb	3.78	0.76	3.79	0.86
As	1.12	0.42	1.13	0.40
Total	100.63	97.25	97.75	98.68

Analysis numbers correspond to those in Figure 20b.

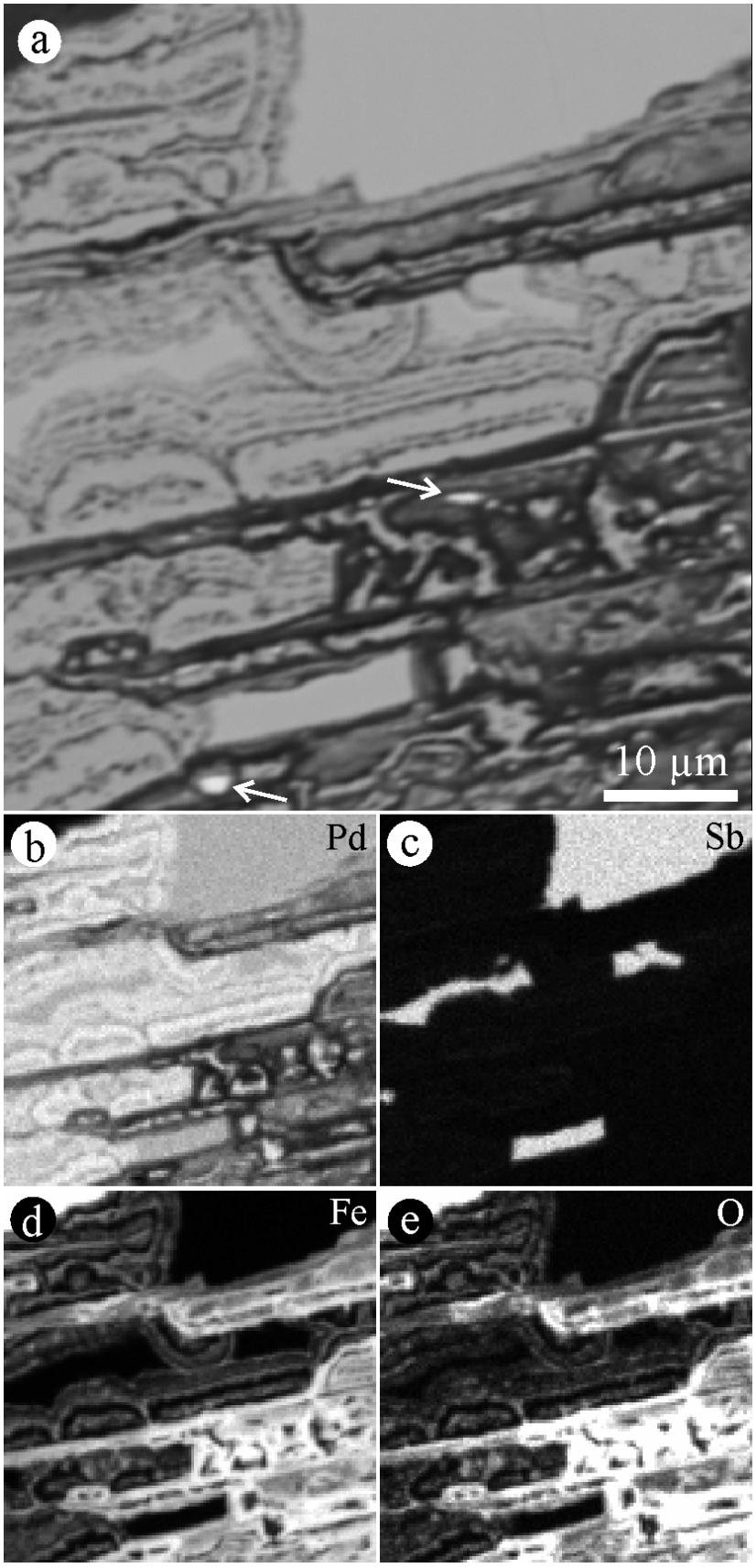

Fig. 24: (a) BSE image of the area squared in Figure 12f. White arrows indicate gold. X-ray element distribution of (a) Pd*L*α, (c) Sb*L*α, (d) Fe*K*α and (e) O*K*α.

Fluid inclusion microthermometry

Crystals of specular hematite were investigated under the infrared microscope for fluid inclusions by V. Lüders (GeoForschungsZentrum Potsdam). The sample material comes from the Sump orebody and consists of specularite intergrown with quartz in pockets and tension gashes. The specularite laths contain numerous fluid inclusions of primary origin (cf. ROEDDER 1984). They occur either isolated within the crystal plates or decorate growth zones. The primary inclusions are highly variable in length, ranging from 20-40 µm for inclusions in growth zones to more than 100 µm for isolated inclusions (Fig. 25). Secondary fluid inclusions are less common, considerably smaller (5-10 µm in length), and occur along trails cross-cutting the crystals. At room temperature, all inclusions consist of an aqueous phase and a vapour bubble. Additionally, many primary fluid inclusions contain daughter crystals of unknown composition (Fig. 25). Homogenisation temperatures and salinities of primary inclusions cluster around 160°C and 10–11wt % NaCl equiv. (Fig. 26). First melting temperatures are between -30.5 and -28°C, well below the eutectic of the pure NaCl–H_2O system and suggest either metastable eutectic melting in the system NaCl–H_2O (CRAWFORD 1981) or the presence of other cations in addition to sodium in the trapped fluids. Daughter crystals in primary fluid inclusions did not dissolve when heated to temperatures of decrepitation (>400°C). Secondary inclusions in specularite are too small to observe phase transitions. The microthermometric data for fluid inclusions in hematite are summarised in Table 9.

Some additional data were obtained from fluid inclusions in quartz (A.R. Cabral, unpublished data, 1996). The sample material comes from quartz-specularite pockets elsewhere at the mine, and may possibly represent another generation (late?) of quartz-specularite veining. The fluid inclusions commonly have an aqueous and vapour phase at room temperature, but some failed to form bubbles on cooling. They are isolated or arranged along trails. The latter are distinctly smaller (up to 10 µm in length) than the isolated inclusions, which may reach up to 50 µm in length. Reconnaissance microthermometry on the apparently primary, isolated fluid inclusions indicates a large salinity range (10–17 wt % NaCl equiv., n = 25) and homogenisation temperatures between 74 and 131°C (n = 16) (Fig. 26). Eutectic temperatures vary from -38 to -32, with a mean value of about -36°C (n = 8), close to that of the NaCl–$MgCl_2$–H_2O system (CRAWFORD 1981).

Table 9: Summary of fluid inclusion (FI) microthermometric data on specular hematite intergrown with quartz

	Eutectic temperature (°C)	Salinity (wt % NaCl equiv.)		Homogenisation temperature (°C)	
	Range (n)	Range	Median (n)	Range	Median (n)
Primary FI	-28 – -30.5 (12)	9.5–11.6	10.7 (32)	148.1–167.4	156.9 (32)

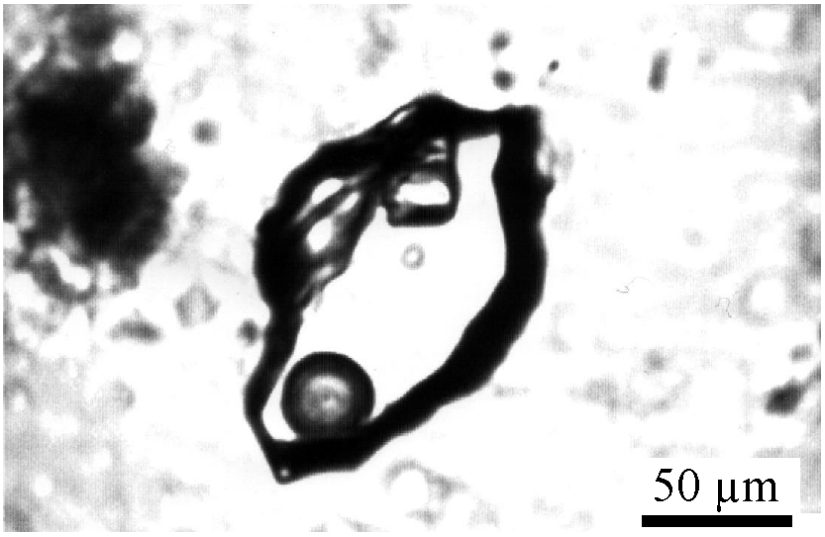

Fig. 25: Primary fluid inclusion in specular hematite with vapour bubble and daughter crystal of unknown composition. Transmitted infrared light, Sump area.

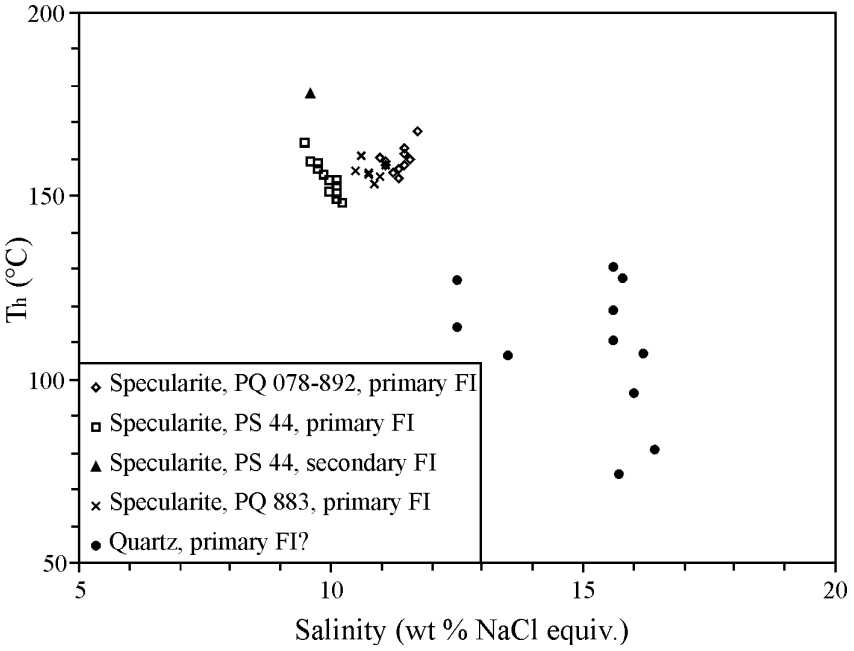

Fig. 26: Salinity vs. homogenisation temperature (T_h) diagram of primary fluid inclusions in specularite from quartz pockets and tension gashes in (auriferous) *jacutinga*, Sump area. Data from quartz (from elsewhere at the mine) are also shown for comparison.

Bulk-rock geochemistry

Geochemical data from samples of *jacutinga* and host itabirite are listed in Table 10. Gold concentrations range from a few ppb up to 50 ppm. It is important to note that the itabirite wallrock may also have gold contents in the ppm range.

Palladium contents vary from below detection limit (<4 ppb) to 790 ppb, and are correlated with gold (Fig. 27a). Although in the ppb range, mercury seems to be a distinctive element of the mineralisation because of its positive correlation with manganese (Fig. 27b). Selenium, present as selenide minerals included in gold, is not detected in the bulk-rock chemical analyses (<0.1 ppm Se). Chromium, in the wt % range in gold-hosted specular hematite (Table 4), is detected in the ppm range in the bulk-rock samples. If palladian gold, as indicated by electron-microprobe data, is indeed related to chromiferous hematite, then only a very small part of the specularite-rich veins is mineralised. In other words, the bulk of the specular hematite that makes up the veins of Figure 9 is barren. Therefore, it appears that palladian gold is restricted to late threadlike fissures, the so-called 'lines of gold' of the old miners (Fig. 8), located not only in specularite-rich veins, but also in the wallrock.

The presence of anomalously high contents of gold in the wallrock led to a reconnaissance study of the dispersion of gold in rocks (itabirite and soft hematite ore) that do not show any obvious relation to *jacutinga* veins (i.e. decimetre-wide specularite-rich veins like those in Figure 9). Gold values as high as 1 ppm were found in soft hematite ore with talc-bearing threadlike fissures and patches (Table 11). Considering all samples in a Hg vs. Au plot, it becomes apparent that the country rocks were hydrothermally affected (Fig. 27c). Some gold is thus dispersed in the country rocks and possibly related to the talcose, specularite-bearing veinlets.

In summary, the *jacutinga* mineralisation is characterised by enrichment in Au, Pd, Fe, Mn, Hg and Cr, compared to fresh itabirite (Table 10). The host itabirite sampled during the gold reconnaissance study has variable and sporadic high values of gold, mercury, palladium, and chromium, which suggests hydrothermal overprint. The composition of the unaltered itabirite, here used as local reference, corresponds to other itabirite data from regional studies (BARBOSA & GROSSI SAD 1973; KESSLER & MÜLLER 1988; KLEIN & LADEIRA 2000).

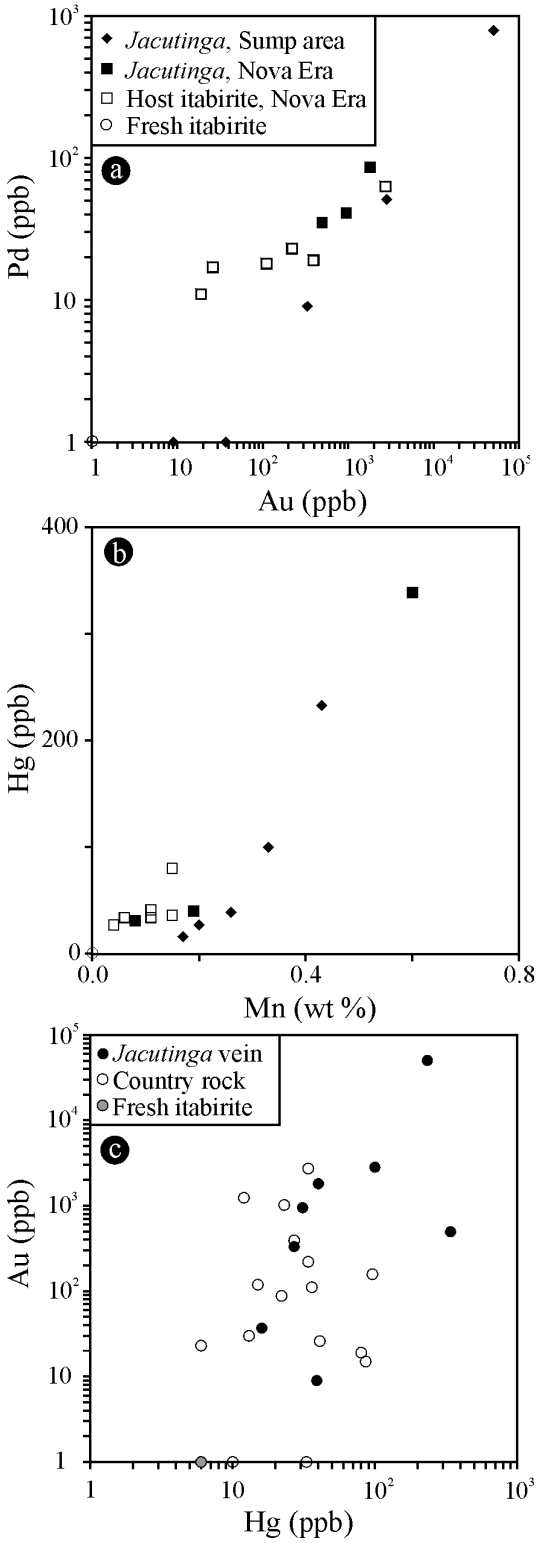

Fig. 27: (a) Pd vs. Au and (b) Hg vs. Mn plots of the bulk-rock chemical analyses in Table 10; legend as in (a). (c) Hg vs. Au plot from data in Tables 10 and 11.

Table 10: Bulk-rock chemical analyses of *jacutinga* veins and host itabirite

	1	2	3	4	5	6	7	8	9	10	11	12	13	14	15	16		17		18	
	PQ-494	PQ-535	PQ-883[§]	PQ-892	PQ-949	AR-02	AR-05	AR-16	AR-04[†]	AR-06[†]	AR-07[†]	AR-01	AR-03	AR-15	F63	x	(n)	x	(n)	x	(n)
(wt %)																					
Fe_2O_3	55.3	84.8	27.2	94.5	90.4	85.21	93.32	71.28	71.95	55.02	75.18	46.96	50.54	38.71	50.34					49.85	(8)
FeO	n.a.	n.a.	n.a.	n.a.	n.a.	<0.10	0.66	<0.10	0.22	0.49	<0.01	<0.01	<0.10	<0.10	n.a.					0.63	(8)
Mn	0.33	0.43	0.20	0.17	0.26	0.19	0.08	0.60	0.11	0.04	0.11	0.06	0.15	0.15	0.02					<0.01	(8)
SiO_2	n.a.	n.a.	n.a.	n.a.	n.a.	6.96	2.43	19.19	19.37	42.49	17.99	49.29	46.97	55.58	48.97					48.52	(8)
Al_2O_3*	1.21	0.77	0.77	0.38	1.78	0.49	1.16	3.55	3.07	0.79	2.42	0.57	0.71	2.30	0.23					0.12	(8)
MgO	0.07	0.28	0.17	0.13	0.10	0.65	0.30	0.26	0.49	0.29	0.37	0.16	0.13	0.02	0.08					0.06	(8)
CaO	<0.01	<0.01	<0.01	<0.01	<0.01	0.07	0.03	0.03	0.05	0.04	0.04	0.04	0.04	0.02	0.02					0.11	(8)
Na_2O	<0.01	<0.01	<0.01	<0.01	<0.01	0.03	0.24	<0.01	0.25	0.06	0.39	0.22	0.01	0.01	0.15					0.18	(8)
K_2O	<0.01	<0.01	<0.01	<0.01	<0.01	<0.01	0.03	0.01	0.06	<0.01	0.07	0.03	0.04	0.02	0.07					<0.01	(8)
TiO_2	0.05	0.03	0.03	0.02	0.03	0.03	0.06	0.22	0.17	0.04	0.14	0.03	0.04	0.14	0.03					0.01	(8)
P_2O_5	0.10	0.10	0.06	0.05	0.05	0.16	0.08	0.25	0.21	0.07	0.14	0.09	0.16	0.11	0.02					0.08	(8)
(ppb)																					
Au	2824	50385	333	37	9	1812	950	496	221	392	26	2729	111	19	1			[8-60]	(8)	[<2-332]	(6)
Hg	100	233	27	16	39	40	31	339	34	27	41	34	36	80	6						
Pd	51	790	9	<4	<4	86	41	35	23	19	17	63	18	11	<4						
Pt	<5	<5	<5	<5	<5	11	<5	5	<5	5	<5	8	<5	<5	<5						
Os	<2	<2	<2	<2	<2	n.a.	n.a.	n.a.	n.a.	n.a.	n.a.	n.a.	n.a.	n.a.	n.a.						
Ir	0.2	<0.1	<0.1	<0.1	<0.1	n.a.	<5	n.a	<5	<5	<5	<5	n.a	n.a	<5						
Ru	<5	<5	<5	<5	<5	n.a.	n.a.	n.a.	n.a.	n.a.	n.a.	n.a.	n.a.	n.a.	n.a.						
Rh	1.1	15.1	<0.2	0.2	0.2	n.a.	n.a.	n.a.	n.a.	n.a.	n.a.	n.a.	n.a.	n.a.	n.a.						
(ppm)																					
Ag	<0.3	1.2	<0.3	<0.3	<0.3	n.a.	<0.3	n.a.	<0.3	<0.3	<0.3	<0.3	n.a.	n.a.	<0.3						
As	7.3	8.8	3.7	5.2	4.7	<5	9	5	23	7	11	9	12	22	2					8.3	(6)
Ba	530	610	<50	<50	<50	13	19	88	14	7	15	12	9	36	20	179	(62)			59	(6)
Be	1	2	<1	1	1	1	2	1	2	<1	1	<1	<1	<1	<1	<2	(89)				
Bi	<0.1	0.5	0.1	<0.1	<0.1	<0.4	<2	<0.4	<2	<2	<2	<2	<0.4	<0.4	n.a.						
Br	<0.5	<0.5	<0.5	<0.5	<0.5	n.a.	<1	n.a.	<1	<1	<1	<1	n.a.	n.a.	<1					<0.4	(6)
Cd	1.6	2.0	1.5	2.6	1.6	n.a.	<0.3	n.a.	<0.3	<0.3	<0.3	0.4	n.a.	n.a.	1.0						
Co	2	4	2	1	6	10	4	3	12	6	8	4	7	<1	<1			117	(54)	248	(8)
Cr	127	467	20	243	33	88	64	67	209	45	137	47	<20	30	9	29	(80)	71	(54)	123	(8)

Table 10: (*Cont.*)

	1	2	3	4	5	6	7	8	9	10	11	12	13	14	15	16		17		18	
	PQ-494	PQ-535	PQ-883§	PQ-892	PQ-949	AR-02	AR-05	AR-16	AR-04†	AR-06†	AR-07†	AR-01	AR-03	AR-15	F63	x	(n)	x	(n)	x	(n)
(ppm)																					
Cs	<1	<1	<1	<1	<1	<5	<0.5	<5	<0.5	<0.5	<0.5	<0.5	<5	<5	<0.5					<0.20	(6)
Cu	10	8	7	2	5	<10	13	14	14	8	13	18	<10	10	7	22	(71)	41	(54)	33	(8)
Ga	n.a.	n.a.	n.a.	n.a.	n.a.	1	n.a.	6	n.a.	n.a.	n.a.	n.a.	1	3	n.a.						
Ge	0.5	0.8	0.2	0.8	0.4	1	n.a.	4	n.a.	n.a.	n.a.	n.a.	1	3	n.a.	<10	(89)				
Hf	<1	<1	<1	<1	<1	<0.2	<0.5	0.8	<0.5	<0.5	<0.5	<0.5	<0.2	0.6	<0.5					<0.11	(6)
In	n.a.	n.a.	n.a.	n.a.	n.a.	<0.2	n.a.	<0.2	n.a.	n.a.	n.a.	n.a.	<0.2	<0.2	n.a.						
Mo	<1	<1	<1	<1	<1	<2	<5	<2	<5	<5	<5	<5	<2	<2	<5	<5	(89)				
Ni	9	15	5	5	3	60	31	<20	72	40	49	23	27	<20	23	21	(70)	162	(54)	19	(8)
Pb	<3	135	10	<3	<3	<5	27	39	42	23	43	30	<5	<5	15						
Rb	<15	<15	<15	<15	<15	2	28	<2	<20	<20	36	<20	<2	2	<20					32	(8)
Sb	0.6	1.8	0.3	1.5	1.5	2.7	4.7	8.0	6.8	3.6	4.8	5.1	3.8	4.2	5.0					2.2	(6)
Sc	2.3	2.5	1.3	1.0	1.5	1.0	1.4	7.0	3.7	1.4	3.5	0.8	2.0	2.0	0.4	<5	(89)			0.19	(6)
Se	<0.1	0.1	<0.1	<0.1	<0.1	n.a.	<3	n.a.	<3	<3	<3	<3	n.a.	n.a.	<3						
Sn	<1	<1	<1	<1	<1	<1	n.a.	<1	n.a.	n.a.	n.a.	n.a.	<1	<1	n.a.	<5	(89)				
Sr	10	61	8	10	12	3	2	4	3	2	4	3	1	2	2					10	(8)
Ta	<0.5	<0.5	<0.5	<0.5	<0.5	<0.1	<1	0.2	<1	<1	<1	<1	<0.1	0.2	<1					<0.15	(5)
Te	<0.1	0.2	<0.1	<0.1	<0.1	n.a.	n.a.	n.a.	n.a.	n.a.	n.a.	n.a.	n.a.	n.a.	n.a.						
Tl	0.1	0.1	<0.1	<0.1	<0.1	<0.1	n.a.	0.2	n.a.	n.a.	n.a.	n.a.	<0.1	<0.1	n.a.						
Th	1.1	<0.2	0.4	0.4	0.8	0.3	0.7	3.2	2.1	<0.5	1.7	<0.5	0.6	1.9	<0.5					<0.10	(6)
U	3.2	10.6	1.9	4.2	3.6	3.4	6.6	5.8	5.2	4.0	5.5	2.4	2.0	1.2	0.8					1.2	(6)
V	17	189	15	20	27	195	103	95	233	76	138	59	51	59	19	35	(73)	132	(54)		
W	<1	<1	<1	<1	4	3	<3	1	<3	<3	<3	<3	1	1	<3	<20	(89)			1.2	(6)
Y*	6	16	3	2	4	9	4	17	9	4	8	3	7	5	7					5	(8)
Zn	20	29	15	11	7	<30	18	31	40	19	24	19	<30	<30	3					42	(8)
Zr	n.a.	n.a.	n.a.	n.a.	n.a.	7	23	20	35	21	33	16	20	22	9					2	(8)

Chemical analysis by Actlabs, Ontario, Canada. Columns: 1-5, hematite-rich vein, Sump area; 6-8, hematite-rich vein, Nova Era area; 9-14: host itabirite, Nova Era area; 15, fresh itabirite sample from drill core FGS-63, 217.0 m deep.

Gold, palladium and platinum determined by fire assay ICP-OEM (other PGE in selected samples by NiS fire assay-INAA); mercury determined by cold vapour FIMS; FeO by titration.

Columns 1–5: elements determined by INAA are: As, Ba, Br, Co, Cr, Cs, Fe, Hf, Ir, Na, Rb, Sb, Sc, Ta, Th, U, W and Y; by ICP-MS: Bi, Ge, In, Se, Sn, Te and Tl; the remaining elements were determined by acid digestion ICP technique.

Columns 7, 9–12, 15: major elements determined by fusion ICP; remaining elements by INAA.

Columns 6, 8, 13, 14: major elements determined by fusion ICP; remaining elements by ICP-MS.

§ Specularite-bearing quartz pocket. † Enclosing itabirite with about 5 cm-thick hematite-rich seam. Elements with (*) may have not been totally digested in the PQ samples.

Columns: 16, BARBOSA & GROSSI SAD (1973); 17, KESSLER & MÜLLER (1988); 18, KLEIN & LADEIRA (2000). Carbonate-rich varieties excluded; (n): number of samples; x: mean. Brackets indicate range. n.a.: not analysed

Table 11: Bulk-rock chemical analyses of itabirite and soft hematite ore

	GS-435	GS-441	GS-442	GS-451	GS-452	GS-461	GS-463	GS-473	GS-474	GS-478
Fe_2O_3 (wt %)	82.23	75.22	72.79	89.09	71.07	87.09	88.37	64.06	71.64	69.93
Mn	0.33	0.15	0.32	0.14	0.98	0.11	0.26	0.05	0.04	0.19
Al_2O_3*	0.62	1.15	3.27	1.02	7.47	1.32	1.15	0.32	0.31	1.35
MgO	0.24	0.17	0.19	0.27	0.40	2.40	0.21	0.22	0.48	0.06
CaO	<0.01	<0.01	<0.01	<0.01	<0.01	<0.01	<0.01	<0.01	<0.01	<0.01
Na_2O	<0.01	<0.01	<0.01	<0.01	<0.01	<0.01	<0.01	<0.01	<0.01	<0.01
K_2O	0.04	0.02	0.01	<0.01	<0.01	<0.01	<0.01	<0.01	<0.01	<0.01
TiO_2	0.02	0.05	0.16	0.02	0.36	0.05	0.02	<0.02	<0.02	0.08
P_2O_5	0.23	0.09	0.12	0.05	0.21	0.06	0.11	0.10	0.03	0.14
SO_4	<0.01	<0.01	<0.01	<0.01	<0.01	<0.01	<0.01	<0.01	<0.01	0.09
Au (ppb)	158	88	1020	119	30	23	1240	<2	<2	15
Hg	96	22	23	15	13	6	12	33	10	86
Ag (ppm)	0.3	<0.3	<0.3	<0.3	0.5	<0.3	<0.3	<0.3	<0.3	<0.3
As	27.5	16.9	23.2	5.4	11.6	6.2	6.1	7.6	6.1	2.5
Ba	330	350	650	120	180	130	<50	100	<50	170
Be	2	1	2	1	3	1	<1	1	<1	2
Cd	2.0	3.0	1.9	2.0	1.7	1.7	2.2	1.1	2.0	2.8
Co	2	5	5	6	20	2	2	5	4	2
Cr	30	25	73	73	129	52	32	15	12	45
Cu	15	7	4	1	4	<1	<1	<1	<1	33
Hf	<1	<1	<1	<1	2	<1	<1	<1	<1	<1
Mo	1	2	<1	<1	<1	<1	<1	2	<1	2
Ni	18	9	13	6	23	5	3	39	6	73
Pb	3	<3	9	3	28	<3	16	<3	<3	<3
Rb	<15	39	<15	33	<15	<15	<15	<15	41	<15
Sb	0.8	0.7	1.4	1.1	1.3	1.0	0.8	13.2	3.5	3.8
Sc	2.0	2.9	6.4	2.4	14.3	2.2	1.5	0.7	0.7	4.7
Sr	14	11	10	13	28	11	15	12	7	8
Ta	<0.5	<0.5	<0.5	0.6	<0.5	<0.5	<0.5	<0.5	<0.5	<0.5
Th	0.6	1.1	2.3	0.5	4.5	0.9	1.1	<0.2	<0.2	2.7
U	5.2	2.8	3.6	4.0	12.5	4.1	4.9	2.3	3.0	2.5
V	7	21	51	19	53	19	18	12	73	19
W	<1	<1	<1	2	2	<1	<1	<1	<1	<1
Y*	10	8	13	6	17	3	2	14	4	14
Zn	11	2	8	<1	12	1	<1	7	<1	91

Sample (local coordinates, rock type): GS-435 (10205N/11424E, friable, ochreous itabirite); GS-441 (10243N/11551E, friable, specular itabirite); GS-442 (10244N/11551E, soft hematite with talc–quartz patches/veinlets); GS-451 (10212N/11430E, soft hematite with talcose patches); GS-452 (10213N/11430E, Mn-bearing, soft hematite with talcose veinlets); GS-461 (10216N/11416E, soft hematite with talcose patches/veinlets); GS-463 (10217N/11416E, Mn-bearing, soft hematite with talcose patches/veinlets); GS-473 (10190N/10353E, friable, ochreous itabirite with coarse-grained porphyroblasts of magnetite); GS-474 (10191N/10351E, friable itabirite); GS-478 (10564N/10954N, friable, ochreous itabirite).

Chemical analysis by Actlabs, Ontario, Canada. Elements determined by INAA: Au, As, Ba, Br, Co, Cr, Cs, Fe, Hf, Ir, Na, Rb, Sb, Sc, Se, Sn, Ta, Th, U, W and Y. The remaining elements were determined by acid digestion ICP technique; Hg by cold vapour FIMS (5 ppb detection limit). The following elements were sought for but not detected: Ir (<5 ppb), Bi (<2 ppm), Br (<0.5 ppm), Cs (<1 ppm), Se (<3 ppm) and Sn (<0.01%). Iron and sulphur as total Fe_2O_3 and SO_4, respectively. Elements with (*) may only be partially extracted.

3
Itabira: another case of palladian gold mineralisation (*ouro preto*)

"*Das Palladiumgold ist im Itabirit fast nur auf kleine Nester und Adern (Linhas) beschränkt (...) nicht selten mit einer limonitähnlichen, braunen, erdigen Kruste bedeckt, die sich als Palladiumoxyd erwies (...)*".

Über das Vorkommen von Palladium und Platin in Brasilien, by E. Hussak, 1906.

Itabira was the locus of a minor gold rush in 1983, when about 5,000 *garimpeiros* washed the waste drainage of iron ore mining for gold. In 1986, CVRD commenced to mine the auriferous *jacutinga* veins, with a mean ore grade of 30 g/t Au (ANDRADE & SÁ 1990). Since then, ore grades have decreased and gold mining at Cauê shall stop in 2003. The decrease in ore grade is illustrated in Figure 28 (GALBIATTI 1999).

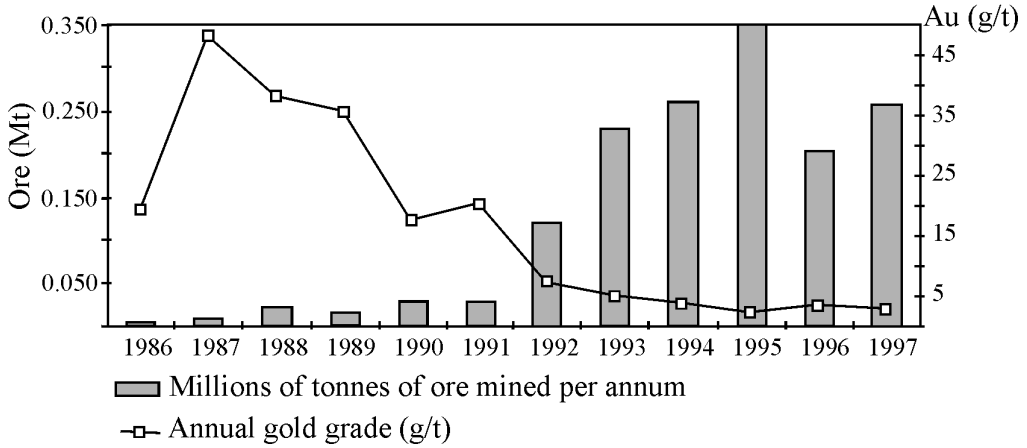

Fig. 28: Annual produce of auriferous ore and its mean gold grade from Cauê mine (GALBIATTI 1999).

The auriferous mineralisation of Itabira is not only economically, but also academically attractive. Concerning mineralogy, a variety of palladium minerals were discovered or redefined from Itabira, such as arsenopalladinite, $Pd_8(As,Sb)_3$, and atheneite, $(Pd,Hg)_3As$ (CLARK et al. 1974; CABRI et al. 1975, 1977), 'palladinite', PdO (JEDWAB et al. 1993), and palladseite, $Pd_{17}Se_{15}$ (DAVIS et al. 1977). This chapter presents mineralogical and geochemical data on the *jacutinga*-style mineralisation as a contribution to the cooperative work with CVRD geologists (GALBIATTI et al. 1997; GALBIATTI 1999; PEREIRA et al. 1999; CABRAL et al. 2002d; KWITKO et al. 2002), and addresses the recent studies by Olivo and co-workers (OLIVO & GAUTHIER 1995; OLIVO et al. 1994, 1995, 1996, 2001).

Geological setting

The world-class Itabira iron ore district is located in the north-eastern extremity of the Quadrilátero Ferrífero (Figs. 1, 6). High-grade hematite ore and auriferous *jacutinga*

mineralisation are hosted by itabirite of the Palaeoproterozoic Cauê Formation, the lower unit of the Itabira Group, i.e. Itabira Iron Formation (Fig. 29). Rocks of the Caraça Group, which underlies the Itabira Group elsewhere in the Quadrilátero Ferrífero, are missing at Itabira (CHEMALE 1987). The Itabira Group is in tectonic contact with subjacent greenstone rocks of the Archaean Rio das Velhas Supergroup (CHEMALE et al. 1987; OLIVO et al. 1995).

Structurally, the Itabira district comprises a regional-scale syncline, with subsidiary synclines (Cauê, Conceição and Dois Córregos) and anticlines (Chacrinha and Periquito) (DORR & BARBOSA 1963; Fig. 29a). Three generations of structures can be distinguished, characteristic fabrics of which are: (1) pervasive S_1 mylonitic foliation and E–W-trending stretching lineation; (2) S_2 axial planar foliation, mesoscopic folding with E–W-trending axis and strike-slip faulting; (3) N–S-trending crenulation cleavage and reverse brittle faults (CHEMALE et al. 1987, 1994; OLIVO et al. 1995; cf. HASUI et al. 1994). These structures are considered to be related to a W-vergent thrusting event of Brasiliano age (CHEMALE et al. 1994; HACKSPACHER et al. 2001).

The Itabira district was affected by more extreme conditions of metamorphism than those in the western and central parts of the Quadrilátero Ferrífero. According to oxygen isotope data, metamorphic temperatures reached a maximum temperature of 660°C (HOEFS et al. 1982), but the mineral paragenesis indicates a lower metamorphic rank (DORR & BARBOSA 1963; PIRES 1995), as manifested in the zonation of metamorphic grade from lower greenschist at Conceição to lower amphibolite facies at Cauê (CHEMALE et al. 1994).

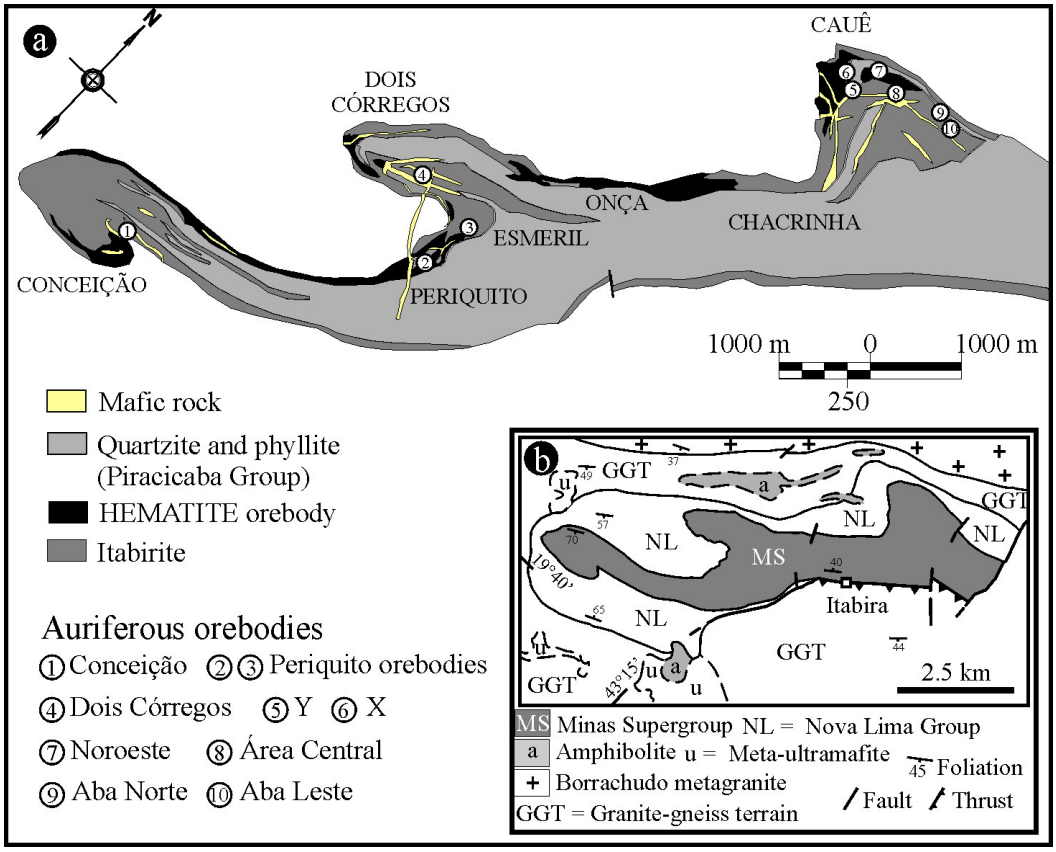

Fig. 29: (a) Simplified geological map of the Itabira district with location of hematite orebodies and auriferous deposits (after GALBIATTI 1999). (b) Geological overview of the Itabira district (after CHEMALE et al. 1987).

The jacutinga-style mineralisation of Itabira

The itabirite-hosted auriferous pockets and veinlets of Itabira provided dark grains of gold (*ouro preto*) for early chemical analyses, in which palladium contents as high as 11.6 wt % were determined (HUSSAK 1906).

Among the *jacutinga*-style gold deposits of the Quadrilátero Ferrífero, those of Itabira have been subject of active research. As a result, two contrasting concepts of *jacutinga* have arisen. One concept defines *jacutinga* as a "hydrothermally altered carbonate-bearing oxide-facies iron formation hosting gold and palladium mineralisation" (OLIVO & GAUTHIER 1995). Accordingly, a main mineralising event is envisaged to have been synchronous with ductile shearing (mylonitic foliation) at peak conditions of metamorphism of about 600°C, assuming parallelism between the auriferous veins and the S_1 mylonitic foliation (Olivo et al. 1995; 2001). A late Transamazonian age of 1.83 ± 0.10 Ga has been suggested for the main mineralising event based on lead isotopic data for palladian gold, quartz and hematite (OLIVO et al. 1996). The analytical data, however, define an 'errorchron', with a mean squared weighted deviation of 7.55 (cf. WENDT & CARL 1991).

The other concept, developed by mine geologists, is based on the mapping of working faces. It defines *jacutinga* mineralisation as fracture infill that truncates the S_1 foliation (Figs. 30, 31) (GALBIATTI et al. 1997; GALBIATTI 1999; see review in DARDENNE & SCHOBBENHAUS 2001). The mineralisation is believed to be Brasiliano in age (GUIMARÃES 1970; GALBIATTI 1999; VARAJÃO et al. 2000).

Fig. 30: Auriferous (*jacutinga*) vein of specularite, quartz (white), with dark patches of manganese oxide, cross-cuts the S_1 foliation of the host itabirite at Central, level 740 (July 2002).

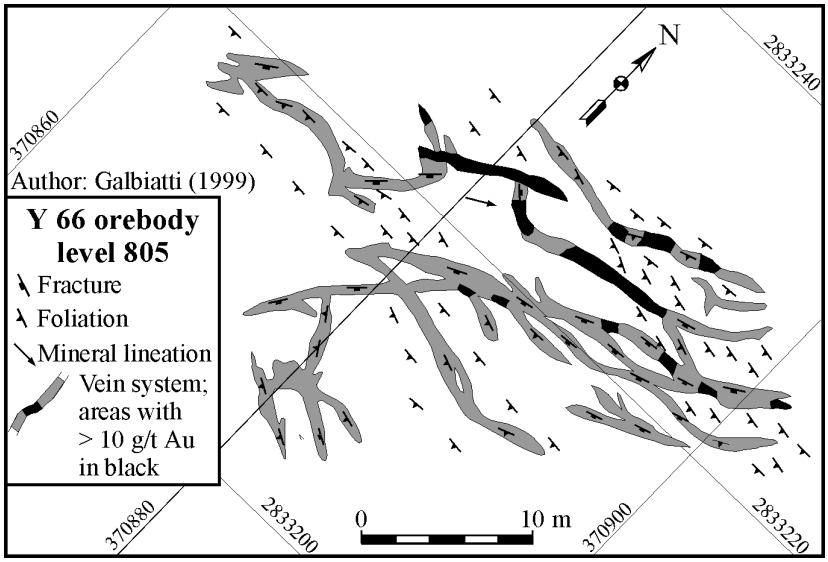

Fig. 31: Sampling channels along auriferous veins and their relationship to the S_1 foliation of the host itabirite (GALBIATTI 1999).

Sample material and analytical techniques

Both the auriferous specularite-quartz veins and the host itabirite are friable. Bulk samples of the veins were taken from the Corpo Y (Y, levels 755 and 725), Área Central (Central, level 740) and Conceição (Lico, level 875) orebodies (Fig. 29a). Gold-bearing compact aggregates of fine-grained magnetite, found as fragments of the host rock in the veins, come from Y, level 802 (CABRAL et al. 2002d). Heavy-mineral concentrates were obtained by panning of selected bulk samples, from which a fraction was separated for geochemical analyses. Some grains were mounted on conductive holders for mineral identification and imaging with a Leiz ISI Super 40/3A scanning electron microscope (TU Clausthal). Backscattered electron (BSE) images of mineral grains were obtained with a Cameca SX100 electron-microprobe (TU Clausthal). Selected grains were then mounted in resin to prepare polished sections for electron-microprobe analysis at TU Clausthal (occasional modifications in the X-ray emissions lines and analytical conditions described in CABRAL et al. (2001) are noted in the tables; cf. section on analytical techniques in the Gongo Soco chapter).

Gold and associated platinum-group minerals (PGM) from heavy-mineral concentrates

Heavy-mineral concentrates are composed essentially of specular hematite. Gold from Central, level 740, is intergrown with specular hematite (Figs. 32a, b, c), but also occurs as independent, dendritic crystals (Fig. 32d) and euhedral crystals on the surface of anhedral gold (Fig. 32e), as well as grains with irregular swellings (Fig. 32f).

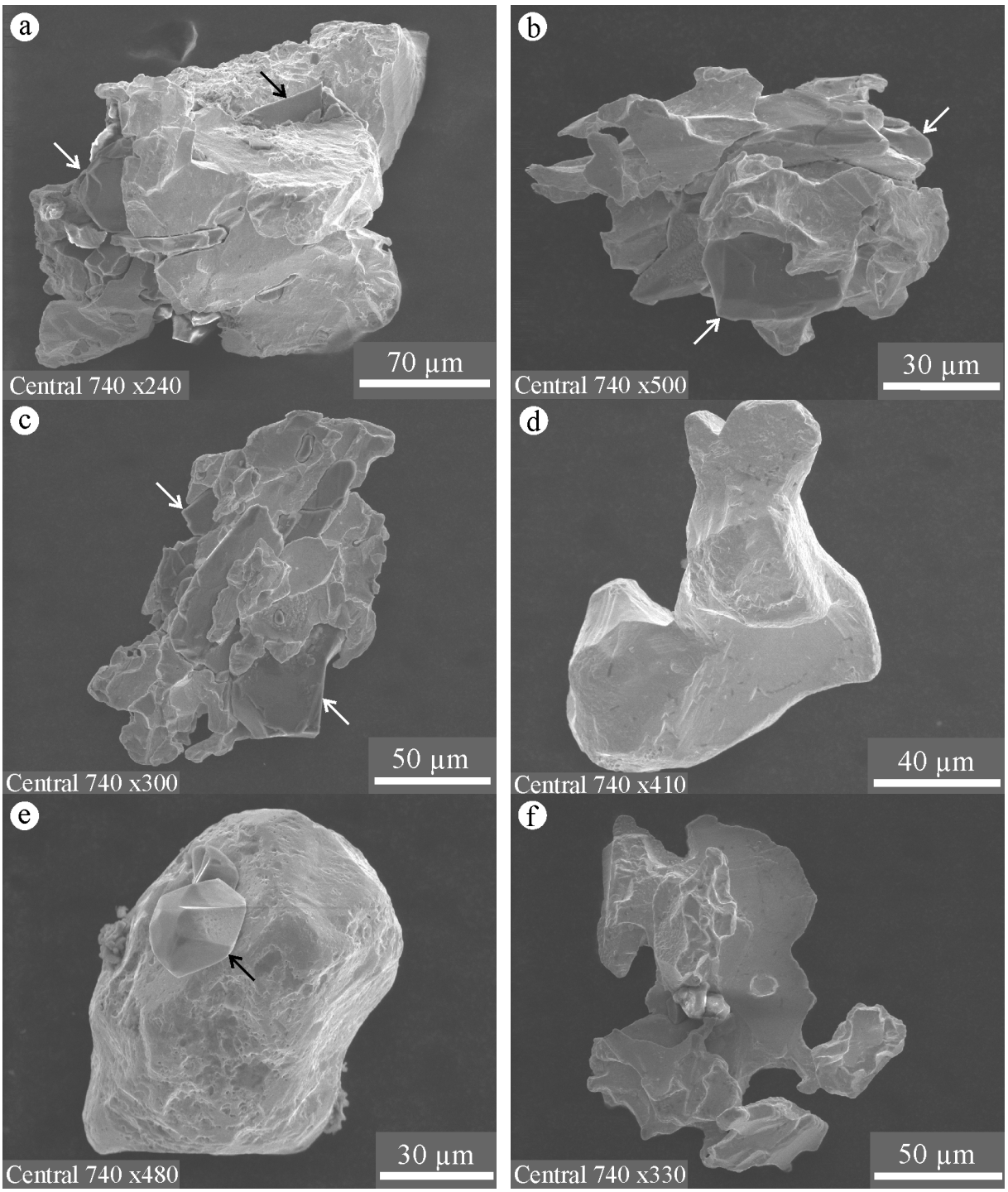

Fig. 32: Secondary electron (SE) images of gold from Central, level 740. (a), (b), (c) Gold intergrowth with specularite (arrows). (d) Dendritic crystal of gold. (e) Euhedral crystal of gold (arrow) on the surface of anhedral gold. (e) Gold with irregular protuberances.

Gold from Conceição (Lico, level 875) is as well intergrown with specular hematite (Fig. 33a) and may have overgrowths of radiating goethite (Figs. 33b, c). Specularite seems to have left triangular impressions on the surface of gold (Fig. 33d). Subhedral and dendritic crystals are illustrated in Figures 33e, f.

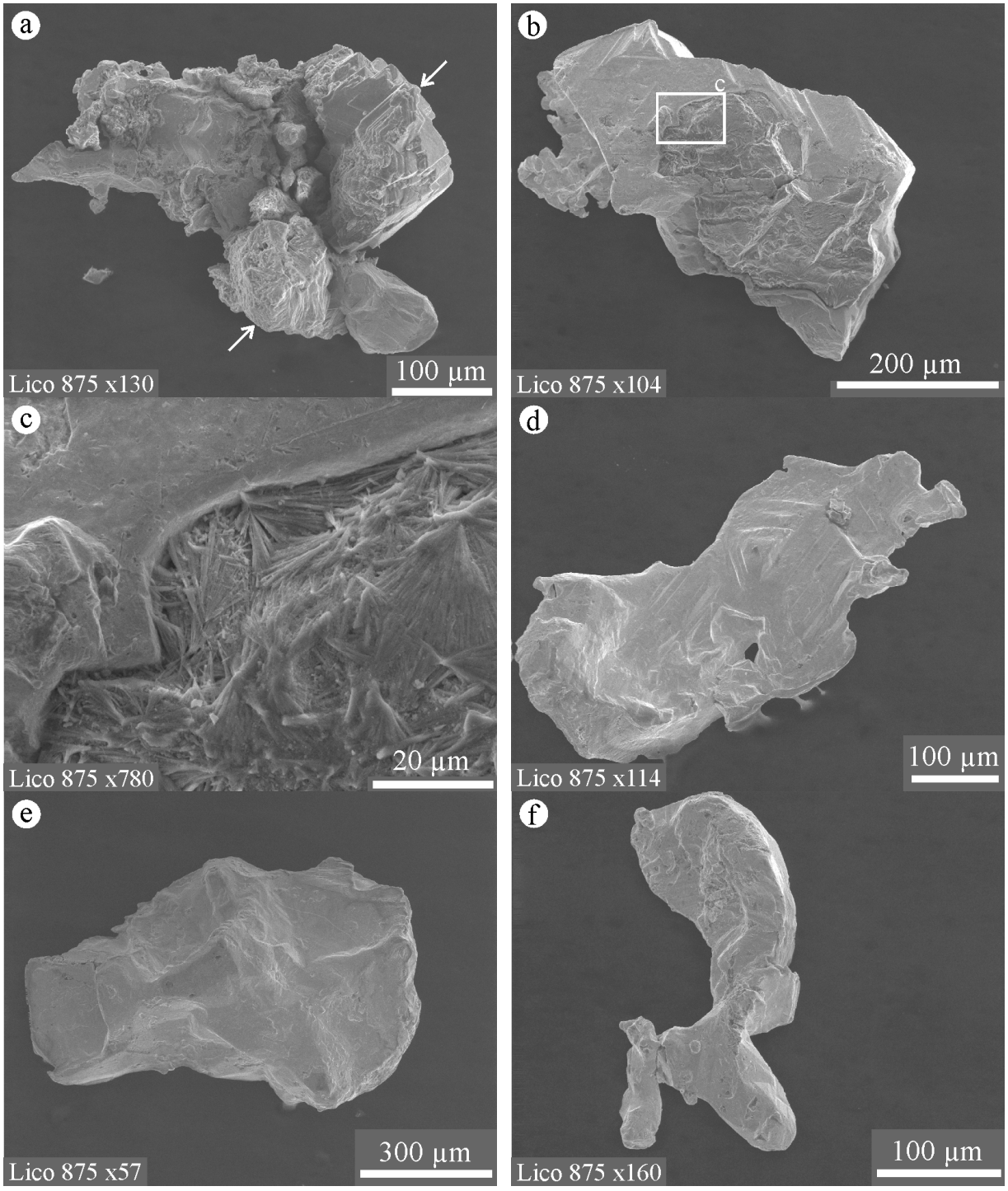

Fig. 33: SE images of gold from Lico, level 875. (a) Gold intergrowth with specularite (arrows). (b) Gold with overgrowth of goethite. (c) Detail of the area squared in (b) to show radiating crystals of goethite. (d) Gold grain with triangular imprints, probably from specularite. (e) Subhedral crystal of gold. (f) Dendritic crystal of gold.

Associated with the gold from Lico, a particular grain of a palladium arsenide-antimonide (isomertieite?) was found in the heavy-mineral concentrate (Fig. 34a). It is characterised by areas where the mineral is covered by spherules (Fig. 34b), compositionally analogous to the substrate, or carved with their moulds (Fig. 34c). The concave-moulded surface has pits, to which spots of a Pd–O phase are spatially related (Fig. 34d).

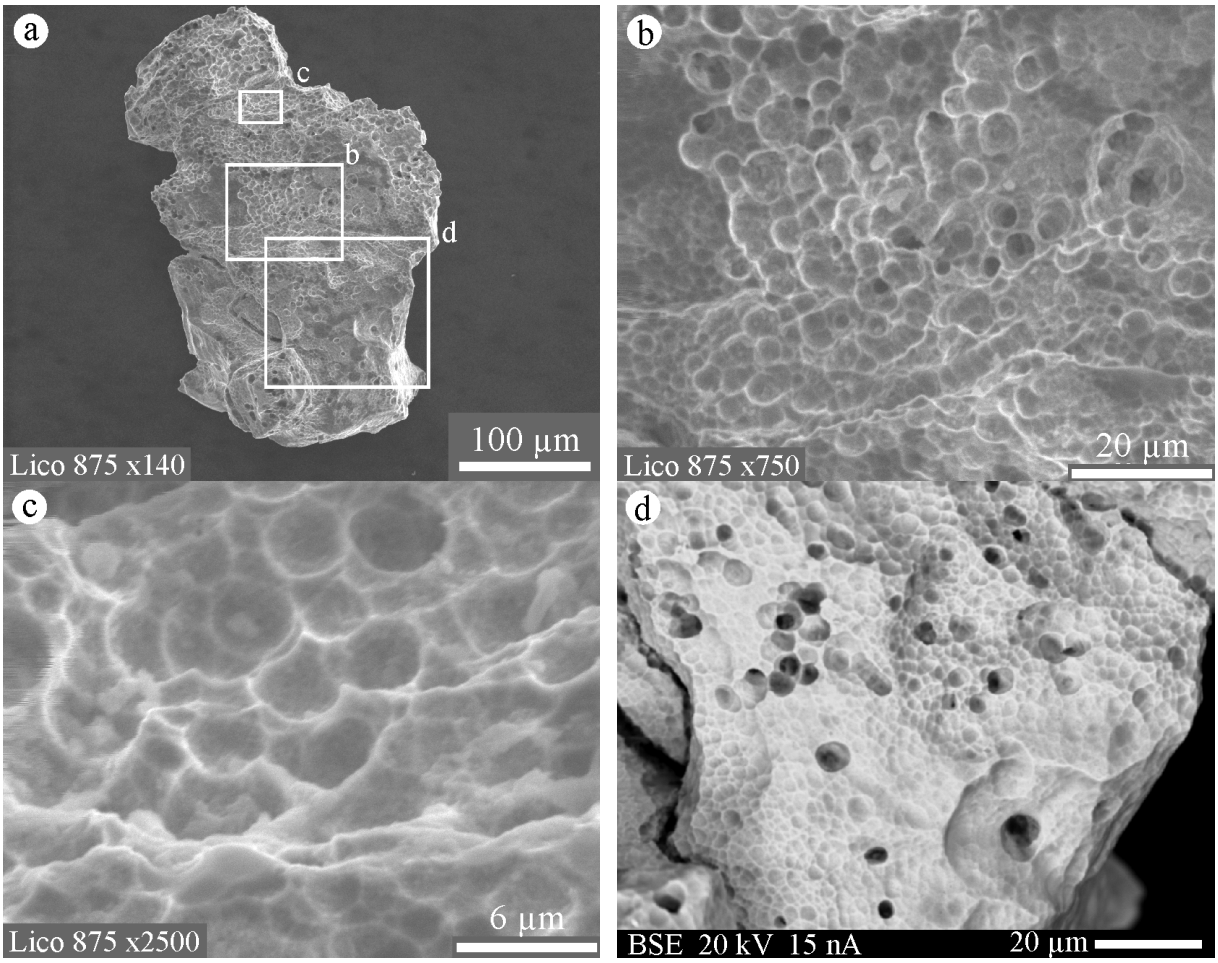

Fig. 34: (a) SE image of a grain of palladium arsenide-antimonide (isomertieite?) from Lico, level 875. (b) SE image of the area squared in (a) to point out spherules compositionally similar to the substrate. (c) SE image of the area squared in (a) to indicate that the substrate also has a concave-moulded surface. (d) BSE image of the area squared in (a) where the concave-moulded surface has pits, with which spots of a Pd–O phase are associated.

Gold from Y, level 725, is likewise intergrown with specularite (Fig. 35a). A distinctive feature, however, is that palladium minerals are partially enclosed in (Figs. 35b, c), and located on the surface of (Figs. 35d, e, f, g), gold.

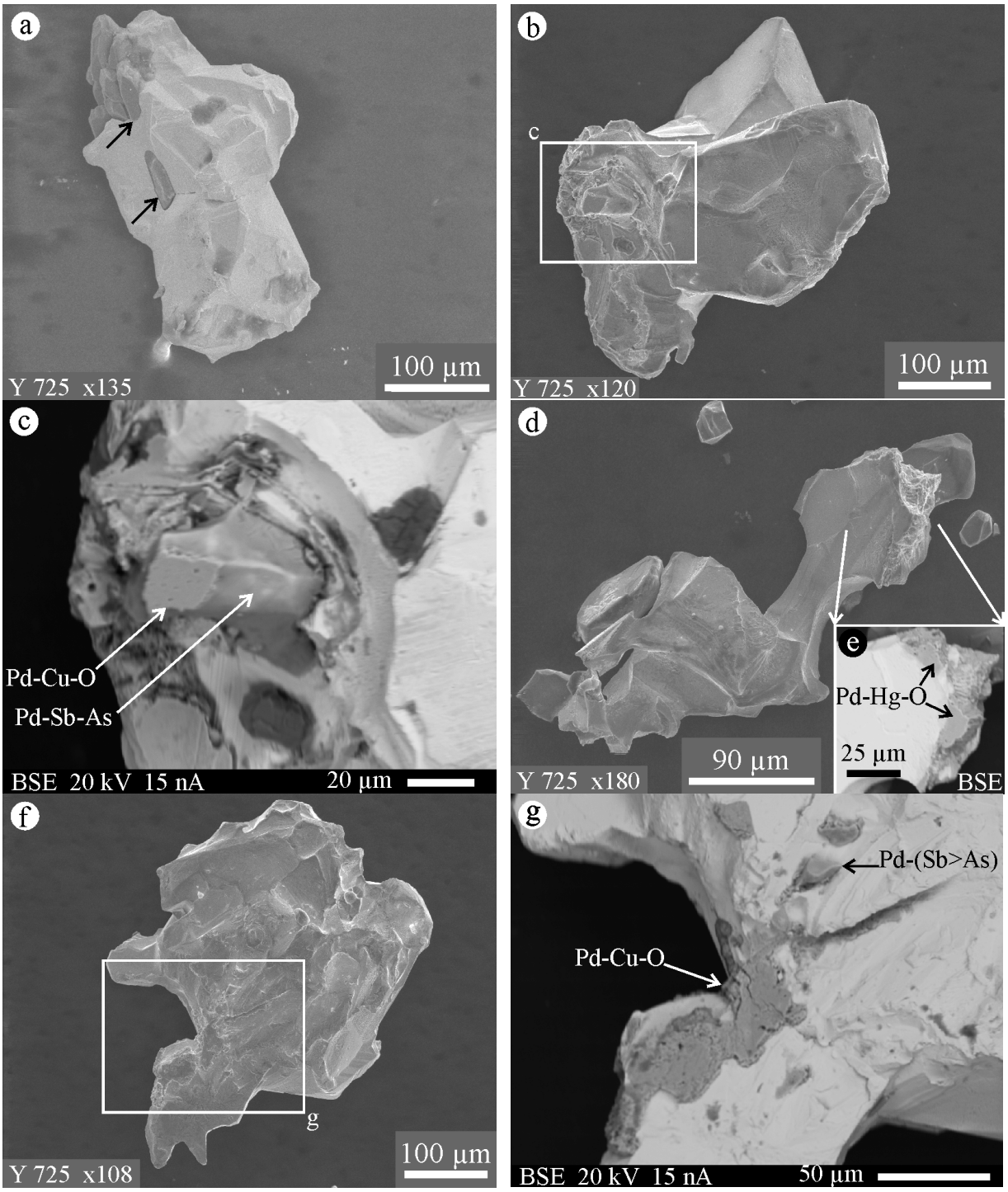

Fig. 35: Gold and associated palladium minerals, Y orebody, level 725. (a) SE image of gold intergrowth with specularite (arrows). (b) SE image of gold with an euhedral termination. (c) BSE image of the area squared in (b) to show a Pd–Sb–As phase (isomertieite?) jutting out from gold. The Pd–Sb–As phase is partially coated by a film of Pd–Cu–O. (d) SE image of a gold grain with hematite crystals (dark grey). (e) BSE image of the area indicated in (d), in which a Pd–Hg–O compound occurs on the surface of gold. (f) SE image of a gold grain, on the surface of which (g) the BSE image shows a coating of Pd–Cu–O and an As-bearing Pd–Sb phase.

Heavy-mineral concentrates obtained from the Central orebody in 1997 provided singular grains of hongshiite, PtCu. They have been described in detail by KWITKO et al. (2002), but as some peculiarities have not been illustrated in that work, further photographic documentation is given here. A number of inclusions of PGM occur in hongshiite. In addition to isomertieite, sperrylite, $PtAs_2$, sudovikovite, $PtSe_2$, and a "guanglinite" -like phase, $Pd_3(As,Sb)$, also atheneite, $(Pd,Hg)_3As$, are present (Fig. 36a). Other than the PGM, barite (Fig. 36b) and a copper selenide (Fig. 36c), of Cu:Se atomic ratio close to 1 (possibly klockmannite, CuSe), as well as an aluminosilicate compositionally analogous to kaolinite (Fig. 36d), are found as inclusions in hongshiite. Rarely observed, an almost imperceptible Te–Bi–Se-bearing Pt mineral is also included in hongshiite (Figs. 36e, f). Specular hematite (no Cr detected by EDS) is likewise found as inclusion in, and appears to be occasionally cross-cut by, hongshiite (Fig. 36e).

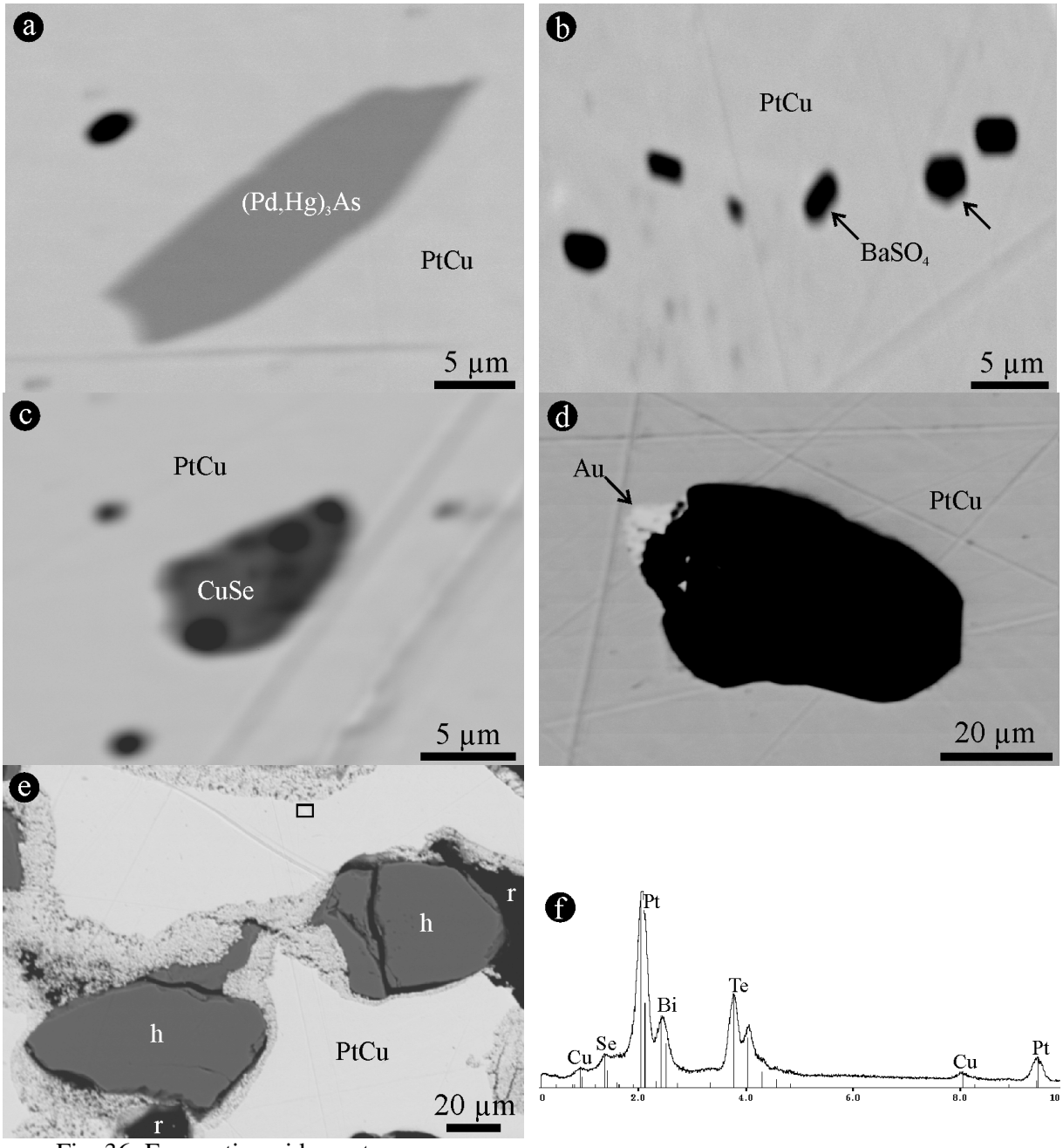

Fig. 36: For caption vide next page.

Fig. 36: BSE images of mineral inclusions in hongshiite, PtCu. (a) Atheneite, $(Pd,Hg)_3As$, and a Mg silicate (black, talc?) (b) Barite, $BaSO_4$ (arrows) and a Mg silicate (black, talc?). (c) Copper selenide, of Cu:Se atomic ratio close to that of klockmannite (CuSe). Black spots are Mg silicate. (d) Aluminosilicate, compositionally analogous to kaolinite (black), associated with gold. (e) Specular hematite, h, appears to have been cross-cut by hongshiite and then corroded by a porous Pt-rich halo (cf. Fig. 37). No Cr in the hematite was detected by EDS. Rectangle indicates an almost imperceptible Te–Bi–Se-bearing Pt mineral. (r, resin). (f) ED spectrum of the area indicated in (e) (rectangle).

Some grains of hongshiite are rimmed by a porous halo (Fig. 37a). The halo is enriched in platinum (Fig. 37b) and impoverished in copper (Fig. 37c). Electron-microprobe analysis indicates residual enrichment to virtually pure native platinum (KWITKO et al. 2002).

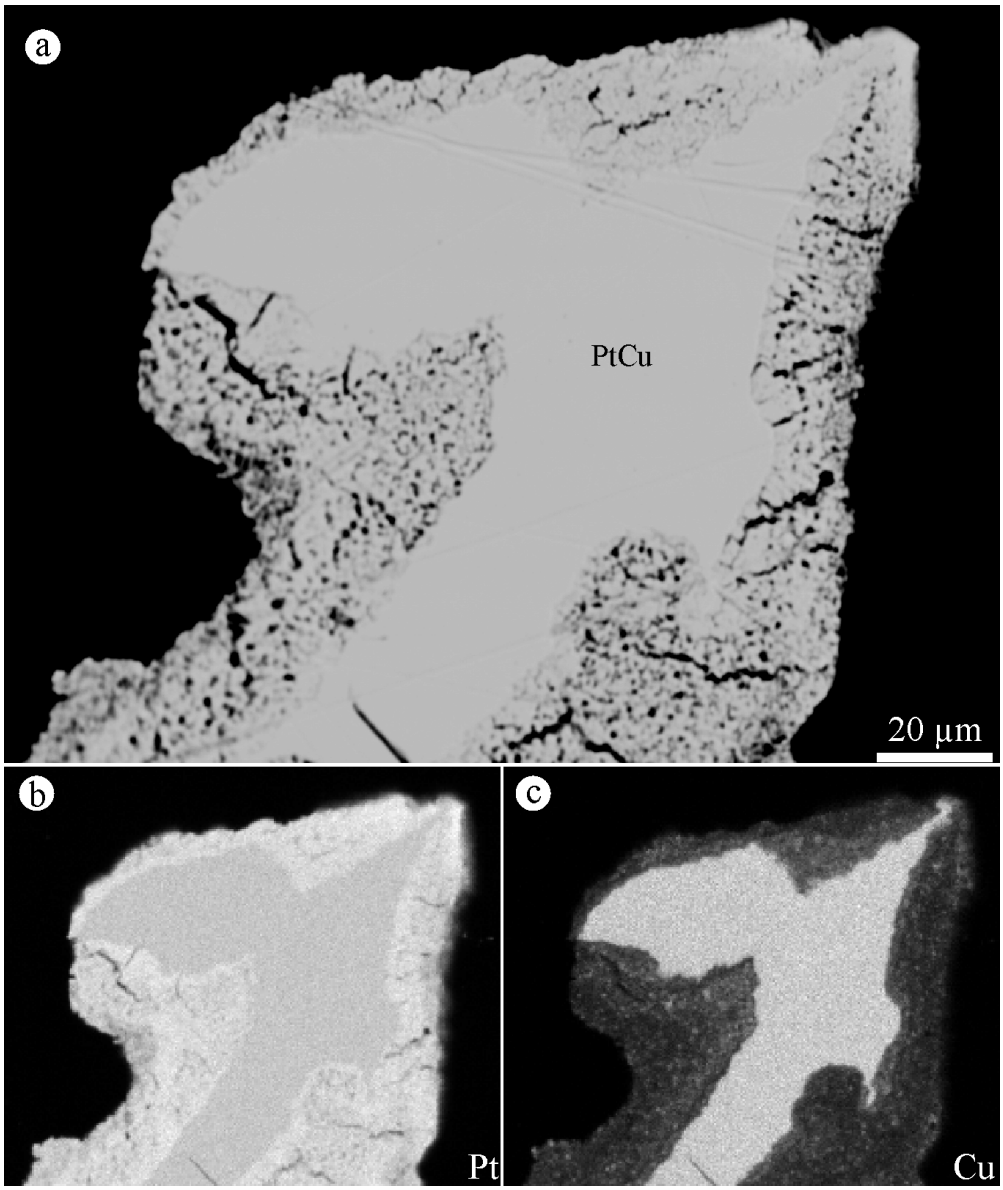

Fig. 37: (a) BSE image of hongshiite (PtCu) haloed by a porous rim. X-ray element-distribution maps of (b) Pt$L\alpha$ and (c) Cu$K\alpha$.

Composition of gold from heavy-mineral concentrates

Electron-microprobe analysis suggests that gold grains from Y (level 725) contain approximately 2 wt % Pd, whereas those from Lico (level 875) have only trace amounts (0.1-0.2 wt % Pd) and those from Central (level 740) are virtually devoid of palladium (Table 12).

Gold-bearing aggregates of fine-grained magnetite

Gold also occurs in wallrock fragments of compact aggregates of fine-grained magnetite within specularite-quartz veins from Y, level 802 (CABRAL et al. 2002d). In the fragments, palladian gold and Cu–Pt–Hg-bearing palladseite infill microfractures and interstices in the magnetite matrix (CABRAL et al. 2002d). The magnetite, extensively oxidised to hematite, i.e. martite, has chromium in amounts as high as 12 wt % Cr_2O_3 (Table 13). Along the aggregate margins, chromiferous magnetite is replaced by specular hematite of planar fabric (Fig. 38a; cf. Fig. 3a of CABRAL et al. 2002d). This specular hematite represents remains of the wallrock S_1 foliation (itabirite). In the replacement process, chromium was leached from magnetite (cf. Fig. 3b of CABRAL et al. 2002d), but only partially incorporated into the foliation-forming hematite as zoned crystals with Cr-poor core and Cr-rich margin (Fig. 38b, Table 13). Titanium, undetected in chromiferous magnetite, but in foliation-forming hematite in amounts of up to about 1 wt % Ti, seems to be extraneous and, to some extent, positively correlated with chromium (Fig. 38c).

Table 12: Electron-microprobe analyses of gold from heavy-mineral concentrates

(wt %)			Au	Pd	Ag	Cu	Total
Y	Fig. 35	Grain					
725	b	1	96.69	1.97	0.79	0.42	99.87
	f	2	96.36	1.89	0.84	0.44	99.54
		5	95.76	1.98	0.94	0.42	99.10
		8	96.32	1.96	0.67	0.44	99.39
	d	10	96.49	2.07	0.48	0.35	99.39
		14	95.75	2.54	0.52	0.33	99.14
Lico	Fig. 33						
875		5	98.00	0.15	1.22	0.08	99.45
	f	6	98.49	0.23	1.60	<0.08	100.32
		7	98.77	0.17	1.25	<0.08	100.20
		8	99.27	0.14	1.43	<0.08	100.84
		10	98.17	0.14	1.34	<0.08	99.65
		12	98.37	0.13	1.43	<0.08	99.93
	d	14	98.43	0.23	1.62	0.09	100.37
Central	Fig. 32						
740	a	1	98.30	<0.04	1.21	0.08	99.58
		4	99.14	<0.04	1.44	<0.07	100.58
		7	97.42	<0.04	1.81	0.08	99.32
	e	14	97.58	<0.04	2.37	0.08	100.03
	f	15	97.75	<0.04	1.16	0.07	98.99

Table 13: Electron-microprobe analyses of magnetite and hematite

	2a	2b	10a	11a	12a	15	18	21	25a	25b
(wt %)										
Fe_2O_3	56.91	90.09	57.86	57.04	56.16	97.93	94.61	97.65	97.64	95.07
FeO	30.86	—	31.15	30.88	30.88	—	—	—	—	—
Cr_2O_3	11.21	9.38	10.90	11.15	11.99	0.74	3.96	1.35	1.00	3.34
TiO_2	<0.03	<0.03	<0.03	<0.03	<0.03	0.78	0.86	0.91	0.76	1.04
V_2O_3	0.06	0.06	0.06	0.06	0.05	0.04	0.03	<0.02	0.05	0.03
MnO	0.18	0.11	0.15	0.17	0.19	<0.02	0.02	0.02	<0.02	0.02
SiO_2	<0.02	0.03	<0.02	<0.02	<0.02	<0.02	<0.02	0.03	<0.02	<0.02
Al_2O_3	0.18	0.17	0.17	0.18	0.18	0.22	0.10	0.10	0.23	0.20
Total	99.40	99.84	100.29	99.48	99.45	99.71	99.58	100.06	99.68	99.70

The mineral was analysed under 20 kV and 40 nA, using the *K*α emission lines and standards as follows (cf. Table 4): Cr (Cr_2O_3), V (pure metal), Si ($MnSiO_3$) and Al (kaersutite).
Microanalyses: 2a, 10a, 11a, 12a: relics of magnetite in crystals (10-50 µm) of martite (hematite); 2b: host martite of 2a; 15, 18, 21, 25a, b: foliation-forming hematite after magnetite (25a and 25b refer to microanalysis in the core and margin, respectively, of the same crystal).

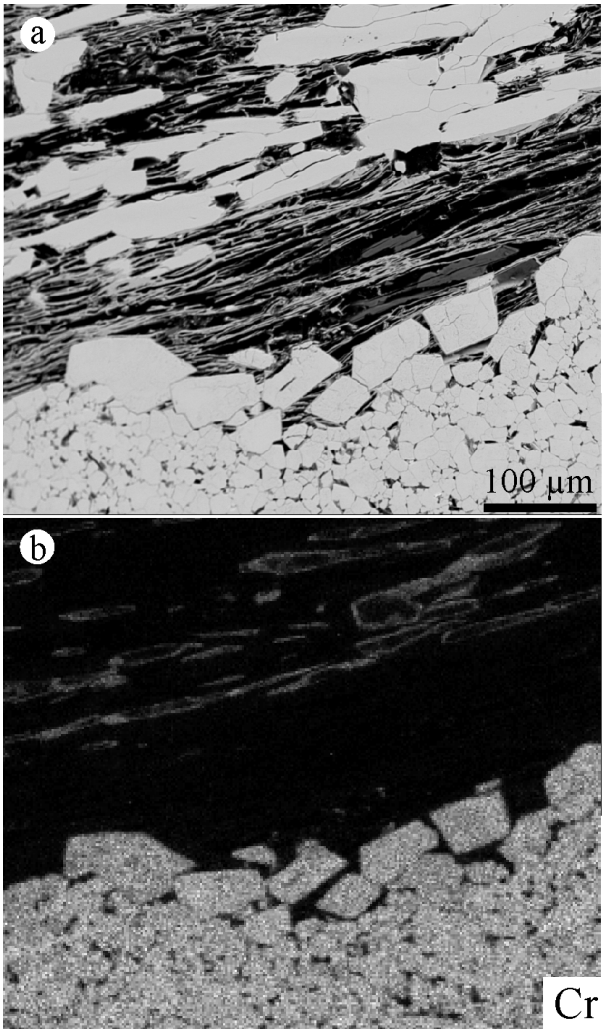

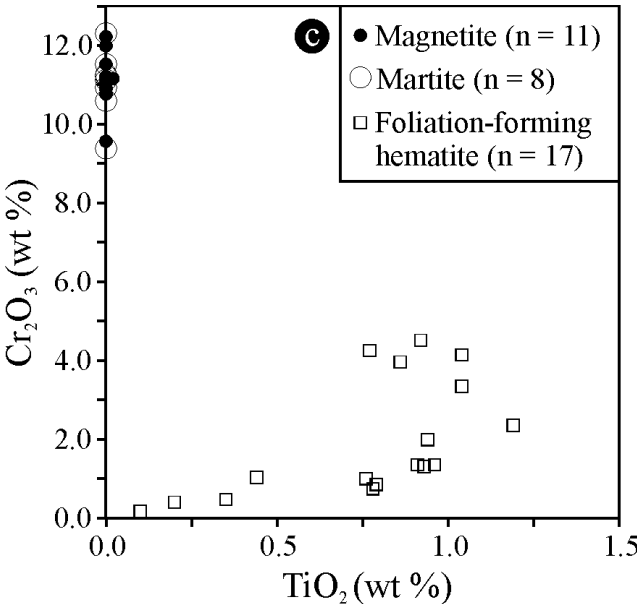

Fig. 38: (a) BSE image of a gold-bearing magnetite aggregate (bottom), i.e. a wallrock fragment within auriferous vein (Y orebody, level 802), at the contact with remains of foliation-forming specular hematite (top) from the wallrock. (b) X-ray distribution of Cr*K*α. Note that Cr is homogeneously distributed in the magnetite aggregate, but shows a zoned pattern in the hematite laths. (c) Cr_2O_3 vs. TiO_2 plot. Vide Table 13 for representative microanalyses.

A late generation of Cr-bearing specular hematite grew over chromiferous magnetite. This specularite is regarded as a vein-related imprint because it is coarser than the foliation-forming hematite, chaotically arranged (i.e. no preferred orientation), and hosts inclusions of chromiferous magnetite and gold (Fig. 39a). The vein-related specularite shows an irregular distribution of chromium (from about 3 to 6 wt % Cr), in contrast to the core-and-mantle pattern of the foliation-forming hematite (Fig. 39b, cf. Fig. 38b). Both the gold included in specularite and that found in interstices of the Cr-magnetite matrix (referred to as 'matrix gold') contain palladium (Figs. 39c, d). The matrix gold appears to have an inhomogeneous distribution of palladium (Table 14, Fig. 39d). Like palladseite (CABRAL et al. 2002d), sudovikovite, though more rarely observed, is an occasional mineral inclusion in vein-related specularite (Fig. 40).

Table 14: Electron-microprobe analyses of minerals indicated in Figure 39

	1	2	3	4	5	7
(wt %)						
Au	94.71	96.34	88.82	1.49	93.83	93.89
Pd	4.29	2.15	9.27	75.38	5.42	5.49
Ag	0.46	0.49	0.25	<0.2	0.20	0.41
Cu	<0.08	<0.08	0.08	0.08	<0.08	0.09
Fe	0.09	0.13	1.41	1.43	0.21	<0.06
Sn	<0.03	<0.03	<0.03	0.05	<0.03	<0.03
Sb	<0.03	<0.03	<0.03	14.60	<0.03	<0.03
As*	<0.05	<0.05	<0.05	8.93	<0.05	<0.05
Total	99.55	99.12	99.84	101.95	99.66	99.88

* The mineral was analysed for As using the $L\alpha$ emission line.
Microanalyses: 1, 2, 3, 5, 7: gold; 4: possibly isomertieite.

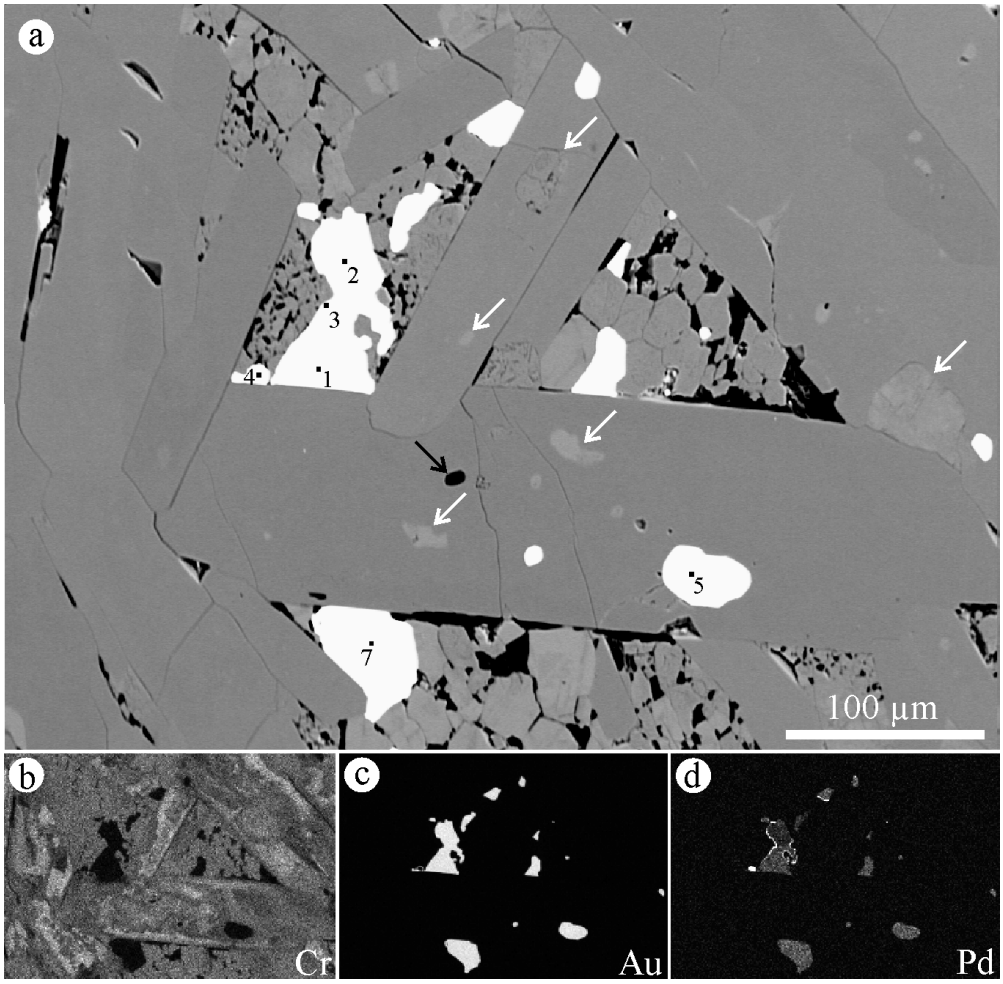

Fig. 39: (a) BSE image of laths of specular Cr-hematite (3–6 wt% Cr) grown chaotically over the granular matrix of chromiferous magnetite from a wallrock fragment within auriferous vein (Y orebody, level 802). Inclusions of gold (white), chromiferous hematite (white arrows) and a Mg silicate (black arrow) occur in the vein-related specularite only, not in the wallrock remains of foliation-forming hematite occasionally found on the surface of the Cr-magnetite aggregates. Numbers refer to microanalyses in Table 14. (b) (c) (d) X-ray element-distribution maps of Cr$K\alpha$, Au$L\alpha$ and Pd$L\alpha$, respectively.

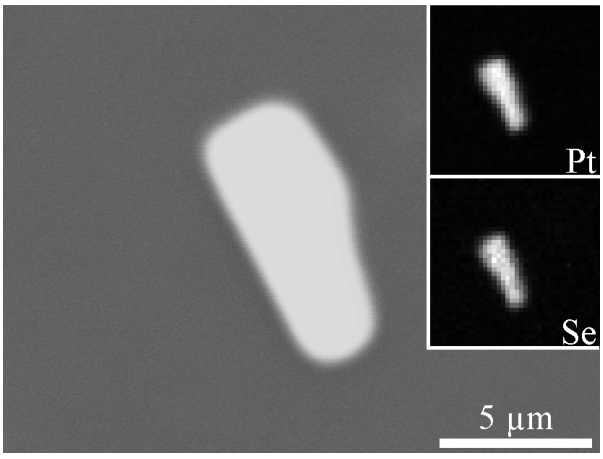

Fig. 40: Crystal of sudovikovite, $PtSe_2$, included in vein-related specularite, which grew over a matrix of Cr-magnetite (Y orebody, level 802), and X-ray element-distribution of Pt$L\alpha$ and Se$K\alpha$.

Bulk-rock geochemistry

Samples of friable specularite-quartz veins, approximately 10 cm in width, were taken from 0.5 m-long channels for panning and geochemical analysis. The geochemical analyses show contents of up to about 25700 ppb Au, 1400 ppb Pd and 190 ppb Pt (Table 15). Gold and palladium are positively correlated (Fig. 41a). Chromium contents are as high as 3780 ppm. There is a striking positive correlation between Cr and Pt, not only in the samples considered here, but also in those analysed by GALBIATTI (1999) (Fig. 41b). No compact aggregates of fine-grained Cr-magnetite like those described above were observed in the samples. Much of the chromium content may conceivably come from specularite. The vein-related Cr-specularite, which grew randomly over Cr-magnetite, has occasional inclusions of sudovikovite (Fig. 40) and Pt-bearing palladseite (CABRAL et al. 2002d). However, the highest values of chromium do not coincide with any noticeable enrichment in selenium, or in other Pt-alloying elements like As, Sb and Cu. It is also apparent that the bulk of the vein-forming specular hematite is not chromiferous, but just a fraction, considering that the chromium content of individual crystals of specularite is in the wt % range (Figs. 39a, b).

The auriferous deposits are situated relatively close to the so-called 'mafic rocks' (Fig. 29). The term applies to a weathered, crumbly, ochreous schist spotted with coarse-grained flakes of talc (cf. SANDERS 1933; DORR & BARBOSA 1963). Chemical analysis of one sample of the 'mafic rock' yields about 600 ppm Ni, 350 ppm Cr and 100 ppm Co, a transition metal assemblage that is compatible with a mafic affiliation. It also has high contents of Ba (1000 ppm) and As (~400 ppm), suggesting hydrothermal overprint. The Ba content broadly corresponds to that of S (calculated as SO_4, 0.07 wt %) and may indicate the presence of barite.

Similar to what has been noted at Gongo Soco, mercury does not reach the ppm range, but has a remarkable positive correlation with manganese (Fig. 41c). This finding seems to be consistent with the observation that local enrichment in manganese would be a guide for gold (HOCHEDER 1833; HENWOOD 1871a; THOMAS 1905; OLIVEIRA 1932).

Compared to the friable host itabirite sampled (Table 15, this study; GALBIATTI 1999), the specularite-quartz veins (*jacutinga*) are distinguished by enrichments in Au, Pd, Pt, Cr, Mn and Hg, and to some extent, Mg and Al. The wallrock has sporadic high values of Au, Pd and Pt of a few hundreds of ppb (GALBIATTI 1999).

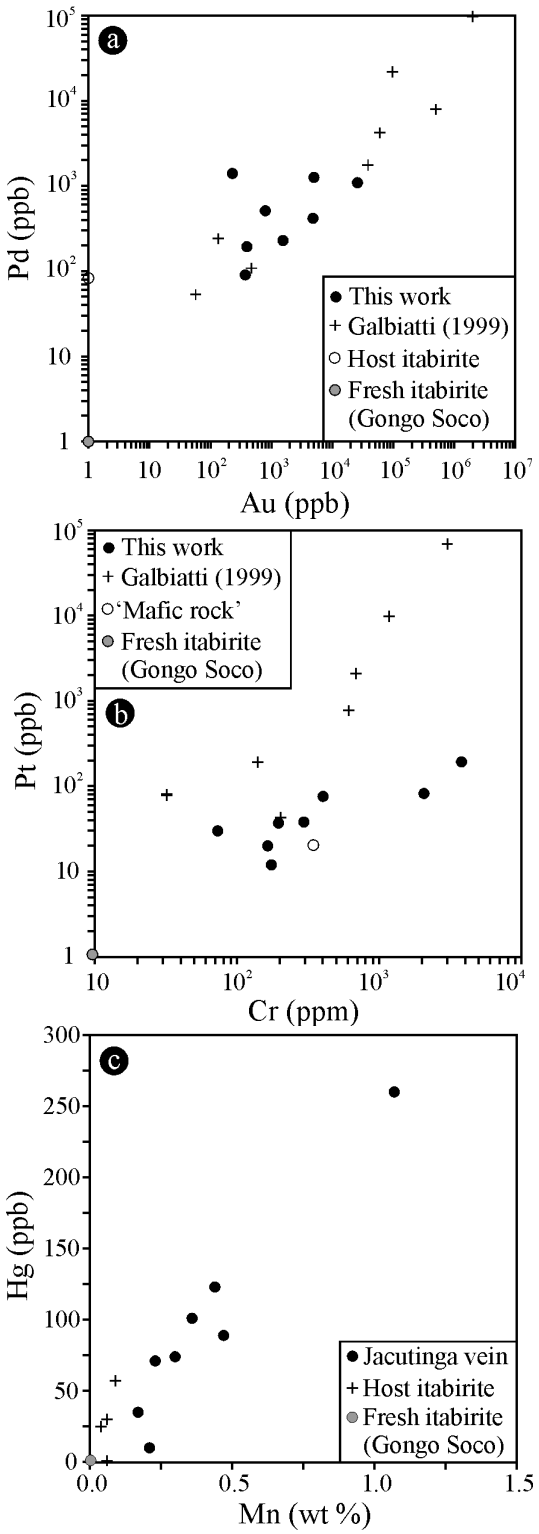

Fig. 41: Variation diagrams. (a) Au vs. Pd, (b) Pt vs. Cr and (c) Hg vs. Mn for *jacutinga* veins (data from Table 15 and GALBIATTI 1999), host itabirite (Table 15) and reference fresh itabirite (Gongo Soco, Table 10). In (b) the 'mafic rock' (crumbly, ochreous schist, Table 15) is plotted for comparison.

Table 15: Bulk-rock chemical analyses of *jacutinga* veins and host itabitite[§]

	1	2[§]	3	4	5	6	7	8	9	10[§]	11[§]	12[§]	13
Fe_2O_3 (wt %)	77.08	69.21	72.79	72.07	53.34	54.05	48.91	76.79	78.79	59.49	46.90	56.20	61.63
Mn	0.21	0.06	0.17	1.07	0.47	0.44	0.23	0.30	0.36	0.06	0.09	0.04	0.76
Al_2O_3*	1.41	1.63	0.79	0.69	1.27	1.02	0.72	0.79	0.44	0.50	0.50	0.23	3.81
MgO	<0.02	<0.02	<0.02	3.78	0.05	<0.02	0.16	0.31	0.22	<0.02	0.03	<0.02	2.83
CaO	0.02	<0.01	0.02	0.02	0.03	0.03	<0.01	0.02	<0.01	0.02	0.03	0.02	0.03
Na_2O	0.01	0.05	0.01	0.03	0.03	0.01	<0.01	<0.01	<0.01	<0.01	<0.01	<0.01	<0.01
K_2O	0.23	0.10	0.11	<0.01	<0.01	0.03	<0.01	<0.01	<0.01	<0.01	0.02	<0.01	<0.01
TiO_2	0.05	0.07	<0.02	0.04	0.03	<0.02	<0.02	<0.02	0.03	0.02	0.02	<0.02	0.08
P_2O_5	0.27	0.06	0.30	0.33	0.16	0.18	0.15	0.20	0.19	0.07	0.10	0.04	0.73
SO_4	0.03	0.01	0.02	0.02	0.01	0.01	0.01	0.01	0.01	<0.01	<0.01	<0.01	0.07
Au (ppb)	373	<2	25747	1553	4824	396	229	796	4983	<2	56	7	2
Hg	10	<5	35	260	89	123	71	74	101	30	57	25	9
Pd	90	83	1095	229	416	194	1398	512	1261	n.a.	n.a.	n.a.	14
Pt	12	9	30	20	193	82	37	38	76	n.a.	n.a.	n.a.	22
Ag (ppm)	0.4	<0.3	0.7	<0.3	0.5	0.4	<0.3	<0.3	0.3	<0.3	<0.3	<0.3	<0.3
As	21.0	6.8	27.4	11.8	<0.5	7.0	9.1	7.9	8.1	3.0	4.5	1.4	364
Ba	<50	<50	<50	<50	<50	<50	<50	<50	<50	160	76	<50	1000
Be	7	3	19	4	7	3	3	4	3	<1	1	<1	18
Bi	0.1	<0.1	0.4	<0.1	0.6	1.3	<0.1	<0.1	<0.1	<2	<2	<2	0.1
Br	<0.5	<0.5	<0.5	<0.5	<0.5	<0.5	<0.5	<0.5	2.3	<0.5	<0.5	<0.5	<0.5
Cd	<0.3	<0.3	<0.3	<0.3	<0.3	<0.3	<0.3	<0.3	<0.3	<0.3	1.3	1.1	<0.3
Co	8	2	26	16	13	18	3	4	4	2	3	1	129
Cr	174	42	73	164	3780	2060	195	294	401	13	12	12	345
Cu	38	7	25	53	8	15	2	5	16	6	5	8	61
Ge	0.6	1.1	0.4	0.5	0.3	0.2	0.4	0.8	0.8	n.a.	n.a.	n.a.	0.4
In	<0.2	<0.2	<0.2	0.4	<0.2	<0.2	<0.2	<0.2	<0.2	n.a.	n.a.	n.a.	3.4
Mo	4	<1	<1	<1	<1	<1	<1	<1	<1	<1	<1	<1	2
Ni	55	5	134	66	3	7	10	9	<1	6	11	3	588
Pb	36	6	8	21	28	84	14	11	12	<3	<3	<3	43
Rb	<15	<15	42	<15	<15	<15	<15	<15	<15	<15	<15	<15	<15
Sb	0.9	0.7	0.6	1.5	2.2	0.4	0.8	1.8	0.8	<0.1	<0.1	0.4	4.7
Sc	12.9	4.7	5.6	2.1	1.2	1.7	1.1	1.4	1.3	0.9	1.2	0.7	40.3
Se	<0.1	<0.1	<0.1	<0.1	0.1	<0.1	0.2	2.0	<0.1	<3	<3	<3	1.0
Sr	7	7	4	23	18	16	14	49	7	4	4	2	91
Te	0.3	<0.1	4.0	<0.1	0.1	0.1	<0.1	<0.1	0.1	n.a.	n.a.	n.a.	0.2
Th	1.9	1.6	0.9	0.7	0.7	0.5	0.6	0.7	0.9	0.7	0.8	0.5	5.5
Tl	<0.1	<0.1	<0.1	0.1	0.5	0.6	<0.1	<0.1	<0.1	n.a.	n.a.	n.a.	<0.1
U	10.9	2.9	47	10.5	8.7	4.7	3.9	4.5	4.7	2.0	3.3	2.1	8.2
V	83	50	96	52	10	7	44	36	93	9	12	4	69
W	4	3	<1	4	<1	<1	<1	<1	<1	<1	<1	<1	31
Y*	21	10	13	24	33	26	49	165	18	6	5	2	41
Zn	57	12	116	73	9	14	36	36	20	28	37	17	362

[§] Friable host rock (itabirite). Samples: 1–3: Lico, level 875; 4–6: Central, level 740; 7–9: Y, level 725; 10–12: Y, level 755; 13: crumbly, ochreous schist (designated as 'mafic rock', Norte area, level 880). Chemical analyses by Actlabs, Ontario, Canada. Elements determined by INAA in all samples except those in parenthesis: Au (1–9, 13), As, Ba, Br, Co, Cr, Cs, Fe, Hf, Ir, Na, Rb, Sb, Sc, Se (1–9, 13), Sn (1–9, 13), Ta, Th, U, W and Y. The remaining elements were determined by ICP. Samples 1–9 were analysed for Bi, Ge, In, Se, Sn, Te and Tl by ICP-MS. Gold, palladium and platinum determined by fire assay ICP-OEM in samples 1–9, 13; mercury by cold vapour FIMS in all samples. The following elements were sought for but not detected: Ir (<5 ppb), Cs (<1 ppm), Hf (<1 ppm), Ta (<0.5 ppm), Sn (<1 ppm* in samples 1–9 and 13, <0.01% in samples 10–12). Iron and sulphur as total Fe_2O_3 and SO_4, respectively. * May only be partially extracted. n.a. = not analysed.

4
Serra Pelada: a startling case of palladian gold mineralisation (*ouro preto*)

"*Deus no céu e Curió aqui na terra*".

Garimpeiro saying at Serra Pelada.

Serra Pelada is the most vivid example of a large-scale gold rush in Amazonia. The *garimpo*, at its peak, in 1983, had a population between 80,000 and 100,000 *garimpeiros*, with a monthly production of more than one tonne of gold. Images of clay-darkened people working in indigent conditions for a pittance were broadcasted throughout the world. The *garimpeiros*, depicted as *formigas humanas* (human ants, Fig. 3), removed with shovels and pickaxes about 12 million tonnes of overburden, turning an entire hill into a 300 x 400-m pit, which ultimately collapsed and flooded at a depth of about 130 m. The *garimpo* of Serra Pelada was the first to be taken over by the Brazilian state. The federal takeover of Serra Pelada was the continuation of the military intervention in the region (Araguaia–Tocantins), which commenced in order to annihilate a small guerrilla uprising by the combatants of the Communist Party of Brazil. Having defeated the guerrillas in 1972, the fascist, CIA-supported dictatorship, instituted by a coup d'état in 1964, had to ensure no recurrence of the guerrilla movement in the region. This was partly accomplished by the state intervention in Serra Pelada, commanded by Curió, major (and supposedly a torturer) of the SNI, the Brazilian security service. The military dictatorship was replaced by a bourgeois democratic state in 1985, but both the rural violence by landowners and the semi-feudal agrarian system of labour exploitation remain. In this context, Curió is still a dominant political figure in the area: his supposed involvement in the assassination of local *garimpeiro* leaders and in militia fomentation to control Serra Pelada has resulted in a military occupation by troops in November 2002 to prevent an armed conflict among the *garimpeiros*.

The gold rush motivated early reports on the mineralisation and mining methods (e.g. FISSGUS 1982; JORGE JOÃO et al. 1982; MEIRELES et al. 1982; MÜLLER 1984; SIEGERS & RENGER 1985; MEIRELES & SILVA 1988), as well as investigations by social scientists (e.g. CLEARY 1990). The gold mined by the *garimpeiros* was found in a near-surface lateritic profile, as bonanza-style ore containing coarse-grained, characteristically dendritic aggregates of palladian gold (MEIRELES & SILVA 1988). The friable, heavily weathered material, in which the bonanza ore occurred, could be removed and washed by the *garimpeiros*. The near-surface bonanza ore was then completely mined out. Consequently, its mineralogy and geochemistry have remained unexamined, and it has generally been assumed that deep tropical weathering was decisive for the extreme metal enrichment (MEIRELES & SILVA 1988, COSTA 1997; TALLARICO et al. 2000a, MORONI et al. 2001; VILLAS & SANTOS 2001; GRAINGER et al. 2002). Remains of the bonanza ore seem to be restricted to one drill, recovered in 1982 from the central part of the *garimpo*. The drill core is exceptionally enriched in gold, palladium and platinum (Fig. 42), and has provided sample material not only for bulk-rock chemical analysis, but also dendritic aggregates of gold for electron-microprobe analysis and quartz crystals for reconnaissance fluid inclusion microthermometry. These data, which complement those published elsewhere (CABRAL et al. 2002a, b), are presented here. This chapter considers the near-surface mineralisation only; the deep-seated mineralisation (>150 m) has

been addressed by TALLARICO et al. (2000a), MORONI et al. (2001), GENER et al. (2002) and GRAINGER et al. (2002).

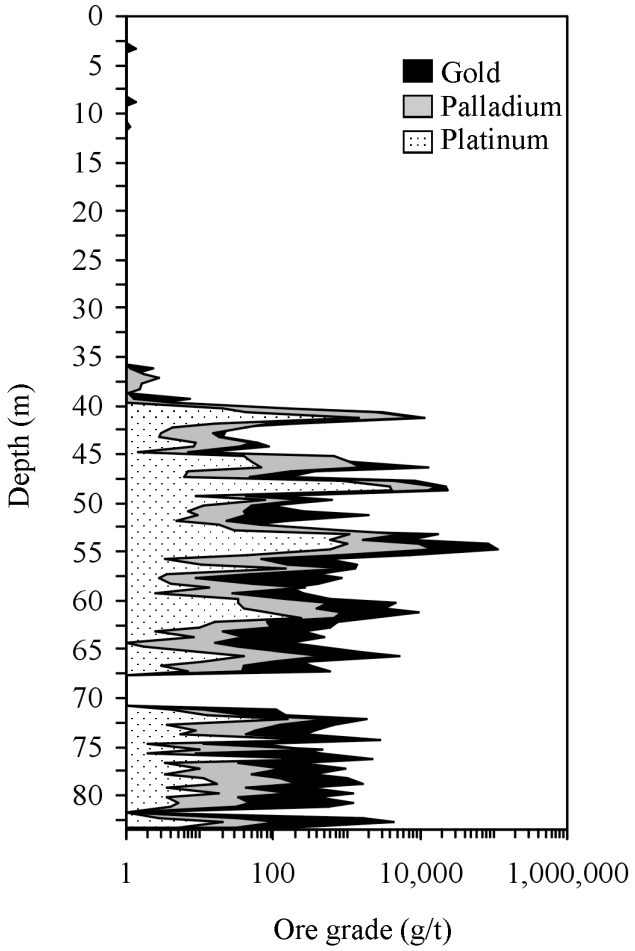

Fig. 42: Distribution of gold, palladium and platinum with depth in drill core SP-32 (from CABRAL et al. 2002a). Gold was determined by atomic absorption spectroscopy (aqua regia digestion) at CVRD; palladium and platinum by fire assay at Nomos, Rio de Janeiro (CVRD, internal files). Data on the interval 67.5–71.0 m are missing. The upper 40 m of the drill core consist of barren, red metasiltstone; the bonanza ore is a soft, powdery, organic carbon-bearing, ferruginous material with silica-, kaolinite- and hematite-rich fragments.

Geological setting and the Serra Pelada deposit

Serra Pelada is one of the diverse ore deposits hosted by the Itacaiúnas Supergroup, which encompass iron oxide copper–gold deposits and world-class deposits of iron and manganese (Fig. 43) (e.g. ANDRADE et al. 1986; COELHO 1986; COELHO & RODRIGUES 1986; HUHN & NASCIMENTO 1997; REQUIA & FONTBOTÉ 2000; RONZÊ et al. 2000; SOUZA & VIEIRA 2000; TAZAVA & OLIVEIRA 2000; TALLARICO et al. 2000b; DARDENNE & SCHOBBENHAUS 2001; VILLAS & SANTOS 2001). The Itacaiúnas Supergroup is an Archaean volcano-sedimentary sequence deposited in a continental rift system (OLSZEWSKI et al. 1989), in which the deposition of a ~400 m-thick sequence of banded iron formation (Carajás Formation, Grão Pará Group) is constrained between ~2750 and ~2740 Ma (U–Pb zircon data, TRENDALL et al. 1998). The volcano-sedimentary belt is delineated by the E–W-trending Carajás and Cinzento strike-slip systems, which record evidence for recurring deformation episodes since *ca.* 2.6–2.7 Ga (PINHEIRO & HOLDSWORTH 1997). The supracrustal rocks of the Itacaiúnas Supergroup were metamorphosed from very low to medium grade and intruded by Archaean to Proterozoic granitoids (OLSZEWSKI et al. 1989; MACHADO et al. 1991; BARROS et al. 1997). Reviews of the geological setting and metallogenesis of the Carajás mineral province can be found elsewhere (e.g. DOCEGEO 1988; DARDENNE & SCHOBBENHAUS 2001; VILLAS & SANTOS 2001).

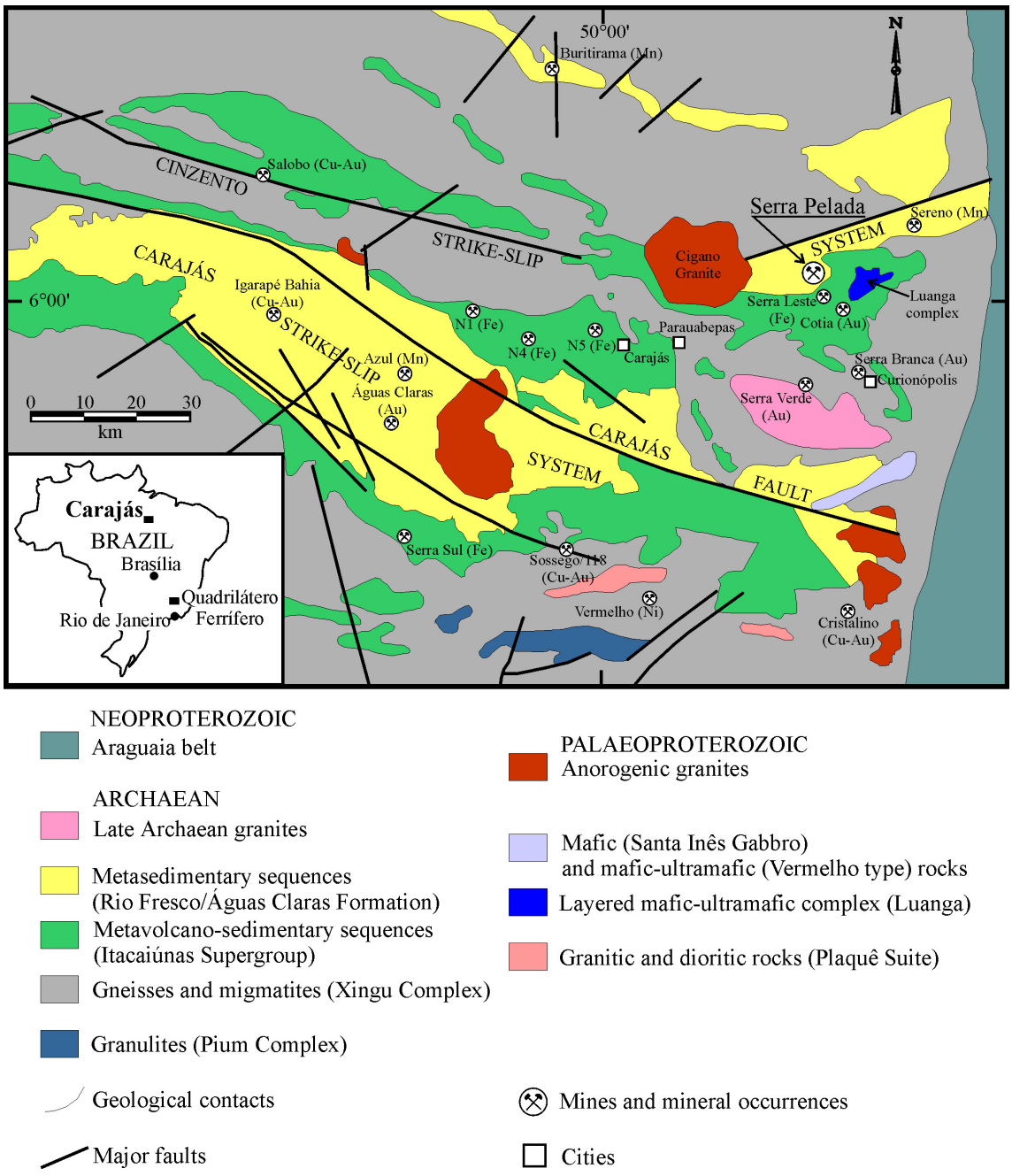

Fig. 43: Simplified geological map of the Carajás mineral province (DARDENNE & SCHOBBENHAUS 2001, and references therein).

The Serra Pelada deposit is hosted by weakly metamorphosed sedimentary rocks of the Rio Fresco Formation, a fluvial to shallow marine sequence of Late Archaean age comprising metaconglomerate, metasandstone, dolomitic marble and metasiltstone (Fig. 44) (CUNHA et al. 1984; MEIRELES & SILVA 1988; DOCEGEO 1988; TALLARICO et al. 2000a; MORONI et al. 2001; GRAINGER et al. 2002). The Rio Fresco Formation rests unconformably on the volcano-sedimentary Rio Novo sequence, which is intruded by the chromite- and PGE-mineralised Luanga layered mafic-ultramafic complex (SUITA & NILSON 1988; DIELLA et al. 1995) of Archaean age (2763 ± 6 Ma; MACHADO et al. 1991) (Fig. 43). Reactivation of the Cinzento strike-slip system at *ca.* 1.9 Ga affected all those rocks (PINHEIRO & HOLDSWORTH 1997).

This fault system shows evidence of neotectonic activity, as indicated by small-scale earthquakes, and hot springs about 50 km west-north-west from Serra Pelada (PINHEIRO & HOLDSWORTH 1997). The 1.88 Ga anorogenic Cigano Granite outcrops about 15 km west from Serra Pelada (MACHADO et al. 1991). The Rio Fresco Formation is also intruded by dioritic dykes and plugs (TALLARICO et al. 2000a), which have tentatively been related to the 2.74 Ga Plaquê Suite by GRAINGER et al. (2002), and by younger, 198 Ma gabbroic dykes (MEIRELES & SILVA 1988). $^{40}Ar/^{39}Ar$ dating of K-poor, Ba-bearing Mn oxide from Serra Pelada has yielded two distinct ages, 35 ± 1 Ma and 44 ± 2 Ma (VASCONCELOS et al. 1994).

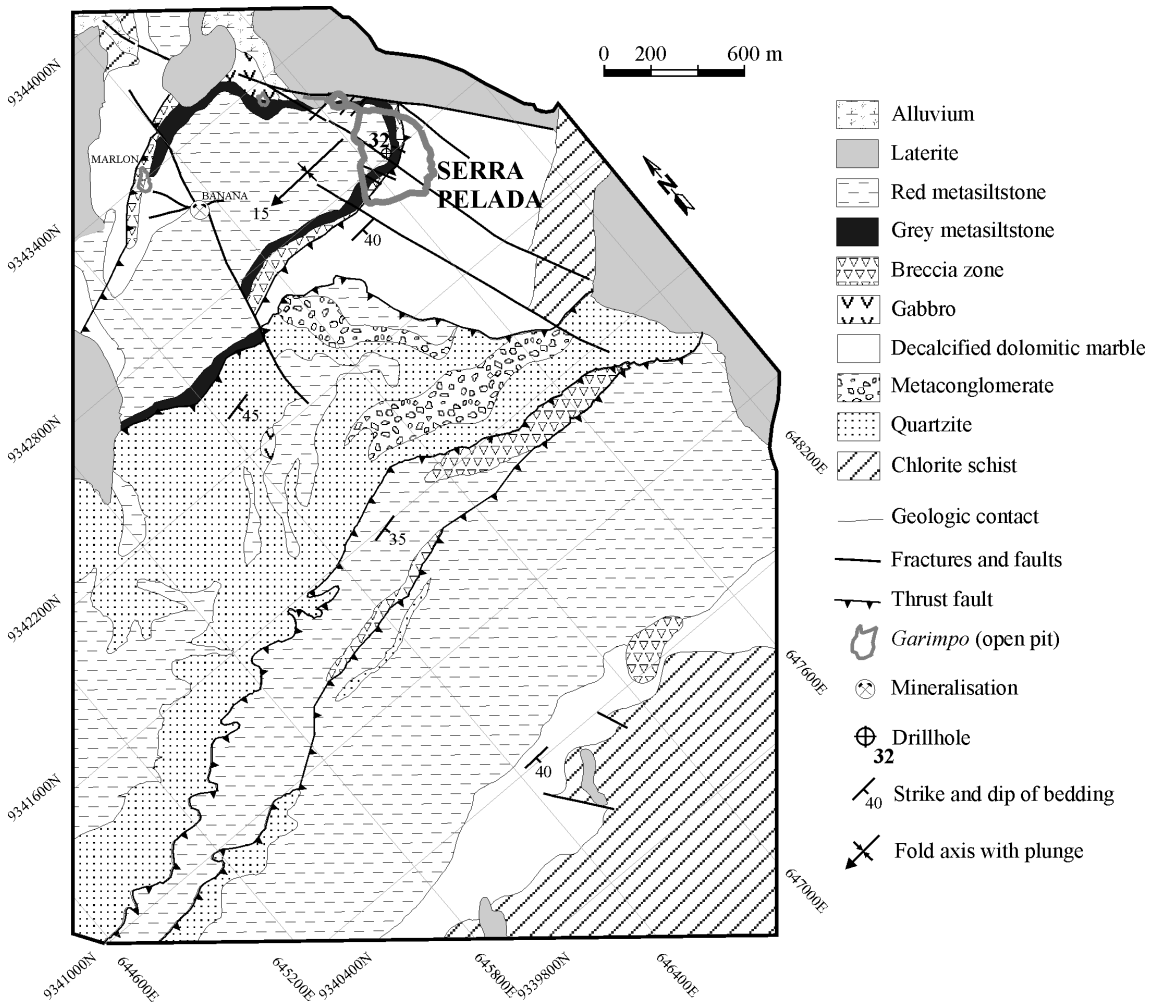

Fig. 44: Simplified geological map of the Serra Pelada area (from TALLARICO et al. 2000a) with location of drill hole SP-32. Thick grey lines delineate the *garimpo* (open pit) of Serra Pelada. Coordinates are in UTM.

The mineralisation is located in the weathered hinge zone of a recumbent syncline and roughly follows the contact between dolomitic marble and carbonaceous metasiltstone (TALLARICO et al. 2000a; GRAINGER et al. 2002). The ore shoots are enveloped by a silicification zone, with which manganiferous breccias are spatially associated. The Mn oxide-cemented breccias are interpreted to be generated by collapse of open spaces left by decalcification of the dolomitic marble (TALLARICO et al. 2000a). The base of the decalcification profile is at a depth of about 300 m (TALLARICO et al. 2000a). The mineralisation found at depth (>150 m) consists of brecciated, fine-grained carbonaceous

rocks with variable amounts of quartz, amorphous carbon (1–10 wt %), white mica, kaolinite, hematite, goethite and manganese oxide (TALLARICO et al. 2000a; MORONI et al. 2001). GRAINGER et al. (2002) specify an ore type associated with massive hematite metasomatism and minor siderite veins in marble. Close to the ore shoots, the metasilstone wallrocks were affected by quartz-chlorite veining with minor sulphides (TALLARICO et al. 2000a). Below the base of decalcification, the dolomitic marble has an alteration assemblage of chlorite, muscovite and magnetite, with minor sulphides (TALLARICO et al. 2000a).

Sample material and analytical techniques

Aggregates of gold were picked from the highest-grade depth interval of drill core SP-32 (54.5–55.0 m with 132,000 g/t Au, 11,400 g/t Pd, 359 g/t Pt; CABRAL et al. 2002a) for imaging with a Leiz ISI Super 40/3A scanning electron microscope (TU Clausthal). Polished sections were then prepared for ore microscopy and electron-microprobe analysis with a Cameca SX100 (TU Clausthal). For analytical conditions, vide corresponding section in the Gongo Soco chapter (or CABRAL et al. 2002a, b).

Euhedral to subhedral crystals of quartz, 1–2 cm in length, were recovered from the powdery material of depth intervals 54.5–55.0 and 61.5–62.0 m for fluid inclusion petrography and microthermometry with a Fluid Inc.-adapted USGS gas-flow heating/freezing stage. The thermocouple was calibrated under operating temperatures of –56.6, 0.0 and 374.1°C using Syn Flinc synthetic fluid inclusion standards. The analytical error is up to 1°C. Salinities were calculated following BODNAR (1993).

Additional samples of the near-surface bonanza ore were collected from drill core SP-32 to complement published data (CABRAL et al. 2002a). The chemical analyses were carried out at Activation Laboratories, Ontario, Canada, using a number of analytical techniques as noted in the tables.

Near-surface bonanza ore

The near-surface ore, as based on drill core SP-32 (Fig. 42), is characterised by dendritic aggregates and threads of Pd-bearing gold (Fig. 45) within a completely disaggregated, soft, ferruginous, carbon-bearing, clayey material. Some euhedral crystals of quartz, up to 2 cm long, are interspersed in the powdery material. Rock fragments of few centimetres in length give the impression that the original rock was a breccia. Macroscopically, the fragments are of (1) whitish, kaolinite-like material, (2) greyish, silica-rich material, (3) greyish to blackish, carbonaceous phyllite and (4) reddish to blackish, hematite-rich material.

The aggregates and threads of dentritic gold have a darkish colour. MEIRELES & SILVA (1988) pointed out that palladian gold is preferentially dark and associated with carbonaceous, grey metasiltstone. Such darkish colour is due not only to a goethite-like coating on palladian gold (Figs. 45a, b), but also to (1) an intergrowth of coarse-grained palladian gold and a Ba-bearing Mn oxide (Fig. 46a), with which fine-grained palladian gold is intimately associated (Fig. 46b), and (2) to minor but notable Pd–O phase on the surface of palladian gold (Fig. 46c). Whereas the arborescent form is similar to the palladian gold from Hope's Nose, Devon, England (HARRISON & FULLER 1987), the presence of Pd–O on the surface of palladian gold makes the Serra Pelada gold comparable to the *ouro preto* of Minas Gerais.

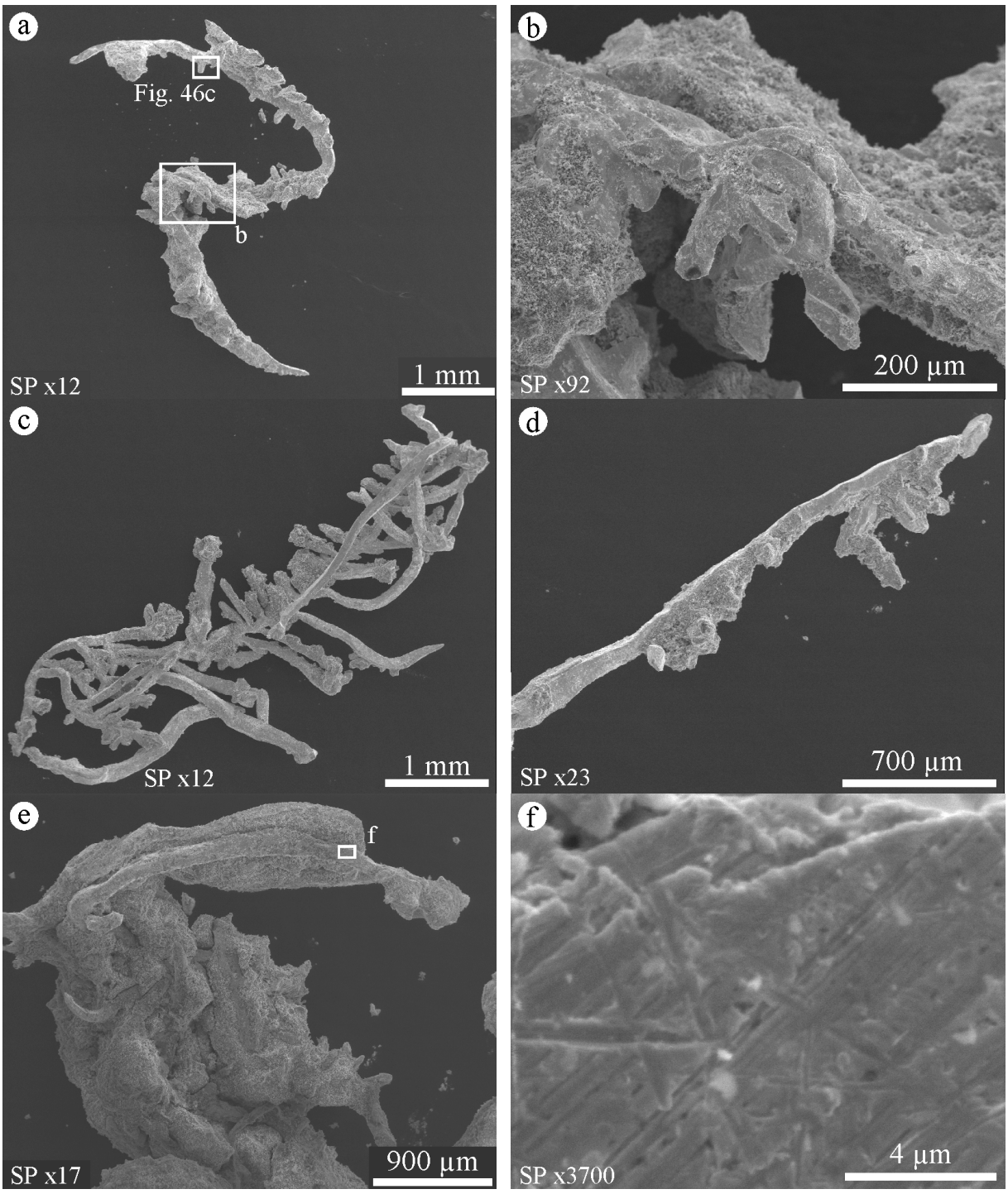

Fig. 45: SE images of aggregates and threads of palladian gold from drill core SP-32 (a-d, depth interval 54.5 to 55.0 m; e-f, 55.0 to 55.5 m). (a) Contorted thread of gold. (b) Detail of the area squared in (a) to show overgrowth of goethite-like masses. (c) Arborescent gold. (d) Thread of gold. (e) Contorted aggregate of dendritic gold. (e) Detail of the squared area in (e) to evince local striae on the surface of gold.

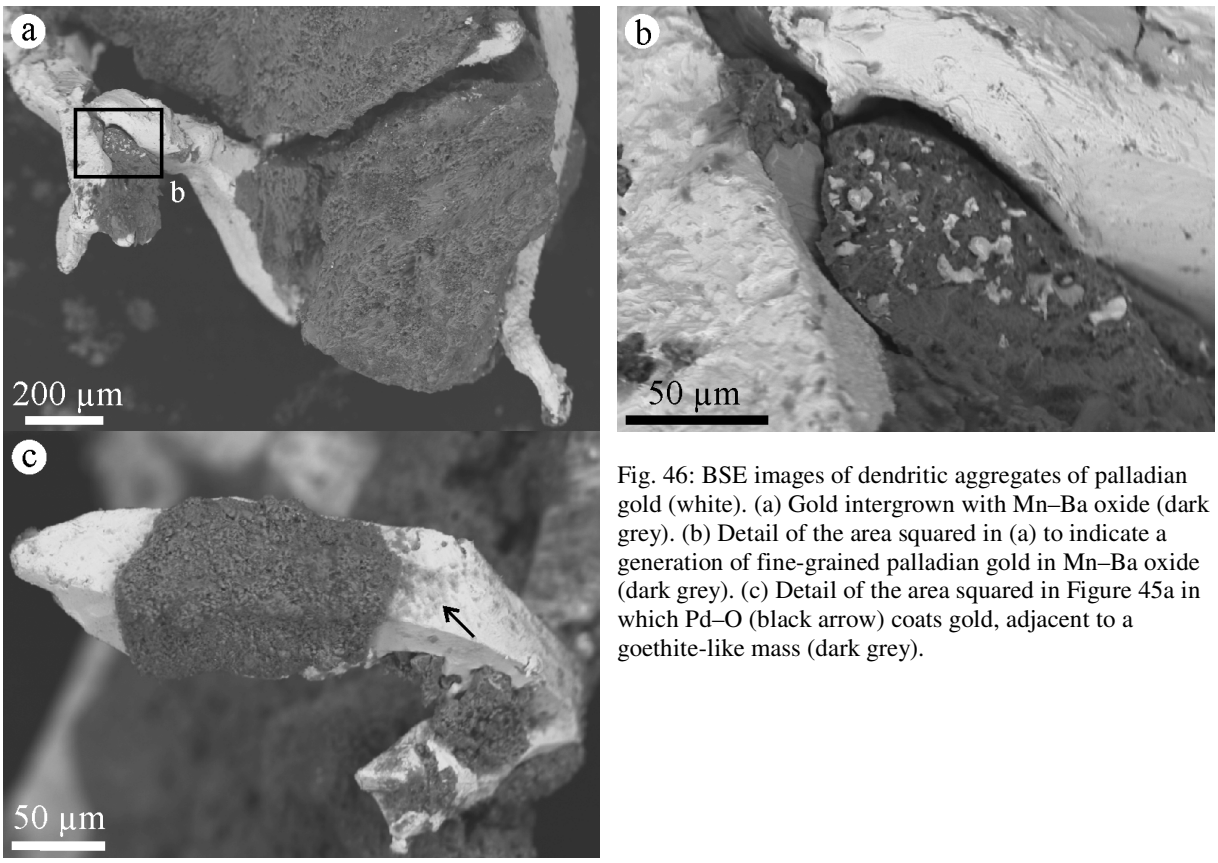

Fig. 46: BSE images of dendritic aggregates of palladian gold (white). (a) Gold intergrown with Mn–Ba oxide (dark grey). (b) Detail of the area squared in (a) to indicate a generation of fine-grained palladian gold in Mn–Ba oxide (dark grey). (c) Detail of the area squared in Figure 45a in which Pd–O (black arrow) coats gold, adjacent to a goethite-like mass (dark grey).

Much of the dendritic gold has a uniform content of about 7 wt % Pd, suggesting an empirical stoichiometry of Au_7Pd (CABRAL et al. 2002a, b). The coarse-grained crystals of "Au_7Pd" occasionally host subhedral to euhedral (5–20 µm in length) inclusions of Pd- and Pt-bearing minerals. Locally abundant, they comprise "guanglinite", Pd_3As, Sb-bearing "guanglinite", $Pd_3(As,Sb)$, sudovikovite, $PtSe_2$, palladseite, $Pd_{17}Se_{15}$, and unnamed alloys of Pd–Pt–Se and Pd–Se (CABRAL et al. 2002a, b). Native palladium characteristically occurs intimately associated with a Pd–O phase in the goethite coating (Fig. 47a, Table 16).

The composition of gold, however, is not ubiquitously constant. This is the case of the fine-grained gold intergrown with a Mn–Ba oxide, possibly romanèchite, as illustrated in Figure 46b. The romanèchite-like matrix, in which the coarse-grained dendritic gold of Figure 46a is set, resembles a breccia. It contains hematite-bearing fragments in a ferruginous matrix, with laths of K-bearing white mica and kaolinite (up to 30 µm in length), which is penetrated by Au-hosting masses of Mn–Ba oxide (Fig. 47b). The Mn–Ba oxide-related gold has about 2 wt % Pd, referred to as Pd-poor gold (cf. CABRAL et al. 2002b), and is intergrown with an isotropic Pd–As–Sb phase compositionally analogous to isomertieite (Fig. 47c, Table 16). The mineral assemblage Pd-poor gold–isomertieite–romanèchite cross-cuts crystals of Pd–Hg-bearing gold, to which crystals of atheneite, $(Pd,Hg)_3As$, are attached (Fig. 47c, Table 16). Eventually, crystals of atheneite are fractured, sealed by Pd-poor gold-hosting romanèchite and partially altered to a Pd–Hg–O phase (Fig. 48).

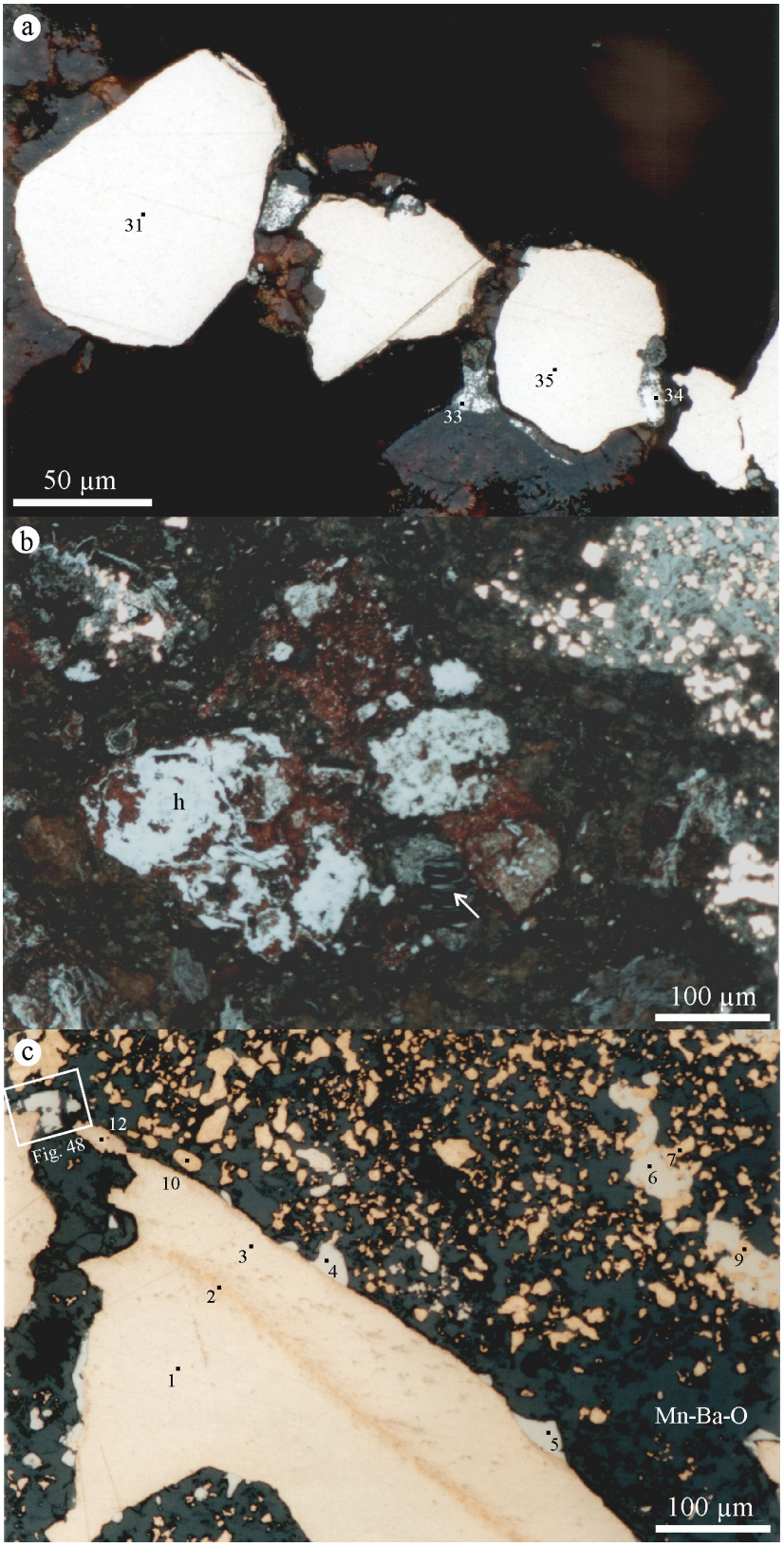

Fig. 47: For caption vide next page.

Fig. 47: Reflected-light photomicrographs of aggregates of gold (oil immersion). Numbers indicate microanalyses in Table 16. (a) Crystals of "Au_7Pd" (whitish yellow) from a thread of gold. The crystals are partially rimmed by a coating of goethite (dark grey), where masses of native palladium (bright white, microanalyses 33 and 34) occur in intimate association with a Pd–O phase (light grey). (b) Hematite-bearing fragment, h, in a goethite-rich matrix with laths of K-bearing white mica and kaolinite. White arrow denotes a crystal of K-bearing white mica with stripes of a Mn–Ba–O phase. The goethite-rich matrix is flooded by a romanèchite-like mass (light grey) spotted with Pd-poor gold, with about 2 wt % Pd (bright whitish yellow). (c) Dendritic, coarse-grained crystal of Pd–Hg-bearing gold (microanalyses 1–3 and 12), on the surface of which crystals of atheneite (microanalyses 4 and 5) are located, is cross-cut by a romanèchite-like mass containing fine-grained crystals of Pd-poor gold (about 2 wt % Pd, microanalyses 7, 9 and 10) and isomertieite (microanalysis 6).

Table 16: Electron-microprobe analyses of gold and associated PGM

	1	2	3	4	5	6	7	9	10	12	31	33	34	35
(wt %)														
Au	90.03	95.96	91.14	0.78	0.90	1.04	96.49	96.34	95.90	93.77	91.97	1.05	1.06	92.13
Pd	8.38	2.52	7.04	68.30	68.16	75.62	2.02	2.34	2.45	5.06	7.45	86.20	97.91	6.99
Ag	<0.2	0.26	0.33	<0.2	0.25	<0.2	<0.2	<0.2	0.32	<0.2	<0.2	<0.2	<0.2	<0.2
Hg	1.64	<0.3	1.13	13.96	14.02	<0.3	<0.3	<0.3	<0.3	0.37	<0.3	<0.3	<0.3	<0.3
Cu	0.59	0.65	0.55	<0.08	<0.08	0.13	0.68	0.68	0.59	0.58	<0.08	0.15	0.12	<0.08
Fe	<0.06	<0.06	<0.06	<0.06	<0.06	<0.06	0.10	<0.06	0.07	<0.06	<0.06	3.05	0.69	<0.06
Sn	<0.03	<0.03	<0.03	<0.03	<0.03	0.05	<0.03	<0.03	<0.03	<0.03	<0.03	<0.03	<0.03	<0.03
Sb	<0.03	<0.03	<0.03	<0.03	<0.03	14.52	<0.03	<0.03	<0.03	<0.03	<0.03	<0.03	<0.03	<0.03
As	<0.05	<0.05	<0.05	17.05	16.65	9.17	<0.05	<0.05	<0.05	<0.05	<0.05	8.40	0.16	<0.05
Total	100.64	99.40	100.20	100.09	99.97	100.53	99.30	99.35	99.33	99.78	99.42	98.86	99.93	99.12
apfu	1	1	1	4	4	15	1	1	1	1	8	1	1	8
Au	0.826	0.931	0.847	0.017	0.019	0.083	0.940	0.938	0.930	0.891	6.957	0.005	0.006	7.015
Pd	0.142	0.045	0.121	2.723	2.727	11.103	0.036	0.042	0.044	0.089	1.043	0.823	0.977	0.985
Ag	—	0.005	0.006	—	0.010	—	—	—	0.006	—	—	—	—	—
Hg	0.015	—	0.010	0.295	0.298	—	—	—	—	0.003	—	—	—	—
Cu	0.017	0.020	0.016	—	—	0.032	0.021	0.020	0.018	0.017	—	0.002	0.002	—
Fe	—	—	—	—	—	—	0.003	—	0.002	—	—	0.056	0.013	—
Sn	—	—	—	—	—	0.006	—	—	—	—	—	—	—	—
Sb	—	—	—	—	—	1.863	—	—	—	—	—	—	—	—
As	—	—	—	0.965	0.946	1.913	—	—	—	—	—	0.114	0.002	—

Microanalyses: 1–3 and 12: coarse-grained palladian gold (Fig. 47c); 4 and 5: atheneite (Fig. 47c); 6: isomertieite (Fig. 47c); 7, 9 and 10: fine-grained gold (Fig. 47c); 31 and 35: "Au_7Pd" (Fig. 47a); 33 and 34: native palladium (Fig. 47a). X-ray line (standard in parenthesis) used: As$L\alpha$ (InAs); all other elements as described in CABRAL et al. (2001).

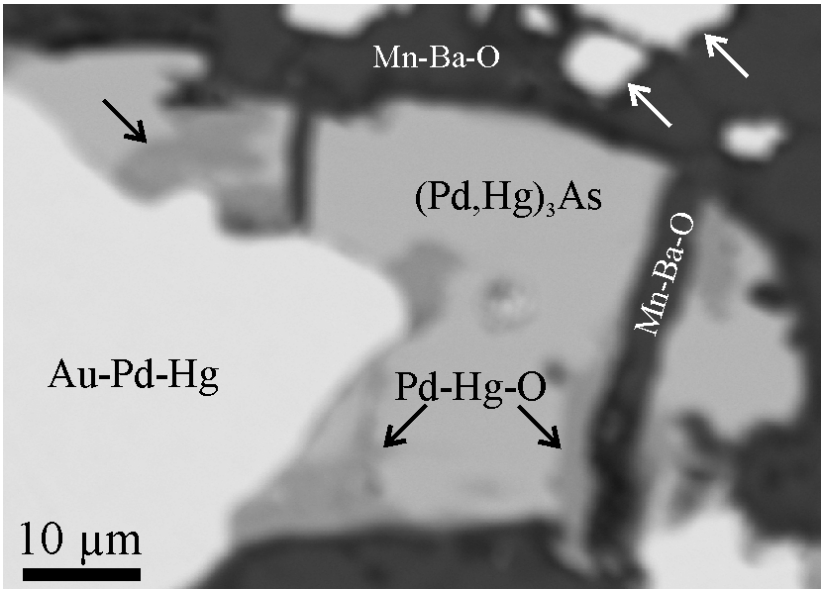

Fig. 48: BSE image of the area squared in Fig. 47c to evince a crystal of atheneite, $(Pd,Hg)_3As$, in which the microfractures are sealed by a Mn–Ba–O phase (possibly romanèchite). White arrows indicate Pd-poor gold (about 2 wt % Pd) intergrown with the Mn–Ba–O phase. The crystal of atheneite is altered to a Pd–Hg–O phase (black arrows).

Some rock fragments of hematite-rich material were recovered to prepare polished sections for ore microscopy. What macroscopically appeared to be porous, ferruginous aggregates has turned out to be a breccia composed of hydrothermal quartz cemented by fine-grained laths of hematite (Fig. 49). The clasts of vein quartz occasionally contain inclusions of zircon (≤10 µm), Fe–Mg-bearing Ca carbonate (≤15 µm); La–Ce-bearing Ca phosphate (≤5 µm), pyrite and Fe–Cu sulphide (≤10 µm). Accessory titanium oxide and traces of sulphide minerals (pyrite, chalcopyrite and a Zn sulphide) are associated with the platy hematite.

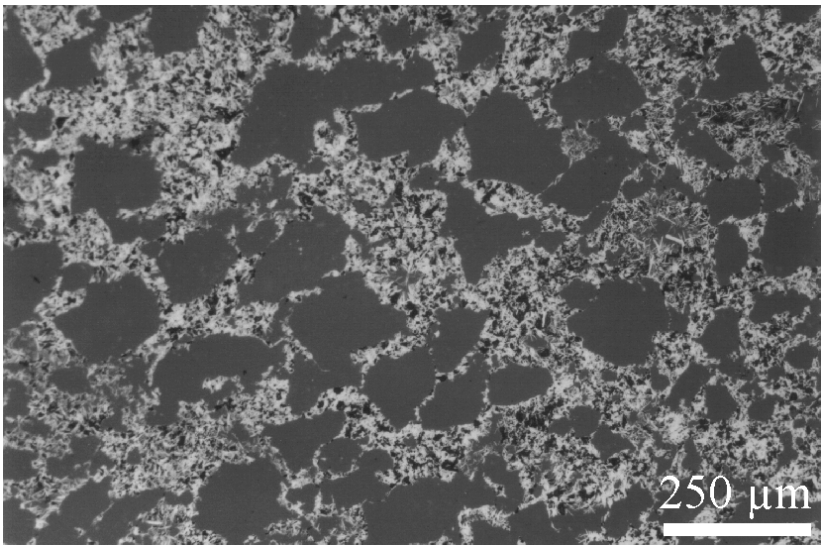

Fig. 49: Reflected-light photomicrograph (air) of a platy hematite-cemented (white) breccia; the clasts are of vein quartz (dark grey). The fragment was recovered from clayey, ferruginous, powdery material at 72.0–72.5 m, drill core SP-32.

In summary, the powdery material of drill core SP-32, in which aggregates of dendritic palladian gold occur, was originally a breccia.

Reconnaissance fluid inclusion microthermometry

Euhedral to subhedral crystals of quartz contain fluid inclusions (10–80 µm in length) of primary origin that decorate growth zones (cf. ROEDDER 1984). Trails of secondary inclusions along cross-cutting microcracks are numerous, but were disregarded in the reconnaissance study. Most primary inclusions consist of an aqueous phase and a vapour bubble, though some have no vapour bubble at room temperature (Fig. 50). After cooling, the vapour bubbles of some fluid inclusions from the depth interval 54.5–55.0 m failed to nucleate, indicating metastability, a common phenomenon in high-density aqueous inclusions with homogenization temperatures below about 150°C (cf. VAN DEN KERKHOF & HEIN 2001). Homogenization temperatures and salinities range from about 97 to 175°C and 22 to 25 wt % NaCl equiv. (Fig. 51, Table 17). First melting temperatures are between -57.3 and -46.2°C, suggesting a Ca-rich component in the trapped fluids (CRAWFORD 1981). In all fluid inclusions examined, salt hydrates of unknown composition were observed in addition to ice; the temperatures of final hydrate melting vary from -16 to -7°C (Table 17).

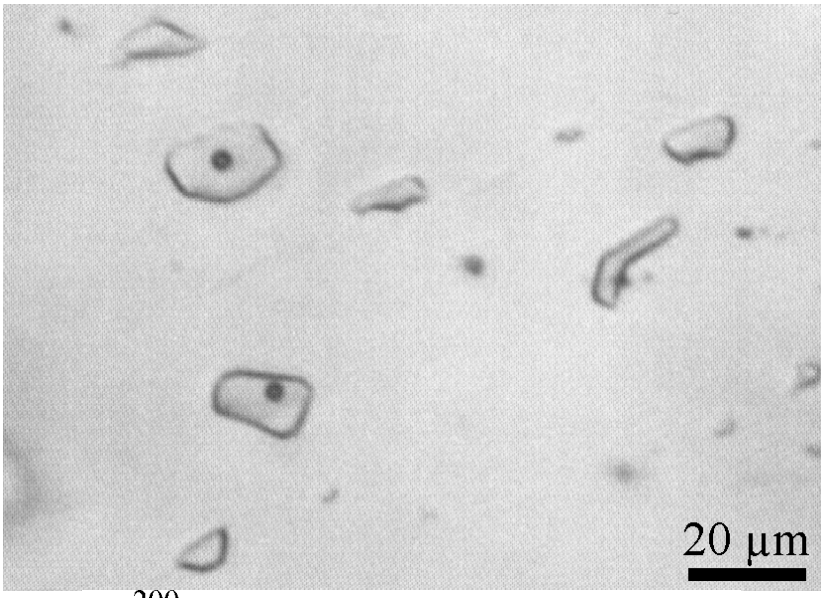

Fig. 50: Photomicrograph of primary fluid inclusions in quartz crystal from depth interval 54.5–55.0 m. Note the presence of aqueous inclusions without vapour bubble at room temperature.

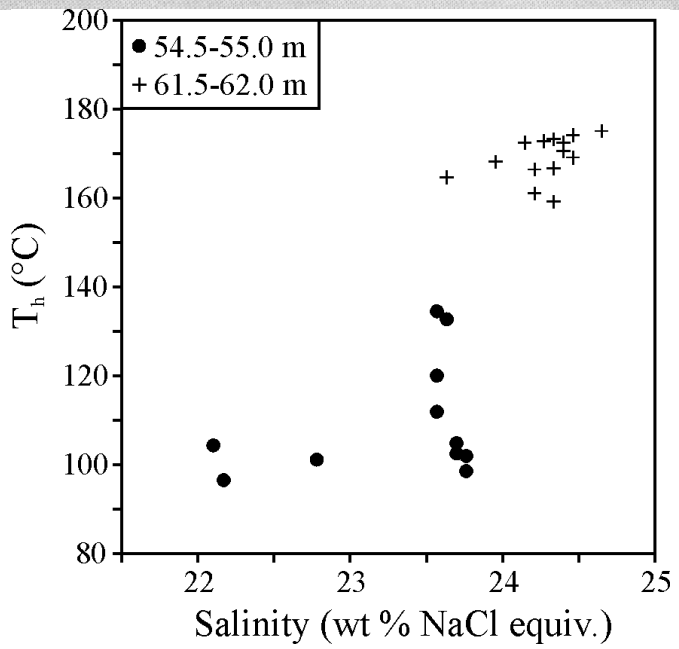

Fig. 51: Salinity vs. homogenisation temperature (T_h) diagram of primary fluid inclusions in subhedral to euhedral crystals of quartz, drill core SP-32. Data from Table 17.

Table 17: Reconnaissance fluid inclusion microthermometric data

	T_e (C°)	T_m (C°)	T_mh (C°)	T_h (C°)	Salinity (wt % NaCl)
SP32, 54.5-55.0 m	-50.5	-22.0	-9.0	102.5	23.7
	-51.0	-20.6	-9.0	101.1	22.8
	-49.5	-22.0	-8.6	104.8	23.7
	-49.4	-19.6		104.3	22.1
	-51.5	-22.1	-15.5	101.9	23.8
	-54.4	-21.8	-16.4	111.9	23.6
	-51.8	-22.1	-8.8	98.5	23.8
	-49.1	-19.7		96.5	22.2
	-46.2	-21.8	-13.1	120.0	23.6
	-52.0	-21.9	-13.4	132.7	23.6
	-47.7	-21.8		134.5	23.6
SP-32, 61.5-62.0 m	-48.7	-22.8	-8.3	166.4	24.2
	-48.0	-21.9	-7.7	164.6	23.6
	-50.1	-22.8	-10.7	161.0	24.2
	-48.8	-22.9	-8.0	172.8	24.3
		-23.2	-8.6	174.1	24.5
	-48.0	-23.0	-7.0	173.2	24.3
	-49.3	-22.7		172.4	24.1
	-49.0	-23.1	-7.5	170.5	24.4
	-53.0	-23.1	-9.5	172.4	24.4
	-51.0	-23.5	-9.7	175.0	24.6
	-49.5	-22.4	-7.5	168.1	24.0
	-55.0	-23.0	-7.9	159.1	24.3
	-57.0	-23.0	-8.6	166.7	24.3
	-57.3	-23.2	-9.3	169.1	24.5

T_e: eutectic temperature; T_m: temperature of final ice melting; T_mh: temperature of final hydrate melting; T_h: homogenisation temperature. Blank spaces indicate no measurement.

Bulk-rock geochemistry

Additional samples from drill core SP-32 were taken to complement geochemical data recorded in CABRAL et al. (2002a). The disaggregated, clayey material from the deeper parts of the drill core shows an extreme variation range of four orders of magnitude and more for gold, palladium, platinum and mercury, and up to three orders of magnitude for silver, arsenic, barium, chromium and antimony in relation to the overlying red metasiltstone (Tables 18 and 19). It should be emphasised that the upper 40 m of the drill core consist of weathered, but well-bedded red metasiltstone.

Some interesting element correlations for drill core SP-32 derive from data presented here in conjunction with those reported in CABRAL et al. (2002a). Gold is positively correlated with palladium (Fig. 52a), and palladium shows positive trends with arsenic (Fig. 52b) and selenium (Fig. 52c), in agreement with the observation that As- and Se-bearing palladium minerals occur as inclusions in dendritic aggregates of palladian gold. Although only few samples were analysed for organic carbon, there is an apparent positive correlation between gold and organic carbon, thereof some control of organic matter on precipitation of gold may tentatively be implied (Fig. 52d). Antimony and, to lesser degree, mercury seem to bear some correlation with chromium (Figs. 52e, f). MORONI et al. (2001) have suggested that gains in chromium are likely related to supergene alteration. However, mercury is commonly lost from the oxidation zones of gold deposits (BOYLE 1979), and extensively oxidising weathering under tropical conditions (lateritisation) is not expected to account for contents as high as 400 ppm Hg (Table 19).

Table 18: Bulk-rock chemical analyses of samples from drill core SP-32: precious metals

Sample no.	Depth (m)	Rock type	Au (g/t)	Ag (ppm)	Pd (g/t)	Pt (g/t)
26	8.85	Red metasiltstone	0.04	<0.3	<0.01	<0.01
27	23.0	Red metasiltstone	<0.01	<0.3	0.03	0.02
28	41.0-41.5	Disaggregated, clayey material	13110	26.7	1350	9086
29	46.0-46.5	Disaggregated, clayey material	10670	53.2	45.03	1333
30	51.0-51.5	Disaggregated, clayey material	146.9	2.7	9.75	41.47
31	72.0-72.5	Disaggregated, clayey material	383.8	0.4	11.57	68.2
32	76.0-76.5	Disaggregated, clayey material	1740	0.4	16.68	196.3
33	82.5-83.0	Disaggregated, clayey material	453.6	<0.3	16.35	87.24

Gold, palladium and platinum were determined by fire assay (gravimetric), except in samples 26 and 27 (fire assay-ICP-OES); silver by 4-acid digestion ICP technique. Iridium was sought for but not detected (<50 ppb, INAA). All analyses by Activation Laboratories, Ontario, Canada.

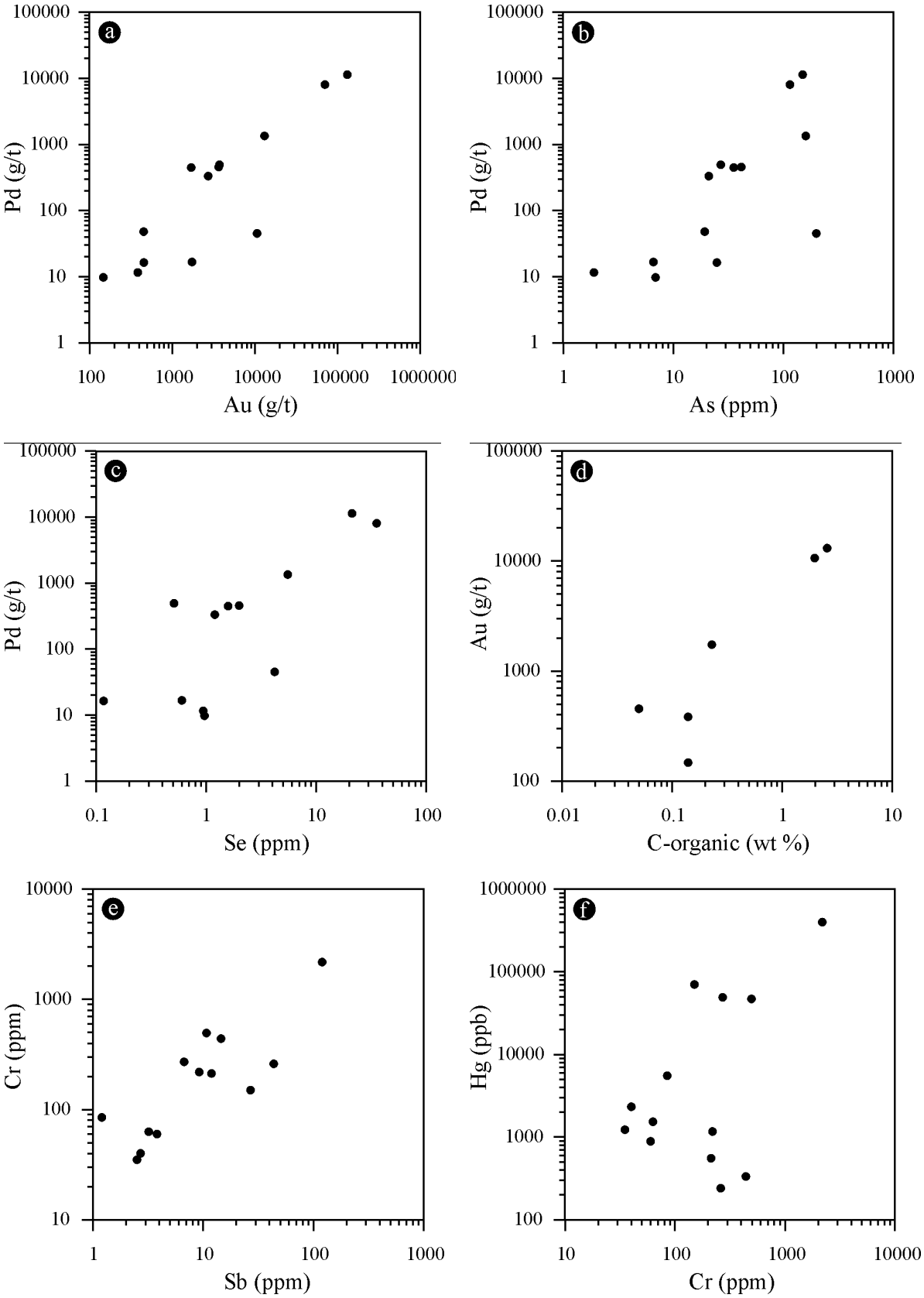

Fig. 52: Variation diagrams for some elements from ore samples of drill core SP-32. Data are from Tables 18 and 19 and CABRAL et al. (2002a).

Table 19: Bulk-rock chemical analyses of samples from drill core SP-32: major and trace elements (for rock types vide Table 18)

Sample no.	26	27	28	29	30	31	32	33
Fe_2O_3 (wt %)	7.39	6.84	6.91	13.54	29.89	8.67	3.99	4.43
Mn	<0.01	0.01	0.07	0.03	3.46	1.26	1.51	1.20
Al_2O_3*	12.88	13.49	13.21	13.21	10.46	4.10	1.60	1.70
MgO	0.24	0.21	0.13	0.03	0.05	0.07	0.04	0.05
CaO	<0.01	<0.01	0.03	0.03	0.06	0.05	0.04	0.03
Na_2O	0.28	0.27	0.04	0.03	0.01	0.04	0.03	0.03
K_2O	3.60	2.94	0.33	0.09	0.03	0.04	0.07	0.03
TiO_2	0.79	0.70	1.38	0.24	0.75	0.22	0.16	0.08
P_2O_5	0.02	0.03	0.28	0.35	0.46	0.11	0.07	0.05
SO_4	0.03	0.03	0.05	0.04	0.03	0.02	0.01	0.02
C-organic	n.a.	n.a.	2.57	1.98	0.14	0.14	0.23	0.05
Hg (ppb)	22	53	70442	400000	47106	2329	1227	1538
Ag (ppm)	<0.3	<0.3	26.7	53.2	2.7	0.4	0.4	<0.3
As	3.9	4.4	160	200	6.9	1.9	6.6	24.9
Ba	850	920	800	3000	2200	700	2100	1500
Be	3	3	4	10	12	3	1	1
Bi	2	<2	10.1	18.7	2.7	0.5	0.4	0.6
Br	<0.5	<0.5	<5	<5	<0.5	<0.5	<0.5	<0.5
Cd	<0.3	<0.3	<0.3	<0.3	<0.3	<0.3	<0.3	<0.3
Co	3	4	59	89	652	170	180	148
Cr	157	131	150	2180	495	40	35	63
Cs	6	6	<2	<2	<1	<1	<1	<1
Cu	4	4	153	55	38	25	48	51
Ge	n.a.	n.a.	0.8	0.2	0.2	<0.1	<0.1	<0.1
Hf	5	4	14	8	19	2	<1	2
In	n.a.	n.a.	0.8	2.1	3.1	0.9	0.5	1.1
Mo	11	7	4	3	1	3	2	2
Ni	75	54	249	269	712	191	179	83
Pb	8	8	82	168	41	14	12	12
Rb	171	145	<30	<30	<15	<15	<15	<15
Sb	1.2	0.6	26.9	120	10.7	2.7	2.5	3.2
Sc	19.2	18.7	36.2	51.3	27.1	6.3	3.7	4.8
Se	<3	<3	5.5	4.2	1.0	0.9	0.6	0.1
Sn*	<100	<100	2	2	2	<1	<1	<1
Sr	40	52	36	19	54	28	14	19
Ta	<0.5	<0.5	<0.5	<0.5	5	<0.5	<0.5	<0.5
Te	n.a.	n.a.	2.0	5.2	0.5	0.2	0.2	0.2
Th	21.2	19.8	12.9	15.2	32.6	4.7	2.4	3.0
Tl*	n.a.	n.a.	1.0	0.1	0.8	0.2	0.3	0.2
U	3.0	2.6	6.5	13.1	20.2	4.1	2.5	2.1
V	101	92	147	199	231	77	39	28
W	<1	<1	<20	<20	5	14	16	26
Y*	3	4	80	111	97	107	46	29
Zn	16	21	90	155	203	52	63	50

Table 19: (*Cont.*)

Sample no.	26	27	28	29	30	31	32	33
La (ppm)	15	16.6	331	50	49.4	12.4	20	12.2
Ce	28	35	300	100	112	32	23	15
Nd	<5	13	265	48	24	22	20	14
Sm	2.1	2.5	40.2	11.4	13.1	6.4	3.5	2.0
Eu	0.7	0.6	7.0	3.1	4.3	2.4	<0.2	1.1
Tb	<0.5	<0.5	2.9	2.4	2.0	2.1	<0.5	<0.5
Yb	2.4	2.2	<0.2	<0.2	16.2	5.5	<1.1	2.0
Lu	0.36	0.34	<0.05	<0.05	2.44	0.77	<0.17	0.3

Chemical analyses by Actlabs, Ontario, Canada. Elements determined by INAA: As, Ba, Br, Ce, Co, Cr, Cs, Eu, Fe, Hf, La, Lu, Na, Nd, Rb, Sb, Sc, Se, Sm, Sn, Ta, Th, Tb, U, W, Y and Yb. The remaining elements were determined by acid digestion ICP technique. Samples 28–33 were analysed for Bi, Ge, In, Se, Sn, Te and Tl by ICP-MS. Mercury was determined by cold vapour FIMS; organic carbon by infrared technology. Iron and sulphur as total Fe_2O_3 and SO_4, respectively.

* May only be partially extracted. n.a. = not analysed

5
Discussion and Conclusions

Gold, perhaps more than any other metal, has inspired tales. Some tales are told from the study of textures of gold grains and provide evidence of their origin and history (cf. CRAIG 2001). As such, grains of palladian gold from Gongo Soco, Itabira and Serra Pelada present microstructures and mineral inclusions that are tentatively deciphered in this chapter. Similarities among those ore deposits with regard to ore mineralogy and geochemistry are stressed, and compared with relevant cases described in the literature, in order to have a general picture of the ore-forming conditions. This chapter is not exhaustive, but intended to be concise and restricted to a few aspects of ore genesis only.

Gongo Soco gold composition

The Gongo Soco gold has diverse composition in terms of palladium and silver (Fig. 13). Individual gold grains are generally homogeneous, with exceptions discussed in the following paragraph. The gold nuggets analysed in Table 3 have an empirical stoichiometry of $(Au,Hg)_3(Ag,Pd,Cu)$. The existence of a natural compound of stoichiometric Au_3Ag (SAMUSIKOV & TSABUL 1977) and of a synthetic ordered Au_3Pd alloy (OKAMOTO & MASSALSKI 1985) suggests that those nuggets of $(Au,Hg)_3(Ag,Pd,Cu)$ may represent a new mineral species awaiting proper definition.

Originally zoned grains of gold become homogenised as a result of the relatively rapid diffusion rates of metals in gold at high temperatures of ≥300°C, whereas intermetallic diffusion would not proceed at ambient temperatures even on a geological timescale (GAMMONS & WILLIAMS-JONES 1995; FRIMMEL & GARTZ 1997). The presence of (1) Ag–Pd-depleted, vermiform patches within compositionally homogeneous nuggets of gold (Fig. 14) and (2) local zoning of an Ag-rich mantle on an Ag-poor core in one coarse-grained aggregate of gold (Figs. 15a, b, 16) may indicate either supergene alteration or rapid cooling after hydrothermal precipitation of gold in order to prevent complete homogenisation by solid state diffusion. In the first case, the compositional inhomogeneity could be ascribed to weathering. However, microprobe data show that silver is preferentially leached compared to palladium (Fig. 14, Table 3), an observation that does not corroborate the suggestion that palladium is more mobile than silver during weathering of palladian gold under lateritic conditions (VARAJÃO et al. 2000). Under such conditions, weathering of gold particles is expected to form an Au-rich, Ag-depleted halo (e.g. MANN 1984; COLIN & VIEILLARD 1991; FREYSSINET et al. 1989; MINKO et al. 1992; COLIN et al. 1997), a phenomenon not observed in the gold nuggets investigated.

The local zoning of an Ag-rich mantle on an Ag-poor gold core (Figs. 15a, b, 16) is unexpected under normal weathering conditions; an Ag-depleted rim, instead, should have formed (KRUPP & WEISER 1992). On the other hand, secondary electrum is reported from tropical weathering profiles where the pH of supergene fluids is buffered to alkaline conditions by carbonate minerals (WEBSTER 1986). Whatever the case, a Pd–Cu–O phase is located along the contact between the core and rim (Figs. 15c–g). A similar Pd–Cu–O phase, which occurs as an alteration halo on mertieite-II, is post-dated by a late generation of Ag-bearing gold. This gold induced an alteration front in the Pd–Cu–O mass (Fig. 12e), and may be related to low-temperature hydrothermal conditions.

Gold-related mineral assemblage and timing of mineralisation at Gongo Soco

The Gongo Soco gold nuggets have a mineral assemblage of arsenide-antimonides and selenides of palladium. The most abundant are isomertieite and mertieite-II. They occur as inclusions in, and attached to the surface of, gold. These minerals are commonly microfractured and brecciated (Fig. 19b, 20a, b; CABRAL et al. 2002c). An empirical $(Pd,Sb,Ag,Hg)_5Se_4$ compound is segmented in a domino-like pattern within gold (Fig. 21c). An aggregate of clausthalite and euhedral Ca–Mg carbonate, brecciated and cemented by chromiferous hematite, is enclosed in gold (Figs. 22a, b). Gold itself is cross-cut and cemented by veinlets of fine-grained, Pd–Hg-enriched gold, specular hematite and kaolinite (Figs. 17a, b). All these microstructures point to episodes of fracturing (brecciation) and hydrothermal self-sealing.

In this context, the presence of mechanically twinned hematite as inclusion in, and in limonite-like coating on, nuggets of palladian gold is not fortuitous (Fig. 18c). Twinning and microfracturing are the main deformation mechanisms observed in hematite at strain rates and temperatures between 10^{-4} and 10^{-5} s^{-1}, and 25 and 450°C, respectively (HENNIG-MICHAELI 1977). Irrespective of the limitations of applying experimental conditions to natural processes, mechanical twinning of hematite is produced at very high strain rates in relation to those prevailing in orogenic regions (10^{-14}–10^{-15} s^{-1}; CARTER & TSENN 1987). The experimental strain rates correspond to those estimated for seismogenic fault failure (NUR 1974; SIBSON et al. 1975). Consequently, twinned hematites are absent in the foliation-forming specular hematite developed during the Brasiliano Orogeny, but occur in younger, brittle faults (HACKSPACHER et al. 2001; ROSIÈRE et al. 2001). Therefore, the writer proposes that the formation of nuggets of palladian gold is post-Brasiliano in age and related to shallow, seismic-related fluid systems. It is pertinent to note that other mechanically twinned minerals have been used to infer seismic-related, short-lived stress peaks (e.g. TREPMANN & STÖCKHERT 2001, and references therein).

Gongo Soco fluid inclusion microthermometry

Microthermometric fluid inclusion data from specularite indicate total homogenisation temperatures around 160°C and salinity of 10–11 wt % NaCl equiv. (Fig. 26). Since no pressure correction can be applied due to lack of geobarometric information, that temperature is regarded as the minimum formation temperature of vein-related hematite. As most selenide minerals are deposited between 65 and 300°C (SIMON et al. 1997), the presence of a selenide paragenesis at Gongo Soco may be an indication that the upper temperature limit does not considerably exceed 300°C. Quartz–iron oxide isotope thermometry in specular hematite–quartz veins elsewhere in the Quadrilátero Ferrífero (Fazenda Alegria, about 30 km SSE, and Morro da Jacutinga, about 40 km E, from Gongo Soco) suggests relatively low temperatures (250–350°C, HOEFS et al. 1982).

Microthermometric fluid inclusion data obtained in quartz have a wider variation range and lower homonenisation temperatures and higher salinities than those in specularite (Fig. 26). The reason for this difference is unclear. It can only be speculated that a late generation of quartz recorded the imprint of more saline, lower-temperature fluids (i.e. cycling of fluids; cf. HENDERSON & MCCAIG 1996).

Formation of native palladium at Gongo Soco

Native palladium is intimately related with Pd–O, from which it emerges by dehydration/deoxygenation (Figs. 12f, 24; cf. McDONALD et al. 1999a; CABRAL & LEHMANN 2003; CABRAL et al. 2003). Alteration of primary minerals of palladium commences with the development of an oxidation halo of Pd–O; Sb and As are leached from the precursor mineral (Figs. 19, 23c), while Mn and, occasionally, Hg are introduced into the Pd–O halo (CABRAL et al. 2001). Where fractured, the precursor minerals (isomertieite and mertieite-II) tend to be more susceptible to alteration (Fig. 20b). Although no cleavage has been reported for isomertieite and mertieite-II (CABRI 2002), the linear fabric of Figure 12f (cf. Fig. 24) suggests a crystallographically controlled alteration of mertieite-II like that observed in the formation of pyrite/marcasite after pyrrhotite (cf. birds eye texture, RAMDOHR 1969).

The alteration process:

$$\text{Pd mineral} \rightarrow \text{Pd–O halo} \rightarrow \text{native Pd}$$

seems to adequately explain why native palladium is deprived of any significant amount of gold (CABRAL & LEHMANN 2003).

Ouro preto from Gongo Soco and Itabira

The alteration of primary minerals of palladium located at the surface of grains of palladian gold produces a dark Pd–O coating. This is the distinctive component that, together with iron oxide/hydroxides, makes up the celebrated *ouro preto* of Minas Gerais (JOHNSON & LAMPADIUS 1837; JEDWAB & CASSEDANNE 1998; CABRAL et al. 2001, CABRAL et al. 2003). The same characteristics are observed in the coarse-grained dendrites of palladian gold from Serra Pelada.

Gongo Soco bulk-rock chemistry

The alteration event responsible for the Hg–Mn-bearing Pd–O halos on primary Pd minerals is perhaps reflected by the positive linear correlation between Mn and Hg in bulk-rock chemical analyses (Fig. 27b). It is interesting to note that late veinlets of Hg-bearing Mn oxide have been recognised elsewhere in the Quadrilátero Ferrífero (CABRAL et al. 2002e).

The bulk-rock data suggest that only a fraction of the decimetre-wide, specularite-rich veins is mineralised in gold. Within the veins there are thin, almost imperceptible veinlets, traditionally regarded as auriferous, i.e. the so-called ‘lines of gold’ (HENWOOD 1871a; TOUZEAU 1892; cf. Fig. 8). These threadlike, specularite–talc-filled fissures possibly account for the high values of gold (up to 3 ppm) found in the wallrock (Table 10) and in soft hematite ore (1 ppm, Table 11) (Fig. 27c).

Itabira auriferous mineralisation

Like in Gongo Soco, the auriferous (*jacutinga*) veins transect the itabirite foliation, to which a Brasiliano age is attributed (CHEMALE et al. 1994; HACKSPACHER et al. 2001; ROSIÈRE et al. 2001). The cross-cutting relationship constrains the vein emplacement to a late or post-Brasiliano age, and disagrees with the late Transamazonian Pb-Pb errorchron age obtained by OLIVO et al. (1996).

No gold nuggets from Itabira were available for investigation and the study had to target on gold grains from heavy-mineral concentrates obtained from friable specularite-quatz veins. Some gold grains are dark due in part to coating of Pd-oxygenated phases, i.e. *ouro preto* (Figs. 35c, e, g). Nevertheless, gold-bearing aggregates of Cr-magnetite, found as wallrock fragments in the veins, were at disposal. They record the imprint of vein-related chromiferous specularite, palladian gold and palladseite on the wallrock aggregate of Cr-magnetite (Fig. 39; cf. CABRAL et al. 2002d). A simplified paragenetic sequence is as follows (cf. CABRAL et al. 2002d):

1. early Cr-magnetite (apparently of very restricted occurrence in the Itabira Iron Formation);
2. ductile deformation and metamorphism: foliation-forming chromiferous hematite after Cr-magnetite;
3. brittle failure: coarse-grained, vein-related Cr-hematite, together with palladian gold and Pd-bearing minerals, precipitated in fissures and interstices in the aggregates of Cr-magnetite. The Cr-magnetite possibly acted as a reducing agent to react with oxidizing fluids and trigger the precipitation of specular hematite, palladian gold and PGM (cf. JAIRETH 1992).

Remains of foliation-forming hematite from the wallrock occur along the margins of the aggregates of Cr-magnetite. The foliation-forming hematite is formed at the expense of magnetite by dissolution and precipitation of Fe^{3+} as hematite platelets to form a ductile planar fabric, i.e. foliation (LAGOEIRO 1998). During the dissolution of Cr-magnetite (no Ti detected), much Cr was lost to Ti-bearing metamorphic fluids (Fig. 38c). Such fluids became enriched in Cr at a late stage of the ductile deformation to precipitate Cr-rich halos on the growing foliation-forming hematite (Fig. 38a, b). With the onset of brittle failure, metamorphic fluids were locally enriched not only in Fe, but also Cr, Au, Pt and Pd to seal fractures with chromiferous hematite and precious metals.

From a narrow stratigraphic perspective (i.e. the itabirite sequence only), the positive linear correlation between chromium and platinum (Fig. 41b) may represent an inheritance from the wallrock (i.e. itabirite). This is to say that some portions of the banded iron formation (itabirite) could originally have been enriched in Cr and Pt (and perhaps other metals like Au, Ag, Hg, Pd, Sb, Se). Syngenetically precious-metal enriched protolith (itabirite) would be a reasonable proposition of source rock for the metal association found in *jacutinga* veins because of occasionally anomalous gold concentrations in fresh itabirites without any obvious relation to late hydrothermal imprint (20–332 ppb, RAMANAIDOU et al. 1991; KLEIN & LADEIRA 2000). Platinum enrichments are known from modern marine ferromanganese deposits, but apparently not palladium (HODGE et al. 1985; STÜBEN et al. 1999, and references therein). Nevertheless, high contents of palladium were detected in ferromanganese nodule reference samples (up to 4 ppm Pd, BALARAM 1999), and unusual concentrations of Cr, Pd, Sb, V and Mn occur in metamorphosed pyritic sedimentary horizons at Brukunga, South Australia (GRAHAM 1978).

Alternatively, the location of Au–Pd–Pt mineralisation relatively close to mappable rocks of possible mafic affiliation (Fig. 29) raises the question whether hydrothermal leaching of those rocks could have provided the precious metals for the *jacutinga* veins. No geochemical data on such mafic rocks from Itabira are available and little can be said based on a single bulk-rock chemical analysis (Table 15), but the evidence presented here that the rock was hydrothermally altered (high contents of As and Ba) justifies further investigation. It is

important to note that GALBIATTI (1999) recognised that *jacutinga*-style mineralisation also occurs along the contact between itabirite and such mafic rocks.

From a somewhat broader stratigraphic perspective, schistose rocks of possible mafic to ultramafic affiliation were recognised in the upper part of the Batatal Formation and the lower part of the Gandarela Formation, encompassing the itabirite sequence (PIRES 1983). The mafic and ultramafic signatures are given by the existence of Ti–Co–Ni–Cr–V-bearing magnetite. These rocks may be potential candidates for source rocks of Cr and PGE. A regional stratigraphic perspective on possible source rocks is given further down.

As observed at Gongo Soco, mercury, though in the ppb range, is positively correlated with manganese (Fig. 41c). It appears that the Mn vs. Hg correlation is characteristic of *jacutinga*-style veins and would explain why old miners used Mn as a pathfinder element for itabirite-hosted gold ore (HOCHEDER 1833; HENWOOD 1871a; THOMAS 1905; OLIVEIRA 1932).

Hongshiite-hosted mineral assemblage

Hongshiite is a rare platinum-group mineral known from mafic-ultramafic rocks and associated placer deposits (CABRI 2002; KWITKO et al. 2002, and references therein). Itabira is perhaps the only case hitherto, where hongshiite occurs in sulphide-free, hematite-rich veins. The hongshiite from Itabira has a typical low-temperature mineral assemblage of Se-bearing minerals, barite and, possibly, kaolinite (Fig. 36). Notably, barite precipitates from oxidising, moderately saline fluids over a temperature range up to about 300°C (BLOUNT 1977).

Weathering of Pd- and Pt-bearing minerals from Itabira

Crystals of hongshiite are commonly haloed by a porous, Cu-depleted, Pt-rich rim approaching pure native platinum (Fig. 37; cf. Table 2 of KWITKO et al. 2002), in the same fashion that alluvial and residual gold grains in lateritic profiles tend to develop a porous, high-purity gold rim (e.g. MANN 1984; GROEN et al. 1990; BOWELL 1992; KRUPP & WEISER 1992). The native platinum rimming on hongshiite crystals is interpreted to be supergene in origin (KWITKO et al. 2002; cf. analogous rimming of native platinum on cooperite recorded in OBERTHÜR 2002). There is a similar rimming of native platinum on Pt–Fe alloy (GORNOSTAYEV et al. 1999) and sperrylite (TOLSTYKH & KRIVENKO 1998) reported from alluvial deposits in the Russian Far East, but an endogenous origin has been proposed in these cases.

A different pattern of alteration is depicted by the palladium arsenide-antimonide grain of Figure 34. The grain is covered by a botryoidal coating that resembles that of supergene gold on detrital gold grains (cf. Fig. 6d of MINKO et al. 1992). The botryoidal coating is compositionally similar to the substrate and could be related to partial dissolution of, and *in situ* precipitation on, the substrate (BOWLES 1986).

Possible sources of fluids and palladian gold mineralisation in the Quadrilátero Ferrífero

Barren specularite–quartz veins in the Ouro Fino area, about 25 km south of Gongo Soco, have been studied by BOIRON et al. (1999) and constitute a possible analogue for the *jacutinga*-style system. There are two types of fluid inclusions in quartz: (1) abundant aqueous, and (2) subordinate aqueous–carbonic inclusions. Due to decrepitation, only a few total homogenisation temperatures were obtained in the range of 104 to 160°C for the aqueous inclusions, and between 250 and 280°C for the aqueous–carbonic ones. The salinity of the

aqueous inclusions ranges from 11 to 16 wt % NaCl equiv., whereas the aqueous–carbonic inclusions have low salinity (1.5–2.6 wt % NaCl equiv.). The Ouro Fino hematite–quartz vein system is characterised by high sulphate, as well as high B, Li and F contents, with low Na/K and Cl/SO_4 ratios close to those found in present-day geothermal systems. It has been suggested that the fluids originated during retrograde metamorphism of late Brasiliano age (BOIRON et al. 1999).

Some fluid inclusion information on quartz from auriferous hematite–quartz veins (*jacutinga*) is available from the work of GALBIATTI (1999) in the Itabira district. Two families of fluid inclusions were found: (1) moderately saline aqueous fluids, with low total homogenisation temperatures (<180°C), and (2) hotter, aqueous–carbonic fluids of high salinity. The second fluid inclusion type contrasts with those observed at Gongo Soco, but appears to be comparable with the aqueous–carbonic inclusions documented from the Ouro Fino area in terms of homogenisation temperatures. If so, the hotter aqueous-carbonic fluids could have been trapped during an initial stage of retrograde metamorphism of Brasiliano age.

Br/Cl ratios from the Ouro Fino specularite–quartz veins indicate an evolved seawater origin from which halite had precipitated, leading to the suggestion that the retrograde metamorphic fluids interacted with evaporites or hydrothermally altered rocks (BOIRON et al. 1999). There is no conclusive evidence for evaporitic rocks in the Itabira Group, but the existence of mineral assemblages with Mg-riebeckite, aegirine, microcline and stilpnomelane reflects a K–Na-bearing system in the Itabira Iron Formation, suggestive of locally evaporitic precursors (PIRES 1995).

Meteoric water, as interpreted elsewhere both in syn- and late-compressive (MOREY 1999; OLIVER & DICKENS 1999; POWELL et al. 1999), and extensional settings (TAYLOR et al. 2001), may have interacted with metamorphic fluids evolved in the Brasiliano Orogeny. Present-day, deep circulation of meteoric water in the Quadrilátero Ferrífero is indicated by thermal spring activity at Água Quente, an old *jacutinga*-style gold mine (HELMREICHEN 1847; HENWOOD 1871b) in the 50 km N–S-trending Água Quente Fault, along which several auriferous (*jacutinga*) deposits are located (Fig. 1). This fault system is a major Brasiliano structure (FERREIRA FILHO & FONSECA 2001) of the Fazendão Thrust Front, of CHEMALE et al. (1994).

Metal enrichment to ore grade is commonly considered to be the result of large-scale, long-lasting processes of fluid–rock interaction (e.g. LEHMANN et al. 2000). In the Olary Domain in South Australia, for instance, replacive and cross-cutting masses of epigenetic iron oxides, which display enrichment in Fe and Au, among other elements, relative to parental iron formation, are viewed as a consequence of regional-scale hydrothermal alteration (ASHLEY et al. 1998). The itabirite-hosted, specular hematite-rich, Au–Pd–Pt-bearing veins (*jacutinga*) of the Quadrilátero Ferrífero may likewise be interpreted from a regional-scale perspective. Ductile-brittle to brittle-ductile, steep reverse and oblique-slip faults were generated and/or reactivated during late- to post-Brasiliano tectonics (CORRÊA NETO 2001). The faults may have facilitated the penetration of meteoric oxidising fluids to deep levels (cf. NESBITT & MUEHLENBACHS 1995; UPTON et al. 1995; MOREY 1999; POWELL et al. 1999). Such fluids could have leached Au, Pd and Pt from the Archaean greenstone rocks and precipitated them as *jacutinga* veins in itabirite (GUIMARÃES 1970). The hydrothermal fractionation of Au, Pd and Pt from other PGE can be explained by the relatively high solubilities of Au, Pd and Pt as chloride complexes under oxidising conditions (e.g. JAIRETH 1992; WOOD et al. 1992; GAMMONS et al. 1993; GAMMONS et al. 1997; WOOD 2002). The magnetite component in the itabirite sequence could then be regarded as a redox trap for the oxidising ore fluids. However, rocks from the enclosing sequences also have Fe^{2+}-bearing minerals that could have

acted as reducing agents, and there is no obvious evidence for an oxidising hydrothermal alteration of the Archaean greenstone rocks.

As highlighted by Hussak (1904), palladian gold seems to be an exclusive feature of the Palaeoproterozoic banded iron formation (itabirite). OLIVO et al. (1995) support the idea, earlier advanced by GUIMARÃES (1970), that Au and Pd could have been leached from the Archaean greenstone rocks. Gold from the Archaean greenstone-hosted lode deposits is alloyed with silver, but not palladium (RIBEIRO-RODRIGUES 1998; LOBATO et al. 2001b). In these deposits Pd-bearing minerals also appear to be absent. The Au-mineralising fluids in the Archaean and the Palaeoproterozoic banded iron formations of the Quadrilátero Ferrífero are different. The Archaean Au-bearing systems were near neutral, reducing, low-salinity, CO_2–H_2O fluids (LOBATO & VIEIRA 1998; LOBATO et al. 2001b) of the classical mesothermal style, i.e. orogenic mesozonal (GROVES et al. 1998), whereas the specular hematite–quartz-bearing (*jacutinga*) vein systems represent oxidising fluids. Whatever the fluid origin is, the known occurrences of palladian gold in the Quadrilátero Ferrífero reflect the particularly oxidising conditions prevailing in the host rock (specular hematite-bearing itabirite and associated hematite ore).

Serra Pelada bonanza ore

Little is known about the near-surface bonanza ore that triggered the gold rush at Serra Pelada. Apparently, only one drill core is all that remains from the bonanza ore. Judging from the friable, powdery, completely disaggregated nature of drill core SP-32, the assertion that supergene enrichment played a fundamental role in the genesis of the bonanza ore is understandable (MEIRELES & SILVA 1988, COSTA 1997; TALLARICO et al. 2000a, MORONI et al. 2001; VILLAS & SANTOS 2001; GRAINGER et al. 2002). However, examination of the only euhedral, coarse-grained mineral phases found in the drill core, dendritic gold and quartz, sheds a different light on the ore genesis.

Astonishingly high grades of gold, palladium and platinum in drill core SP-32 (Fig. 42) are expressed as coarse-grained dendrites of palladian gold, with which Pd- and Pt-bearing minerals are associated. Dendritic morphology of gold indicates crystallisation from Au-supersaturated solutions by a continuous growth mechanism (SUNAGAWA 1981) and dendrites of gold can form via a 25°C disproportionation reaction of aurous chloride complexes (GAMMONS et al. 1997). In nature, coarse-grained dendrites of electrum occur in the weathering profile at Wau, Papua New Guinea (WEBSTER & MANN 1984). On the other hand, dendritic gold also is known from epithermal and hot-spring gold deposits (Saunders 1994; Sherlock & Lehrman 1995), and a low-temperature hydrothermal origin has been proposed for the dendritic aggregates of Pt–Pd and Pd–Hg–Au alloys from Bom Sucesso, Minas Gerais (CASSEDANNE et al. 1996; FLEET et al 2002). The dendrites of palladian gold from Serra Pelada have a Pd–Pt–As–Sb–Se–Hg mineralogical signature (CABRAL et al. 2002a, b), of which Pd- and Se-bearing minerals are typically found in selenide-bearing hydrothermal veins (JOHAN 1989; CABRI et al. 1991; MERNAGH et al. 1994; PAAR et al. 1998, 2000; NICKEL 2002; ROBERTS et al. 2002; STANLEY et al. 2002), commonly formed at temperatures of about 100°C (SIMON et al. 1997). Such a low-temperature hydrothermal environment is suggested by fluid inclusion data in quartz (Fig. 51), which also identify the fluid phase as Ca-rich brines.

The origin of the Ca-rich brines cannot be constrained here. There is evidence that the breakdown of dolomite in the presence of an aqueous fluid enhances the fluid salinity, and that the salinity of metamorphic fluids is related to the original distribution of evaporites

and/or connate brines (YARDLEY & GRAHAM 2002, and references therein). Regardless of the origin of fluids, the decalcification of the underlying dolomitic marble sequence, whose base is located at a depth of about 300 m, could have involved Ca-rich brines. If this is indeed the case, then the decalcification and related manganiferous collapse breccias, regarded as supergene in origin (TALLARICO et al. 2000a; GRAINGER et al. 2002), are not entirely derived by weathering, but primarily by a shallow hydrothermal fluid system (cf. hypogene carbonate dissolution and related collapse breccias in Carlin-type gold deposits, HOFSTRA & CLINE 2000). It is interesting to note that (1) a sample of Mn oxide breccia from the *garimpo* dump has a Ba–Co–Cu–Ni–Hg geochemical signature (CABRAL et al. 2002a) comparable to that observed in hot spring-related Co-rich Mn oxide mineralisation (CRESPO et al. 1995), and (2) the Mn oxide minerals commonly observed in supergene environments (e.g. cryptomelane, pyrolusite, romanèchite) may also be deposited by low-temperature hydrothermal fluids (~120°C) of moderate salinity (RODDY et al. 1988).

An episodic ore-forming process is suggested by the late generation of palladian gold–isomertieite intergrown with Mn–Ba oxide (possibly romanèchite) that post-dates coarse-grained dendrites of palladian gold (Figs. 47c). The ore mineralogy defines a Ba–Sb–As association typical of hydrothermal manganese oxide veins (e.g. HEWETT 1964; NICHOLSON 1992, and references therein).

The near-surface bonanza ore is geochemically and mineralogically distinct from the deep-seated mineralisation (CABRAL et al. 2002a), for which a skarn-like model related to dioritic rocks of unknown age (TALLARICO et al. 2000a; VILLAS & SANTOS 2001) and a distal relationship to the Fe oxide Cu–Au deposits of Carajás (linked to either ca. 1.88 Ga, subalkaline to alkaline granitoids or ca. 2.57 Ga, A-type alkaline granitoids; GRAINGER et al. 2002) have been proposed. Nevertheless, DARDENNE & SCHOBBENHAUS (2001, and references therein) have pointed out that the mineralising fluids could also have been generated during reactivation of regional shear faults. The Cinzento strike-slip system, where Serra Pelada is situated in its eastern segment, had several periods of reactivation and shows evidence of neotectonic activity (PINHEIRO & HOLDSWORTH 1997). In this regard, the 198 Ma-old gabbroic dyke, located along a NW-trending fault adjacent to the *garimpo* (Fig. 44), or even younger reactivations of the fault system could have had some influence on the formation of the near-surface bonanza mineralisation (cf. JORGE JOÃO et al. 1982, p. 55). Currently, no conclusive genetic model can be elaborated, but the geochemical and mineralogical signature (Au–Pd–Pt–As–Sb–Se–Hg) of the bonanza ore is characteristic of shallow hydrothermal systems (cf. epithermal gold selenide category of LINDGREN 1928).

Quadrilátero Ferrífero and Carajás: regional aspects of palladian gold mineralisation

Apart from local and regional particularities, the palladian gold deposits of the Quadrilátero Ferrífero and the Serra Pelada *garimpo* have similar metallogenetic settings:

1. The palladian gold mineralisation is within world-class iron ore districts; the *jacutinga* veins are hosted by itabirite and associated hematite ore, whereas Serra Pelada is spatially and stratigraphically close to the Carajás Formation (banded iron formation).
2. The Serra Pelada and the *jacutinga*-style mineralisations are hosted by sedimentary rocks resting on greenstone sequences.
3. The Quadrilátero Ferrífero and the Carajás mineral province experienced resurgent tectonics that reactivated older structures through the Proterozoic and in Phanerozoic times (PINHEIRO & HOLDSWORTH 1997; SANT'ANNA et al. 1997).

4. Meteoric oxidising fluids are still circulating to deep levels, as indicated by present day thermal-spring activity in the Cinzento strike-slip system (PINHEIRO & HOLDSWORTH 1997), in the eastern segment of which Serra Pelada is situated, and in the Água Quente Fault (DORR 1969; FERREIRA FILHO & FONSECA 2001), along which several *jacutinga*-style gold deposits occur (Fig. 1).

Concluding remarks

Gongo Soco, Itabira and Serra Pelada have a number of features in common:

1. coarse-grained palladian gold;
2. abundant hematite;
3. sulphide-poor ore-mineral assemblages;
4. a low-pressure (As–Sb–Se–Hg) mineralogical signature;
5. dominantly brittle ore-hosting structures;
6. open-space filling ore textures.

These characteristics warrant comparisons with other Au–Pd–Pt occurrences related to oxidising fluids (e.g. Kupferschiefer, Poland, KUCHA & PRZYBY£OWICZ 1999; Waterberg district, South Africa, WAGNER 1929; MCDONALD et al. 1999b), of which only two are briefly considered here:

1. Dendritic palladian gold, mertieite-II, isomertieite and a variety of selenide minerals including chrisstanleyite and verbeekite occur in hematite-bearing carbonate veins hosted by hematitised limestone of Middle Devonian age at Hope's Nose, Devon, England (CLARK & CRIDDLE 1982; HARRISON & FULLER 1987; STANLEY et al. 1990; PAAR et al. 1998; ROBERTS et al. 2002). Fluid inclusions in the calcite gangue and associated bipyramidal quartz are Ca-rich brines (20–23 wt % NaCl equiv.) that homogenise over the temperature range of 65 to 120°C (SCRIVENER et al. 1982).

2. With an indicated resource of 4.85 Mt at 4.31 g/t Au, 0.65 g/t Pd and 0.19 g/t Pt (CARVILLE et al. 1990), the Coronation Hill Au–Pd–Pt (±U) deposit is situated in the Palaeoproterozoic Pine Creek inlier of the Northern Territory, Australia, and has a distinct Au–PGM–selenide association (CARVILLE et al. 1990; MERNAGH et al. 1994). This association occurs in late quartz–carbonate–hematite veinlets and disseminations in pervasively chlorite–sericite-altered volcaniclastic and intrusive dioritic rocks. It includes electrum and Pd- and Pt-bearing minerals, such as palladseite, sudovikovite and a PdSbSe phase, as well as stibiopalladinite, Pd_5Sb_2, sudburyite, PdSb, native palladium and platinum. Tiemannite and clausthalite are also present. A component of replacive pyrite may also be found, mainly in the altered igneous rocks. Fluid inclusion, mineralogical and isotopic data indicate a low-temperature mineralisation at around 140°C derived from acidic, highly oxidising, Ca-rich brines (about 26 wt % $CaCl_2$ equiv.) of meteoric origin (MERNAGH et al. 1994).

The Hope's Nose and Coronation Hill ore fluids are low-temperature (<200°C), Ca-rich brines like those suggested by reconnaissance fluid inclusion microthermometry for the Serra Pelada bonanza ore. Similarly oxidising, relatively low-temperature hydrothermal fluids of moderate salinity are suggested for the Gongo Soco *jacutinga*-style veins. Under such conditions, Au, Pd and Pt can efficiently be transported as chloride complexes in equilibrium with hematite (e.g. WOOD et al. 1992; WOOD 2002). Among the different mechanisms of depositing Au, Pd and Pt, reduction is considered to be very effective (cf. JAIRETH 1992). Reduction of highly oxidising, mineralising fluids caused by (1) organic carbon and (2)

magnetite may have been important at Serra Pelada (Fig. 52d) and Itabira (Fig. 39), respectively.

More research is still necessary for an adequate understanding of the mineralising processes at Gongo Soco, Itabira and Serra Pelada. Irrespective of intrinsic peculiarities and different geological settings, Gongo Soco, Itabira and Serra Pelada are the result of hydrothermal deposition from acidic, saline, highly oxidising fluid systems under relatively low-pressure (shallow-level) conditions.

References

ALKMIM, F.F. & MARSHAK, S. (1998): Transamazonian orogeny in the Southern São Francisco craton region, Minas Gerais, Brazil: evidence for Paleoproterozoic collision and collapse in the Quadrilátero Ferrífero.— Precamb. Res., **90:** 29-58.

ANDRADE, F.G., NAKASHIMA, J. & PODESTÁ, P.R. (1986): Depósito de manganês da Serra de Buritirama, Pará.— In: SCHOBBENHAUS, C. & COELHO, C.E.S. (Eds.): Principais depósitos minerais do Brasil, **2:** 153-166; Brasília (Departamento Nacional da Produção Mineral, Companhia Vale do Rio Doce).

ANDRADE, L.P. & SÁ, E.L. (1990): Lavra seletiva de minério aurífero nos itabiritos.— Minérios, **161:** 34-40.

ASHLEY, P.M., LOTTERMOSER, B.G. & WESTAWAY, J.M. (1998): Iron-formations and epigenetic ironstones in the Palaeoproterozoic Willyama Supergroup, Olary Domain, South Australia.— Mineral. Petrol., **64:** 187-218.

AUGÉ, T. & LEGENDRE, O. (1994): Platinum-group element oxides from the Pirogues ophiolitic mineralization, New Caledonia, origin and significance.— Econ. Geol. **89:** 1454-1468.

BABINSKI, M., CHEMALE JR., F. & VAN SCHMUS, W.R. (1995): The Pb/Pb age of the Minas Supergroup carbonate rocks, Quadrilátero Ferrífero, Brazil.— Precamb. Res., **72:** 235-245.

BALARAM, V. (1999): Determination of precious metal concentrations in a polymetallic nodule reference sample from the Indian ocean by ICP-MS.— Marine Georesources and Geotechnology, **17:** 17-26.

BARBOSA, A.L.M. & GROSSI SAD, J.H. (1973): Tectonic control of sedimentation and trace-element distribution in iron ores of central Minas Gerais (Brazil).— In: Proceedings of the Kiev Symposium, 1970, Unesco, Earth Sciences, **9:** 125-131.

BARROS, C.E.M., DALL'AGNOL, R., BARBEY, P. & BOULLIER, A.M. (1997): Geochemistry of the Estrela granite complex, Carajás region, Brazil: an example of an Archaean A-type granitoid.— J. South Amer. Earth Sci., **10:** 321-330.

BENSUSAN, A.J. (1929): Auriferous jacutinga deposits.— Bull. Inst. Min. Metall., **300:** 450-483.

BLOUNT, C.W. (1977): Barite solubilities and thermodynamic quantities up to 300°C and 1400 bars.— Am. Mineral., **62:** 942-957.

BODNAR, R.J. (1993): Revised equation and table for determining the freezing point depression of H_2O–NaCl solutions.— Geochim. Cosmochim. Acta, **57:** 683-684.

BOIRON, M.-C., MOISSETTE, A., CATHELINEAU, M., BANKS, D., MONNIN, C. & DUBESSY, J. (1999): Detailed determination of palaeofluid chemistry: an integrated study of sulphate-volatile rich brines and aquo-carbonic fluids in quartz veins from Ouro Fino (Brazil).— Chem. Geol., **154:** 179-192.

DE BOVET, A. (1883): A industria mineral na Provincia de Minas-Geraes. Primeira parte: ferro e ouro.— Annaes da Escola de Minas de Ouro Preto, **2:** 25-99.

BOWELL, R.J. (1992): Supergene gold mineralogy at Ashanti, Ghana: implications for the supergene behaviour of gold.— Mineral. Mag., **56:** 545-560.

BOWLES, J.F.W. (1986): The development of platinum-group minerals in laterites.— Econ. Geol., **81:** 1278-1285.

BOYLE, R.W. (1979): The geochemistry of gold and its deposits.— 584 p.; Ottawa (Geological Survey of Canada, Bulletin 280).

BURTON, R.F. (1869): The highlands of the Brazil.— Volume I, 443 p.; London (Tinsley Brothers).

CABRAL, A.R. & LEHMANN, B. (2003): A two-stage process of native palladium formation at low temperatures: evidence from a palladian gold nugget (Gongo Soco iron ore mine, Minas Gerais, Brazil).— Mineral. Mag., in press.

CABRAL, A.R. & SATTLER, C.D. (2001): Contrasting pyrophanite–ilmenite solid-solution compositions from the Conta História Fe–Mn deposit, Quadrilátero Ferrífero, Minas Gerais, Brazil.— N. Jb. Miner. Mh., 271-288.

CABRAL, A.R., LEHMANN, B., KWITKO, R., JONES, R.D., PIRES, F.R.M., ROCHA FILHO, O.G. & INNOCENTINI, M.D. (2001): Palladium-oxygenated compounds of the Gongo Soco mine, Quadrilátero Ferrífero, central Minas Gerais, Brazil.— Mineral. Mag., **65:** 169-179.

CABRAL, A.R., LEHMANN, B., KWITKO & CRAVO COSTA, C.H. (2002a): The Serra Pelada Au-Pd-Pt deposit, Carajás mineral province, northern Brazil: reconnaissance mineralogy and chemistry of very high grade palladian gold mineralization.— Econ. Geol., **97:** 1127-1138.

CABRAL, A.R., LEHMANN, B., KWITKO, R. & CRAVO COSTA, C.H. (2002b): Palladium and platinum minerals from the Serra Pelada Au–Pd–Pt deposit, Carajás mineral province, northern Brazil.— Can. Mineral., **40:** 1451–1463.

CABRAL, A.R., LEHMANN, B., KWITKO, R. & JONES, R.D. (2002c): Palladian gold and palladium arsenide-antimonide minerals from Gongo Soco iron ore mine, Quadrilátero Ferrífero, Minas Gerais, Brazil. — Trans. Instn Min. Metall. (Sect. B: Appl. earth sci.), **111:** B74-B80.

CABRAL, A.R., LEHMANN, B., KWITKO, R., GALBIATTI, H.F. & PEREIRA, M.C. (2002d): Palladseite and its oxidation: evidence from Au-Pd vein-type mineralization (jacutinga), Cauê iron-ore mine, Quadrilátero Ferrífero, Minas Gerais, Brazil.— Mineral. Mag., **66:** 327–336.

CABRAL, A.R., LEHMANN, B., SATTLER, C.D., PIRES, F.R.M. & KANEKO, K. (2002e): Hg–Tl-bearing manganese oxide from Conta História manganese deposit, Quadrilátero Ferrífero, Minas Gerais, Brazil.— Trans. Instn Min. Metall. (Sect. B: Appl. earth sci.), **111:** B123-B127.

CABRAL, A.R., LEHMANN, B., KWITKO, R., JONES, R.D. & ROCHA FILHO, O.G. (2003): On the association of palladium-bearing gold, hematite and gypsum in an *ouro preto* nugget.— Can. Mineral., **41:** 473-478.

CABRI, L.J. (2002): The platinum-group minerals.— In: CABRI, L.J. (Ed.): The geology, geochemistry, mineralogy and mineral beneficiation of platinum-group elements:13-129; Montreal (Canadian Institute of Mining, Metallurgy and Petroleum, Special Volume 54).

CABRI, L.J., CLARK, A.M. & CHEN, T.T. (1977): Arsenopalladinite from Itabira, Brazil, and from the Stillwater complex, Montana.— Can. Mineral., **15:** 70-73.

CABRI, L.J., LAFLAMME, J.H.G., STEWART, J.M., ROWLAND, J.F. & CHEN, T.T. (1975): New data on some palladium arsenides and antimonides.— Can. Mineral., **13:** 321-335.

CABRI, L.J., LAFLAMME, J.H.G., ROBERTS, A.C., CRIDDLE, A.J. & HULBERT, L.J. (1991): Jolliffeite and unnamed CoAsSe: two new arsenoselenides from the north shore of Lake Athabasca, Saskatchewan.— Can. Mineral., **29:** 411-418.

CARTER, N.L. & TSENN, M.C. (1987): Flow properties of continental lithosphere.— Tectonophysics, **136:** 27-63.

CARVILLE, D.P., LECKIE, J.F., MOORHEAD, C.F., RAYNER, J.G. & DURBIN, A.A. (1990): Coronation Hill gold-platinum-palladium deposit. In: HUGHES, F.E. (Ed.): Geology of the mineral deposits of Australia and Papua New Guinea: 759-762; Melbourne (The Australasian Institute of Mining and Metallurgy).

CASSEDANNE, J.P., JEDWAB, J. & ALVES, J.N. (1996): Apport d'une prospection systématique à l'étude de l'origine de l'or et du platine alluviaux du Córrego Bom Sucesso (Serro – Minas Gerais).— An. Acad. Bras. Ciênc., **68:** 569-582.

CHAUVET, A. & MENEZES, M. (1992): Évolution structurale du sud du Craton São Fransisco: implications sur les minéralisations aurifères de la région d'Ouro Preto, Brésil.— C. R. Acad. Sci. Paris, Série II, **315:** 495-501.

CHAUVET, A., FAURE, M., DOSSIN, I. & CHARVET, J. (1994): A three-stage structural evolution of the Quadrilátero Ferrífero: consequences for the Neoproterozoic age and the formation of gold concentrations of the Ouro Preto area, Minas Gerais, Brazil.— Precamb. Res., **68:** 139-167.

CHAUVET, A., PIANTONE, P., BARBANSON, L., NEHLIG, P. & PEDROLETTI, I. (2001): Gold deposit formation during collapse tectonics: structural, mineralogical, geochronological, and fluid inclusion constraints in the Ouro Preto gold mines, Quadrilátero Ferrífero, Brazil.— Econ. Geol., **96:** 25-48.

CHEMALE JR., F. (1987): Tektonische, lagerstättenkundliche und petrographische Untersuchungen im Eisenerzrevier Itabira, Minas Gerais, Brasilien.— 140 p.; Clausthal-Zellerfeld (Clausthaler Geowissenschaftliche Dissertation, Technische Universität Clausthal).

CHEMALE JR., F., QUADE, H. & CARBONARI, F.S. (1987): Economic and structural geology of the Itabira Iron District, Minas Gerais, Brazil.— Zbl. Geol. Paläont. Teil I, **(7/8):** 743-752.

CHEMALE JR., F., ROSIÈRE, C.A., & ENDO, I. (1994): The tectonic evolution of the Quadrilátero Ferrífero, Minas Gerais, Brazil.— Precamb. Res., **65:** 25-54.

CLARK, A.M. & CRIDDLE, A.J. (1982): Palladium minerals from Hope's Nose, Torquay, Devon.— Mineral. Mag., **46:** 371-377.

CLARK, A.M., CRIDDLE, A.J. & FEJER, E.E. (1974): Palladium arsenide-antimonides from Itabira, Minas Gerais, Brazil.— Mineral. Mag., **39:** 528-543.

CLEARY, D. (1990): Anatomy of the Amazon Gold Rush.— 245 p.; Hampshire (The Macmillan Press).

COELHO, C.E.S. (1986): Depósito de ferro da Serra dos Carajás, Pará.— In: SCHOBBENHAUS, C. & COELHO, C.E.S. (Eds.): Principais depósitos minerais do Brasil, **2:** 29-64; Brasília (Departamento Nacional da Produção Mineral, Companhia Vale do Rio Doce).

COELHO, C.E.S. & RODRIGUES, O.B. (1986): Jazida de manganês do Azul, Serra dos Carajás, Pará.— In: SCHOBBENHAUS, C. & COELHO, C.E.S. (Eds.): Principais depósitos minerais do Brasil, **2:** 145-152; Brasília (Departamento Nacional da Produção Mineral, Companhia Vale do Rio Doce).

COLIN, F. & VIEILLARD, P. (1991): Behavior of gold in the lateritic equatorial environment: weathering and surface dispersion of residual gold particles, at Dondo Mobi, Gabon.— Appl. Geochem. **6:** 279-290.

COLIN, F., SANFO, Z., BROWN, E., BOURLÈS, D. & MINKO, A.E. (1997): Gold: a tracer of the dynamics of tropical laterites.— Geology, **25:** 81-84.

CORREA DA COSTA, L.A. (1878): Estudo geologico da região de S. Bartholomeu e da mina de ouro da Tapéra perto de Ouro-Preto.— Archivos do Museu Nacional, **3:** 17-31.

CORRÊA NETO, A.V. (2001): Análise estrutural nos setores sul e sudeste do Sistema de Cisalhamento Fundão-Cambotas, Quadrilátero Ferrífero, Brasil.— 166 p.; Rio de Janeiro (unpubl. Ph.D. thesis, Departamento de Geologia, Instituto de Geociências, Universidade Federal do Rio de Janeiro).

COSTA, M.L. (1997): Lateritization as a major process of ore deposit formation in the Amazon region.— Explor. Mining Geol., **6:** 79-104.

CRAIG, J.R. (2001): Ore-mineral textures and the tales they tell.— Can. Mineral., **39:** 937-956.

CRAWFORD, M.L. (1981): Phase equilibria in aqueous fluid inclusions.— In: HOLLISTER, L.S. & CRAWFORD, M.L. (Eds.): Short course in fluid inclusions: applications to petrology. Short course handbook, **6:** 75-100; Calgary (Mineralogical Association of Canada).

CRESPO, A., LUNAR, R., OYARZUN, R. & DOBLAS, M. (1995): Unusual case of hot springs-related Co-rich Mn mineralization in central Spain: the Pliocene Calatrava deposits.— Econ. Geol., **90:** 433-437.

CUNHA, B.C.C., SANTOS, D.B. & PRADO, P. (1984): Contribuição ao estudo da estratigrafia da região dos Gradaús, com ênfase no Grupo Rio Fresco.— In: Congresso Brasileiro de Geologia, 33, Anais, **2:** 873-885; Rio de Janeiro (Sociedade Brasileira de Geologia).

DARDENNE, M.A. & SCHOBBENHAUS, C. (2001): Metalogênese do Brasil.— 392 p.; Brasília (Editora Universidade de Brasília).

DAVIS, R.J., CLARK, A.M. & CRIDDLE, A.J. (1977): Palladseite, a new mineral from Itabira, Minas Gerais, Brazil.— Mineral. Mag., **41:** 123, M10-M13.

DIELLA,V., FERRARIO, A. & GIRARDI, V.A.V. (1995): PGE and PGM in the Luanga mafic-ultramafic intrusion in Serra dos Carajás (Pará State, Brazil).— Ore Geol. Rev., **9:** 445-453.

DOCEGEO, EQUIPE-DISTRITO AMAZÔNIA (1988): Revisão litoestratigráfica da Província Mineral de Carajás.— In: Província Mineral de Carajás – Litoestratigrafia e principais depósitos minerais: Congresso Brasileiro de Geologia, 35, Anexo: 11-56; Belém (Sociedade Brasileira de Geologia).

DORR, J.V.N. (1965): Nature and origin of the high-grade hematite ores of Minas Gerais, Brazil.— Econ. Geol., **60:** 1-46.

DORR, J.V.N. (1969) Physiographic, stratigraphic and structural development of the Quadrilátero Ferrífero, Minas Gerais, Brazil.— U.S. Geol. Surv. Prof. Paper, **641-A:** 110 p.

DORR, J.V.N. & BARBOSA, A.L.M. (1963): Geology and ore deposits of the Itabira district, Minas Gerais, Brazil.— U.S. Geol. Surv. Prof. Paper, **341-C:** 110 p.

DORR, J.V.N., GAIR, J.E., POMERENE, J.B. & RYNEARSON, G.A. (1957): Revisão da estratigrafia precambriana do Quadrilátero Ferrífero, Minas Gerais, Brazil.— Rio de Janeiro (Departamento Nacional da Produção Mineral, Divisão de Fomento da Produção Mineral), Avulso **81:** 31 p.

DOSSIN, I.A., DOSSIN, T.M., CHARVET, J. & CHEMALE JR., F. (1992): Tectonique du Protérozoïque supérieur au sud-est du Craton São Francisco (Minas Gerais, Brésil).— C. R. Acad. Sci. Paris, Série II, **315:** 629-636.

ESCHWEGE, W.L.V. (1833): Pluto Brasiliensis.— 622 p.; Berlin (G. Reimer).

FARADAY, W. (1828): In: Imperial Brazilian Mining Association – Fifth report of the directors, addressed to the share-holders at the half-yearly meeting, on the 13th of November, 1828; and an appendix, containing extracts of the various communications received from the mines, the account of the produce of the gold washings from the 1st of January, to 30th June, 1828, and the auditors' statement of accounts for the same period: 89-95; London (The Philanthropic Society).

FERRAND, M.P. (1894): L'or a Minas Geraes (Brésil).— Volume II, 164 p.; Ouro Preto (Imprensa Official do Estado de Minas Geraes).

FERREIRA FILHO, F.A. & FONSECA, M.A. (2001): Partição da deformação em regimes contracionais com obstáculos no antepaís: exemplo do sistema de falhas Água Quente, borda leste do Quadrilátero Ferrífero, MG.— Revista Brasileira de Geociências, **31:** 267-278.

FISSGUS, S. (1982): Goldgewinnung in der Serra Pelada, Brasilien.— Erzmetall, **35:** 467-469.

FLEET, M.E., DE ALMEIDA, C.M. & ANGELI, N. (2002): Botryoidal platinum, palladium and potarite from the Bom Sucesso stream, Minas Gerais, Brazil: compositional zoning and origin.— Can. Mineral., **40:** 341-355.

FREYBERG, B.V. (1932): Ergebnisse geologischer Forschungen in Minas Geraes (Brasilien).— N. Jb. Miner. Geol. Paläont., Sonderband II: 403 p.

FREYSSINET, PH., ZEEGERS, H. & TARDY, Y. (1989): Morphology and geochemistry of gold grains in lateritic profiles of southern Mali.— J. Geochem. Expl., **32:** 17-31.

FRIMMEL, H.E. & GARTZ, V.H. (1997): Witwatersrand gold particle chemistry matches model of metamorphosed, hydrothermally altered placer deposits.— Mineral. Deposita, **32:** 523-530.

GALBIATTI, H.F. (1999): Natureza e controle estrutural da mineralização aurífera (jacutinga) na mina do Cauê, Itabira, MG.— 150 p.; Ouro Preto (unpubl. M.Sc. thesis, Departamento de Geologia, Universidade Federal de Ouro Preto).

GALBIATTI, H.F., PEREIRA, M.C. & FONSECA, M.A. (1997): Estruturação dos corpos auríferos (jacutingas) na mina do Cauê – Itabira – MG.— In: Simpósio de Geologia de Minas Gerais, 9, Boletim **14:** 60-62; Ouro Preto (Sociedade Brasileira de Geologia).

GAMMONS, C.H. & WILLIAMS-JONES, A.E. (1995): Hydrothermal geochemistry of electrum: thermodynamic constraints.— Econ. Geol. **90:** 420-432.

GAMMONS, C.H., YU, Y. & BLOOM, M.S. (1993): Experimental investigation of the hydrothermal geochemistry of platinum and palladium: III. The solubility of Ag-Pd alloy + AgCl in NaCl / HCl solutions at 300°C.— Geochim. Cosmochim. Acta, **57:** 2469-2479.

GAMMONS, C.H., YU, Y. & WILLIAMS-JONES, A.E. (1997): The disproportionation of gold(I) chloride complexes at 25 to 200°C.— Geochim. Cosmochim. Acta, **61:** 1971-1983.

GARDNER, D. (1826): In: Imperial Brazilian Mining Association – Reports of the directors addressed to the share-holders: 117-119; London (The Philanthropic Society).

GARDNER, D. (1827): In: Imperial Brazilian Mining Association – Second annual report of the directors, addressed to the share-holders on the 2d March, 1827, and an appendix, containing the reports of the directors to the special general meeting on the 8th February, 1827; and of the Committee appointed by that Special General Meeting: also, extracts of the various communications received from the mines, and the account of the produce of the gold washings from the commencement to the 30th Nov. 1826: 43-45; London (The Philanthropic Society).

GEHLEN, A.F. (1811): Platin und Palladium in Brasilien und St. Domingo gefunden.— Journal für Chemie und Physik, **1:** 362-373.

GORCEIX, H. (1881): Estudo chimico e geologico do centro da provincia de Minas Geraes.— Annaes da Escola de Minas de Ouro Preto, **1:** 1-12.

GORNOSTAYEV, S.S., CROCKET, J.H., MOCHALOV, A.G. & LAAJOKI, K.V.O. (1999): The platinum-group minerals of the Baimka placer deposits, Aluchin Horst, Russian Far East.— Can. Mineral., **37:** 1117-1129.

GRAHAM, J. (1978): Manganochromite, palladium antimonide, and some unusual mineral associations at the Nairne pyrite deposit, South Australia.— Amer. Mineral., **63:** 1166-1174.

GRAINGER, C.J., GROVES, D.I. & CRAVO COSTA, C.H. (2002): The epigenetic sediment-hosted Serra Pelada Au-PGE deposit and its potential genetic association with Fe oxide Cu-Au mineralization within the Carajás mineral province, Amazon craton, Brazil.— Society of Economic Geologists, Special Publication **9:** 47-64. Also in: PORTER, T.M. (Ed.): Hydrothermal iron oxide copper-gold and related deposits: a global perspective, **2:** 227-245; Adelaide (PGC Publishing).

GROEN, J.C., CRAIG, J.R. & RIMSTIDT, J.D. (1990): Gold-rich rim formation on electrum grains in placers.— Can. Mineral., **28:** 207-228.

GROVES, D.I., GOLDFARB, R.J., GEBRE-MARIAM, M., HAGEMANN, S.G. & ROBERT, F. (1998): Orogenic gold deposits: a proposed classification in the context of their crustal distribution and relationship to other gold deposit types.— Ore Geol. Reviews, **13:** 7-27.

GUIMARÃES, D. (1970): Arqueogênese do ouro na região central de Minas Gerais.— Rio de Janeiro (Departamento Nacional da Produção Mineral, Divisão de Fomento da Produção Mineral), Boletim **139:** 51 p.

HACKSPACHER, P.C., OLIVEIRA JR., V.T., SIEMES, H., ROSIÈRE, C.A. & MORENO, M.M.T. (2001): Textures of hematitic and itabiritic iron ores in the Conceição mine, Quadrilátero Ferrífero, Minas Gerais, Brazil.— Z. dt. Geol. Ges., **152:** 467-478.

HARDER, E.C. & CHAMBERLIN, R.T. (1915): The geology of central Minas Geraes, Brazil.— J. Geol., **23:** 341-378, 385-424.

HARRISON, S. & FULLER, J. (1987): Gold from Hope's Nose, Torquay, Devon, England.— Mineral. Record, **18:** 85-88.

HART, R. (1827): In: Imperial Brazilian Mining Association – Third report of the directors, addressed to the share-holders at the half-yearly meeting, on the 12th of October, 1827, being an adjourned meeting from the 14th September preceding; and an appendix, containing extracts of the various communications received from the mines up to 8th August, and the account of the produce of the gold washings from the 1st December, 1826, to the 30th June, 1827: 41-42; London (The Philanthropic Society).

HARTT, C.F. (1870): Geology and physical geography of Brazil.— 620 p.; Boston (Fields, Osgood & Co.).

HASUI, Y., MAGALHÃES, F.S., RAMOS, J.M.S., CARBONARI, F.S. & SANDRONI, S.S. (1994): Modelo estrutural da mina de ferro do Cauê.— Geociências, **13:** 149-165.

HELMREICHEN, V. v. (1847): Reisebericht aus Minas Geraes vom 6. Mai 1846.— Berichte über die Mitteilungen von Freuden der Naturwissenschaft in Wien, **2:** 137-151.

HENDERSON, I.H.C. & MCCAIG, A.M. (1996): Fluid pressure and salinity variations in shear zone-related veins, central Pyrenees, France: implications for the fault-valve model.— Tectonophysics, **262:** 321-348.

HENNIG-MICHAELI, C. (1977): Microscopic structure studies of experimentally and naturally deformed hematite ores.— Tectonophysics, **39:** 255-271.

HENWOOD, W.J. (1846): Notice of the Itabira and Santana mines, in Brazil.—Trans. Royal Geol. Soc. Cornwall, **6:** 227-229.

HENWOOD, W.J. (1871a): On the gold mines of Minas Geraes, in Brazil.—Trans. Royal Geol. Soc. Cornwall, **8:** 168-370.

HENWOOD, W.J. (1871b): On subterranean temperature, Brazil.—Trans. Royal Geol. Soc. Cornwall, **8:** 725-732.

HERZ, N. (1978): Metamorphic rocks of the Quadrilátero Ferrífero, Minas Gerais, Brazil.— U.S. Geol. Surv. Prof. Paper, **641-C:** 81 p.

HEWETT, D.F. (1964): Veins of hypogene manganese oxide minerals in the southwestern United States.— Econ. Geol., **59:** 1429-1472.

HOCHEDER, J.C. (1833): On the geological position of rocks in which the Gongo mine is situated, with a particular view to mining.— In: Fifteenth report of the directors of the Imperial Brazilian Mining Association, read at the half-yearly general meeting, on Thursday, November 14th, 1833, and an appendix, containing extracts of communications from Brazil, account of daily workings, for the half-year ending June 30th, 1833, and financial statement for the same period: 53-57; London (The Philanthropic Society).

HODGE, V.F., STALLARD, M., KOIDE, M. & GOLDBERG, E.D. (1985): Platinum and the platinum anomaly in the marine environment.— Earth Planet. Sci. Letters, **72:** 158-162.

HOEFS, J., MÜLLER, G. & SCHUSTER, A.K. (1982): Polymetamorphic relations in iron ores from the Iron Quadrangle, Brazil: the correlation of oxygen isotope variations with deformation history.— Contrib. Mineral. Petrol., **79:** 241-251.

HOFSTRA, A.H. & CLINE, J.S. (2000): Characteristics and models for Carlin-type gold deposits.— In: HAGEMANN, S.G. & BROWN, P.E. (Eds.): Gold in 2000, Reviews in Economic Geology, **13:** 163-220 (Society of Economic Geologists).

HIPPERTT, J. & DAVIS, B. (2000): Dome emplacement and formation of kilometre-scale synclines in a granite-greenstone terrain (Quadrilátero Ferrífero, southeastern Brazil).— Precamb. Res., **102:** 99-121.

HUHN, S.R.B. & NASCIMENTO, J.A.S. (1997): São os depósitos cupríferos de Carajás do tipo Cu-Au-U-ETR?— In: COSTA, M.L. & ANGÉLICA, R.S. (Eds.): Contribuições à geologia da Amazônia: 143-160; Belém (FINEP–Financiadora de Estudos e Projetos/Sociedade Brasileira de Geologia).

HUSSAK, E. (1904): Über das Vorkommen von Palladium und Platin in Brasilien.— Sitzungsberichte der mathematisch-naturwissenschaftlichen Klasse der Kaiserlichen Akademie der Wissenschaften, **113:** 379-468.

HUSSAK, E. (1906): Über das Vorkommen von Palladium und Platin in Brasilien.— Z. prakt. Geol., **14:** 284-293.

JAIRETH, S. (1992): The calculated solubility of platinum and gold in oxygen-saturated fluids and the genesis of platinum-palladium and gold mineralization in the unconformity-related uranium deposits.— Mineral. Deposita, **27:** 42-54.

JEDWAB, J. & CASSEDANNE, J. (1998): Historical observations on oxygen-bearing compounds of platinum and palladium in Minas Gerais, Brazil.— Can. Mineral., **36:** 887-893.

JEDWAB, J., CASSEDANNE, J., CRIDDLE, A.J., RY, P. DU, GHYSENS, G., MEISSER, N., PIRET, P. & STANLEY, C.J. (1993): Rediscovery of palladinite PdO from Itabira (Minas Gerais, Brazil) and from Ruwe (Shaba, Zhaire).— Terra Nova, Abstract Supplement, **2:** 22.

JOHAN, Z. (1989): Merenskyite, $Pd(Te,Se)_2$, and the low-temperature selenide association from the Pøíbram uranium deposit, Czechoslovakia.— N. Jb. Miner. Mh., 179-191.

JOHNSON, P.N. & LAMPADIUS, W.A. (1837): Ueber brasilianisches Palladgold und dessen Ausbringen und Scheidung.— J. prakt. Chemie **11:** 309-315.

JORGE JOÃO, X. DA S., NEVES, A.P. & LEAL, J.W.L. (1982): Ouro de Serra Pelada – aspectos da geologia e garimpagem.— In: Simpósio de Geologia da Amazônia, 1, Volume **2:** 52-61; Belém (Sociedade Brasileira de Geologia).

KESSLER, W. & MÜLLER G. (1988): Minor and trace-element data of iron oxides from iron-formations of the Iron Quadrangle, Minas Gerais, Brazil.— Mineral. Petrol., **39:** 245-250.

KLEIN, C. & LADEIRA, E.A. (2000) Geochemistry and petrology of some Proterozoic banded iron-formations of the Quadrilátero Ferrífero, Minas Gerais, Brazil.— Econ. Geol., **95:** 405-428.

KRUPP, R.E. & WEISER, T. (1992): On the stability of gold-silver alloys in the weathering environment.— Mineral. Deposita, **27:** 268-275.

KUCHA, H. & PRZYBYŁOWICZ, W. (1999): Noble metals in organic matter and clay-organic matrices, Kupferschiefer, Poland.— Econ. Geol., **94:** 1137–1162.

KWITKO, R., CABRAL, A.R., LEHMANN, B., LAFLAMME, J.H.G., CABRI, L.J., CRIDDLE, A.J. & GALBIATTI, H.F. (2002): Hongshiite (PtCu) from itabirite-hosted Au–Pd–Pt mineralization (jacutinga), Itabira district, Minas Gerais, Brazil.— Can. Mineral., **40:** 711-723.

LADEIRA, E.A. (1991): Genesis of gold in Quadrilátero Ferrífero: a remarkable case of permanency, recycling and inheritance – a tribute to Djalma Guimarães, Pierre Routhier and Hans Ramberg.— In: LADEIRA, E.A. (Ed.): Brazil Gold '91: 11-30; Rotterdam (Balkema).

LAGOEIRO, L.E. (1998): Transformation of magnetite to hematite and its influence on the dissolution of iron oxide minerals.— J. Metamorphic Geol., **16:** 415-423.

LEHMANN, B., DIETRICH, A. & WALLIANOS, A. (2000): From rocks to ore.— Int. J. Earth Sci., **89:** 284-294.

LINDGREN, W. (1928): Mineral deposits.— 1049 p.; New York (McGraw Hill, 3rd ed.).
LOBATO, L.M. & VIEIRA, F.W.R. (1998): Styles of hydrothermal alteration and gold mineralization associated with the Nova Lima Group of the Quadrilátero Ferrífero: Part II, the Archean mesothermal gold-bearing hydrothermal system.— Revista Brasileira de Geociências, **28:** 355-366.
LOBATO, L.M., RIBEIRO-RODRIGUES, L.C., ZUCCHETTI, M., NOCE, C.M., BALTAZAR, O.F., SILVA, L.C., & PINTO, C.P. (2001a): Brazil's premier gold province. Part I: The tectonic, magmatic, and structural setting of the Archean Rio da Velhas greenstone belt, Quadrilátero Ferrífero.— Mineral. Deposita, **36:** 228-248.
LOBATO, L.M., RIBEIRO-RODRIGUES, L.C. & VIEIRA, F.W.R. (2001b): Brazil's premier gold province. Part II: geology and genesis of gold deposits in the Archean Rio das Velhas greenstone belt, Quadrilátero Ferrífero.— Mineral. Deposita, **36:** 249-277.
LÜDERS, V., GUTZMER, J. & BEUKES, N.J. (1999): Fluid inclusion studies in cogenetic hematite, hausmannite, and gangue minerals from high-grade manganese ores in the Kalahari manganese field, South Africa.— Econ. Geol. **94:** 589-596.
MACHADO, N., LINDENMAYER, Z., KROGH, T.E. & LINDENMAYER, D. (1991): U-Pb geochronology of Archean magmatism and basement reactivation in the Carajás area, Amazon shield, Brazil.— Precamb. Res. **49:** 329-354.
MANN, A.W. (1984): Mobility of gold and silver in lateritic weathering profiles: some observations from Western Australia.— Econ. Geol., **79:** 38-49.
MARSHAK, S., ALKMIM, F.F. & JORDT-EVANGELISTA, H. (1992): Proterozoic crustal extension and the generation of dome-and-keel structure in an Archaean granite-greenstone terrain.— Nature, **357:** 491-493.
MCDONALD, I., OHNENSTETTER, D., OHNENSTETTER, M. & VAUGHAN, D.J. (1999a): Palladium oxides in ultramafic complexes near Lavatrafo, Western Adriamena, Madagascar.— Mineral. Mag., **63:** 345-352.
MCDONALD, I., OHNENSTETTER, D., ROWE, J.P., TREDOUX, M., PATTRICK, R.A.D. & VAUGHAN, D.J. (1999b) Platinum precipitation in the Waterberg deposit, Naboomspruit, South Africa.— S. Afr. J. Geol., **102:** 184–191.
MEIRELES, E. DE M. & SILVA, A.R.B. (1988): Depósito de ouro de Serra Pelada, Marabá, Pará.— In: SCHOBBENHAUS, C. & COELHO, C.E.S. (Eds.): Principais depósitos minerais do Brasil, **3:** 547-557; Brasília (Departamento Nacional da Produção Mineral, Companhia Vale do Rio Doce).
MEIRELES, E. DE M., TEIXEIRA, J.T. & MEDEIROS FILHO, C.A. (1982): Geologia preliminar do depósito de ouro de Serra Pelada.— In: Simpósio de Geologia da Amazônia, 1, Volume **2:** 74-83; Belém (Sociedade Brasileira de Geologia).
MERNAGH, T.P., HEINRICH, C.A., LECKIE, J.F., CARVILLE, D.P., GILBERT, D.J., VALENTA, R.K. & WYBORN, L.A.I. (1994): Chemistry of low-temperature hydrothermal gold, platinum, and palladium (±uranium) mineralization at Coronation Hill, Northern Territory, Australia.— Econ. Geol., **89:** 1053-1073.
MINKO, A.E., COLIN, F., TRESCASES, J.-J. & LECOMTE, P. (1992): Altération latéritique du gîte aurifère d'Ovala (Gabon), et formation d'une anomalie superficielle de dispersion. — Mineral. Deposita, **27:** 90-100.
MOORE, S.L. (1969): Geology and ore deposits of Antônio dos Santos, Gongo Soco and Conceição do Rio Acima quadrangles, Minas Gerais, Brazil.— U.S. Geol. Surv. Prof. Paper, **341-I:** 48 p.
MORONI, M., GIRARDI, V.A.V. & FERRARIO, A. (2001): The Serra Pelada Au-PGE deposit, Serra dos Carajás (Pará State, Brazil): geological and geochemical indications for a composite mineralising process.— Mineral. Deposita, **36:** 768-785.

MOREY, G.B. (1999): High-grade iron ore deposits of the Mesabi Range, Minnesota–product of a continental-scale Proterozoic ground-water flow system.— Econ. Geol., **94:** 133-142.

MÜLLER, G. (1984): Die Goldlagerstätte Morro da Babilônia im Staate Pará, Brasilien.— Aufschluss, **35:** 279-291.

NESBITT, B.E. & MUEHLENBACHS, K. (1995): Geochemical studies of the origins and effects of synorogenic crustal fluids in the southern Omineca Belt of British Columbia, Canada.— Geol. Soc. America Bull., **107:** 1033-1050.

NICHOLSON, K. (1992): Contrasting mineralogical-geochemical signatures of manganese oxides: guides to metallogenesis.— Econ. Geol., **87:** 1253-1264.

NICKEL, E.H. (2002): An unusual occurrence of Pd, Pt, Au, Ag, and Hg minerals in the Pilbara region of Western Australia.— Can. Mineral., **40:** 419-433.

NUR, A. (1974): Matsushiro, Japan, earthquake swarm: confirmation of the dilatancy-fluid diffusion model.— Geology, **2:** 217-221.

OBERTHÜR, T. (2002): Platinum-group element mineralization of the Great Dyke, Zimbabwe.— In: CABRI, L.J. (Ed.): The geology, geochemistry, mineralogy and mineral beneficiation of platinum-group elements: 483-506; Montreal (Canadian Institute of Mining, Metallurgy and Petroleum, Special Volume 54).

OKAMOTO, H. & MASSALSKI, T.B. (1985): The Au-Pd (gold-palladium) system.— Bull. Alloy Phase Diagrams, **6:** 229-235.

OLIVEIRA, E.P. (1932): Genesis of the deposits of auriferous jacutinga.— Econ. Geol., **32:** 744-749.

OLIVER, N.H.S. & DICKENS, G.R. (1999): Hematite ores of Australia formed by syntectonic heated meteoric fluids. — In: STANLEY et al. (Eds.): Mineral deposits: process to processing: 889-892; Rotterdam (Balkema).

OLIVO, G.R. & GAUTHIER, M. (1995): Palladium minerals from the Cauê iron mine, Itabira district, Minas Gerais, Brazil.— Mineral. Mag., **59:** 455-463.

OLIVO, G.R., GAUTHIER, M. & BARDOUX, M. (1994): Palladian gold from the Cauê iron mine, Itabira district, Minas Gerais, Brazil.— Mineral. Mag., **58:** 579-587.

OLIVO, G.R., GAUTHIER, M., BARDOUX, M., SÁ, E.L., FONSECA, J.T.F. & SANTANA, F.C. (1995): Palladium-bearing gold deposit hosted by Proterozoic Lake Superior-type iron-formation at the Cauê iron mine, Itabira district, southern São Francisco craton, Brazil: geologic and structural controls.— Econ. Geol., **90:** 118-134.

OLIVO, G.R., GAUTHIER, M., GARIÉPY, C. & CARIGNAN, J. (1996): Transamazonian tectonism and Au-Pd mineralization at the Cauê mine, Itabira district, Brazil: Pb isotopic evidence.— J. South Amer. Earth Sci., **9:** 273-279.

OLIVO, G.R., GAUTHIER, M., WILLIAMS-JONES, A.E., & LEVESQUE, M. (2001): The Au-Pd mineralization at the Conceição iron mine, Itabira district, southern São Francisco craton, Brazil: an example of a jacutinga-type deposit.— Econ. Geol., **96:** 61-74.

OLSZEWSKI, W.J., WIRTH, K.R., GIBBS, A.K. & GAUDETTE, H.E. (1989): The age, origin, and tectonics of the Grão Pará Group and associated rocks, Serra dos Carajás, Brazil: Archean continental volcanism and rifting.— Precamb. Res., **42:** 229-254.

PAAR, W.H., ROBERTS, A.C., CRIDDLE, A.J. & TOPA, D. (1998): A new mineral, chrisstanleyite, $Ag_2Pd_3Se_4$, from Hope's Nose, Torquay, Devon, England.— Mineral. Mag., **62:** 257-264.

PAAR, W.H., AMANN, G., TOPA, D. & SUREDA, R.J. (2000): Gold and palladium in the Sierra de Umango and Los Llantenes selenide districts, La Rioja, Argentina.— In: Memoria del XIV Congreso Geologico Boliviano: 465-469; La Paz.

PEREIRA, M.C., GALBIATTI, H.F. & FONSECA, M.A. (1999): Mineralização aurífera (jacutinga) associada a fraturas em zonas transcorrentes, mina Conceição, Itabira, MG.— In:

Simpósio de Geologia do Centro-Oeste, 7, Boletim de Resumos: 75; Brasília (Sociedade Brasileira de Geologia).

PINHEIRO, R.V.L. & HOLDSWORTH, R.E. (1997): Reactivation of Archaean strike-slip fault systems, Amazon region, Brazil. — J. Geol. Soc. London, **154:** 99-103.

PIRES, F.R.M. (1983): Greenstones as a part of the Minas Supergroup in the Quadrilátero Ferrífero, Minas Gerais, Brazil.— Revista Brasileira de Geociências, **13:** 106-112.

PIRES, F.R.M. (1995): Textural and mineralogical variations during metamorphism of the Proterozoic Itabira Iron Formation in the Quadrilátero Ferrífero, Minas Gerais, Brazil.— An. Acad. Bras. Ciênc., **67:** 77-105.

POLÔNIA, J.C. & SOUZA, A.M.S. (1988): O comportamento em microescala do ouro no minério de ferro de Itabira, Minas Gerais.— In: Congresso Brasileiro de Geologia, 35, Volume **1:** 58-69; Belém (Sociedade Brasileira de Geologia).

POWELL, C.MCA., OLIVER, N.H.S., LI, Z.-X., MARTIN, D.MCB. & RONASZEKI, J. (1999): Synorogenic hydrothermal origin for giant Hamersley iron oxide orebodies.— Geology, **27:** 175-178.

RAMANAIDOU, E., CATHELINEAU, M., DUBESSY, J. & LE GLEUHER, M. (1991): Gold mobility during hydrothermal and supergene alteration of BIF (Itabirites), Ouro Fino syncline, Brazil.— In: LADEIRA, E.A. (Ed.): Brazil Gold '91: 729-733; Rotterdam (Balkema).

RAMDOHR, P. (1969): The ore minerals and their intergrowths.— 1174 p.; Oxford (Pergamon Press, 3rd ed.).

RENGER, F.E., NOCE, C.M., ROMANO, A.W. & MACHADO, N. (1994): Evolução sedimentar do Supergrupo Minas: 500 ma. de registro geológico no Quadrilátero Ferrífero, Minas Gerais, Brasil.— Geonomos, **2**: 1-11.

REQUIA, K. & FONTBOTÉ, L. (2000): The Salobo iron oxide copper-gold deposit, Carajás, northern Brazil.— In: PORTER, T.M. (Ed.): Hydrothermal iron oxide copper-gold and related deposits: a global perspective, **1:** 225-236; Adelaide (PGC Publishing).

RIBEIRO-RODRIGUES, L.C. (1998): Gold mineralization in Archaean banded iron-formation of the Quadrilátero Ferrífero, Minas Gerais, Brazil – The Cuiabá Mine.— 262 p.; Aachen (Aachener Geowissenschaftliche Beiträge, Band 27).

ROBERTS, A.C., PAAR, W.H., COOPER, M.A., TOPA, D., CRIDDLE, A.J. & JEDWAB, J. (2002): Verbeekite, monoclinic $PdSe_2$, a new mineral from the Musonoi Cu-Co-Mn-U mine, near Kolwezi, Shaba Province, Democratic Republic of Congo.— Mineral. Mag, **66:** 173-179.

RODDY, M.S., REYNOLDS, S.J., SMITH, B.M. & RUIZ, J. (1988): K-metasomatism and detachment-related mineralization, Harcuvar Mountains, Arizona.— Geol. Soc. America Bull., **100:** 1627-1639.

ROEDDER, E. (1984): Fluid inclusions.— Reviews in Mineralogy, **12**; 644 p. (Mineralogical Society of America).

RONZÊ, P.C., SOARES, A.D.V., DOS SANTOS, M.G.S. & BARREIRA, C.F. (2000): Alemão copper-gold (U-REE) deposit, Carajás, Brazil.— In: PORTER, T.M. (Ed.): Hydrothermal iron oxide copper-gold and related deposits: a global perspective, **1:** 191-202; Adelaide (PGC Publishing).

ROSIÈRE, C.A., SIEMES, H., QUADE, H., BROKMEIER, H.-G. & JANSEN, E.M. (2001): Microstructures, textures and deformation mechanisms in hematite.— J. Struct. Geol., **23:** 1429-1440.

SAINT-HILAIRE, A. (1830): Viagens pelas províncias do Rio de Janeiro e Minas Gerais.— 378 p.; Belo Horizonte (Itatiaia, 1975).

SAMUSIKOV, V.P. & TSABUL, L.N. (1977): Vliyanie probnosti samorodnogo zolota na skorost ego rastvoreniya.— Dokl. Akad. Nauk CCCP, **235:** 462-465.

SANDERS, B.H. (1933): Iron ores at Itabira, Brazil.— Instn Min. Metall. Bull., **346:** 1-23.

SANT'ANNA, L.G., SCHORSCHER, H.D. & RICCOMINI, C. (1997): Cenozoic tectonics of the Fonseca Basin region, eastern Quadrilátero Ferrífero, MG, Brazil.— J. South Amer. Earth Sci., **10:** 275-284.

SAUNDERS, J.A. (1994): Silica and gold textures in bonanza ores of the Sleeper deposit, Humboldt County, Nevada: evidence for colloids and implications for epithermal ore-forming processes.— Econ. Geol., **89:** 628-638.

SCOTT, H.K. (1902): The gold field of the state of Minas Geraes, Brazil.— Trans. Amer. Inst. Min. Eng., **33:** 406-444.

SCRIVENER, R.C., COOPER, B.V., GEORGE, M.C. & SHEPHERD, T.J. (1982): Gold-bearing carbonate veins in the Middle Devonian Limestone of Hope's Nose, Torquay.— Proceedings of the Ussher Society, **5:** 393.

ᵍ ENER, A.K., GRAINGER, C.J. & GROVES, D.I. (2002): Epigenetic gold–platinum-group element deposits: examples from Brazil and Australia.— Trans. Instn Min. Metall. (Sect. B: Appl. earth sci.), **111:** B65-B73.

SHERLOCK, R.L. & LEHRMAN, N.J. (1995): Occurrences of dendritic gold at the McLaughlin Mine hot-spring deposit.— Mineral. Deposita, **30:** 323-327.

SIBSON, R.H., MOORE, J.MCM. & RANKIN, A.H. (1975): Seismic pumping – a hydrothermal fluid transport mechanism.— J. Geol. Soc. London, **131:** 653-659.

SIEGERS, A. & RENGER, F.E. (1985): Gold mining in Brazil.— Erzmetall, **38:** 351-358.

SIMON, G., KESLER, S.E. & ESSENE, E.J. (1997): Phase relations among selenides, sulfides, tellurides, and oxides: II. Applications to selenide-bearing ore deposits.— Econ. Geol., **92:** 468-484.

SOUZA, L.H. & VIEIRA, E.A.P. (2000): Salobo 3 Alpha deposit: geology and mineralisation.— In: PORTER, T.M. (Ed.): Hydrothermal iron oxide copper-gold and related deposits: a global perspective, **1:** 213-224; Adelaide (PGC Publishing).

STANLEY, C.J., CRIDDLE, A.J. & LLOYD, D. (1990): Precious and base metal selenide mineralization at Hope's Nose, Torquay, Devon.— Mineral. Mag., **54:** 485-493.

STANLEY, C.J., CRIDDLE, A.J., FÖRSTER, H.-J. & ROBERTS, A.C. (2002): Tischendorfite, $Pd_8Hg_3Se_9$, a new mineral species from Tilkerode, Harz Mountains, Germany.— Can. Mineral., **40:** 739-745.

STÜBEN, D., GLASBY, G.P., ECKHARDT, J.D., BERNER, Z., MOUNTAIN, B.W. & USUI, A. (1999): Enrichments of platinum-group elements in hydrogenous, diagenetic and hydrothermal marine manganese and iron deposits.— Explor. Mining Geol., **8:** 233-250.

SUITA, M.T.F. & NILSON, A.A. (1988): Geologia do complexo máfico-ultramáfico Luanga (Província de Carajás, Pará) e das unidades encaixantes.— In: Congresso Brasileiro de Geologia, 35, Anais, **6:** 2813-2823; Belém (Sociedade Brasileira de Geologia).

SUNAGAWA, I. (1981): Characteristics of crystal growth in nature as seen from the morphology of mineral crystals.— Bull. Minéral., **104:** 81-87.

TALLARICO, F.H.B., COIMBRA, C.R. & CRAVO COSTA, C.H. (2000a): The Serra Leste sediment-hosted Au-(Pd-Pt) mineralization, Carajás Province.— Revista Brasileira de Geociências, **30:** 226-229.

TALLARICO, F.H.B., OLIVEIRA, C.G. & FIGUEIREDO, B.R. (2000b): The Igarapé Bahia Cu-Au mineralization, Carajás province.— Revista Brasileira de Geociências, **30:** 230-233.

TAYLOR, D., DALSTRA, H.J., HARDING, A.E., BROADBENT, G.C. & BARLEY, M.E. (2001): Genesis of high-grade hematite orebodies of the Hamersley Province, Western Australia.— Econ. Geol., **96:** 837-873.

TAZAVA, E. & OLIVEIRA, C.G. (2000): The Igarapé Bahia Au-Cu-(REE-U) deposit, Carajás mineral province, northern Brazil.— In: PORTER, T.M. (Ed.): Hydrothermal iron oxide copper-gold and related deposits: a global perspective, **1:** 203-212; Adelaide (PGC Publishing).

THOMAS, O.R. (1905): Minas Geraes, Brazil.— The Engineering and Mining Journal, **80:** 453-455.

TOLSTYKH, N.D. & KRIVENKO, A.P. (1998): Native high-purity platinum, its origin, and the nomenclature of Pt–Fe alloys.— Dokl. Earth Sci., **361A:** 775-777.

TOUZEAU, E.M. (1892): Gold-mining in Brazil.— Trans. Fed. Inst. Mining Engineers, **4:** 219-232.

TRENDALL, A.F., BASEI, M.A.S., LAETER, J.R. & NELSON, D.R. (1998): SHRIMP zircon U-Pb constrains on the age of the Carajás Formation, Grão Pará Group, Amazon Craton.— J. South Amer. Earth Sci., **11:** 265-277.

TREPMANN, C. & STÖCKHERT, B. (2001): Mechanical twinning of jadeite – an indication of synseismic loading beneath the brittle–plastic transition.— Int. J. Earth Sciences, **90:** 4-13.

UPTON, P., KOONS, P.O. & CHAMBERLAIN, C.P. (1995): Penetration of deformation-driven meteoric water into ductile rocks: isotopic and model observations from the Southern Alps.— New Zealand J. Geol. Geophys., **38:** 535-543.

VAN DEN KERKHOF, A.M. & HEIN, U.F. (2001): Fluid inclusion petrography.— Lithos, **55:** 27-47.

VARAJÃO, C.A.C., FIALIN, M., COLIN, F. & VIEILLARD, P. (1999): Chemical composition including oxygen of an undefined Pd-Cu-bearing phase from Maquiné mine, Minas Gerais, Brazil.— Zbl. Geol. Paläont. Teil I, (**7/8):** 871-881.

VARAJÃO, C.A.C., COLIN, F., VIEILLARD, P., MELFI, A.J. & NAHON, D. (2000): Early weathering of palladium gold under lateritic conditions, Maquiné mine, Minas Gerais, Brazil.— Appl. Geochem. **15:** 245-263.

VASCONCELOS, P.M., RENNE, P.R., BRIMHALL, G.H. & BECKER, T.A. (1994): Direct dating of weathering phenomena by $^{40}Ar/^{39}Ar$ and K-Ar analysis of supergene K-Mn oxides.— Geochim. Cosmochim. Acta, **58:** 1635-1665.

VILLAS, R.N. & SANTOS, M.D. (2001): Gold deposits of the Carajás mineral province: deposit types and metallogenesis.— Mineral. Deposita, **36**, 300-331.

WAGNER, P.A. (1929): The platinum deposits and mines of South Africa.— 326 p.; Edinburgh (Oliver and Boyd).

WEBSTER, J.G. (1986): The solubility of gold and silver in the system Au-Ag-S-O_2-H_2O at 25°C and 1 atm.— Geochim. Cosmochim. Acta, **50:** 1837-1845.

WEBSTER, J.G. & MANN, A.W. (1984): The influence of climate, geomorphology and primary geology on the supergene migration of gold and silver.— J. Geochem. Expl., **22:** 21-42.

WENDT, I. & CARL, C. (1991): The statistical distribution of the mean squared weighted deviation.— Chem. Geol., **86:** 275-285.

WOOD, S.A. (2002): The aqueous geochemistry of platinum-group elements with applications to ore deposits.— In: CABRI, L.J. (Ed.): The geology, geochemistry, mineralogy and mineral beneficiation of platinum-group elements: 211-249; Montreal (Canadian Institute of Mining, Metallurgy and Petroleum, Special Volume 54).

WOOD, S.A., MOUNTAIN, B.W. & PAN, P. (1992): The aqueous geochemistry of platinum, palladium and gold: recent experimental constraints and a re-evaluation of theoretical predictions.— Can. Mineral., **30:** 955-982.

YARDLEY, B.W.D. & GRAHAM, J.T. (2002): The origins of salinity in metamorphic fluids.— Geofluids, **2:** 249-256.